

**UNDERSTANDING *STAPHYLOCOCCUS AUREUS* β -LACTAM RESISTANCE: A
STRUCTURAL INVESTIGATION**

by

John Andrew Nelson Alexander

B.Sc. Hons., The University of the Fraser Valley, 2014

A THESIS SUBMITTED IN PARTIAL FULFILLMENT OF
THE REQUIREMENTS FOR THE DEGREE OF

DOCTOR OF PHILOSOPHY

in

THE FACULTY OF GRADUATE AND POSTDOCTORAL STUDIES
(Biochemistry and Molecular Biology)

THE UNIVERSITY OF BRITISH COLUMBIA

(Vancouver)

August 2020

© John Andrew Nelson Alexander, 2020

The following individuals certify that they have read, and recommend to the Faculty of Graduate and Postdoctoral Studies for acceptance, the dissertation entitled:

Understanding *Staphylococcus aureus* β -lactam resistance: a structural investigation

submitted by John Andrew Nelson
Alexander in partial fulfilment of the requirements for

the degree of Doctor of philosophy

in Biochemistry and Molecular Biology

Examining Committee:

Natalie Strynadka, Biochemistry and Molecular Biology

Supervisor

Lindsay Eltis, Microbiology and Immunology

Supervisory Committee Member

Dieter Brömme, Oral Biological and Medical Sciences

University Examiner

Erin Gaynor, Microbiology and Immunology

University Examiner

Additional Supervisory Committee Members:

Robert Hancock, Microbiology and Immunology

Supervisory Committee Member

Abstract

Methicillin-resistant *Staphylococcus aureus* (MRSA) infections increase mortality and morbidity worldwide, threatening public health. MRSA is resistant to many classes of antibiotics including the most commonly prescribed β -lactam antibiotic class, making treatment of infections difficult. In MRSA β -lactam resistance is primarily mediated by PBP2a, a β -lactam resistant penicillin-binding protein and to some extent, PC1, a β -lactamase. Additionally, β -lactam resistance in *S. aureus* has also been recently shown to be facilitated independently of PBP2a by mutations in the gene coding for penicillin-binding protein 4 (PBP4), though the mechanisms of resistance have remained mysterious.

In an effort to understand the mechanism of PBP4-mediated β -lactam resistance, two ligand-free and six acyl-enzyme intermediate X-ray crystallographic structures of mutant and wild-type PBP4 were solved. Localised within the transpeptidase active site cleft, the two substitutions appear to have different effects depending on the drug. Kinetic analysis shows the missense mutations impaired the K_M value for ceftobiprole 150-fold, decreasing the proportion of inhibited PBP4. However, ceftaroline resistance appeared to be mediated by other factors, possibly including mutation of the *pbp4* promoter. These findings suggest PBP4 mediated β -lactam resistance is mediated by at least two separate mechanisms.

The expression of the genes coding PC1 and PBP2a are controlled by two integral membrane proteins: BlaR1 and MecR1 respectively, which consist of a zinc metalloprotease domain and an extracellular C-terminal β -lactam sensing domain which activates the proteolytic domain when acylated by a β -lactam antibiotic. Here, avibactam, a diazabicyclooctane β -lactamase inhibitor, was found to induce expression of *pbp2a* (which codes for PBP2a) and *blaZ* (which codes for PC1) in a clinical strain of MRSA. The X-ray crystallographic structures of the

BlaR1 and MecR1 sensor domains show avibactam binds to MecR1 as has been observed for the Class-D β -lactamases. In contrast, BlaR1 has two avibactam binding poses orientated 180° to each other. As avibactam upregulates expression of *blaZ* and *pbp2a* antibiotic resistance genes, we suggest further research is needed to explore the effect of administering β -lactam-avibactam combinations to treat MRSA infections.

Together, these findings improve our understanding of β -lactam resistance in MRSA and provide molecular details to facilitate improved inhibitors of MRSA.

Lay summary

Expanding antimicrobial resistance is threatening to undo the advances of modern medicine. Without antibiotics, risks of infection will dramatically increase, making even a simple cut or routine surgery much more dangerous. In an effort to reduce increasing antibiotic resistance, this thesis furthers our understanding of the mechanisms of antibiotic resistance in methicillin-resistant *Staphylococcus aureus* (MRSA), a particularly problematic “superbug” that is found worldwide in hospitals and the community. Using X-ray crystallography, a technique that allows the positions of atoms in a molecule to be determined, this work demonstrates how proteins responsible for mediating resistance interact with antibiotics. Additionally, by comparing the shape of proteins aiding resistance in susceptible and resistant strains of MRSA, it can uncover the molecular details of the resistance mechanism. Insight into how antibiotics bind proteins and how protein shape evolves contributes to the understanding of resistance and facilitates the development of new and improved antibiotics.

Preface

I was responsible for all writing and figure making for this thesis with editing of the final version by Dr Strynadka. Chapter 2 is based on two publications and was conducted in collaboration with Dr Henry Chambers' lab.

Alexander, J. A. N., Chatterjee, S. S., Hamilton, S. M., Eltis, L. D., Chambers, H. F., and Strynadka, N. C. J. (2018) Structural and kinetic analysis of penicillin-binding protein 4 (PBP4)-mediated antibiotic resistance in *Staphylococcus aureus*. *J. Biol. Chem.* **293**, 19854–19865.

Under the guidance of Dr Strynadka, I designed and conducted all experiments, analysed all the data, made all the figures, and wrote the manuscript. Drs Som Chatterjee, Stephanie Hamilton, and Henry Chambers provided guidance on project design and reviewed the manuscript. Dr Lindsay Eltis gave valuable advice on the design and analysis of the kinetics data and reviewed the manuscript.

Hamilton, S. M., **Alexander, J. A. N.**, Choo, E. J., Basuino, L., Da Costa, T. M., Severin, A., Chung, M., Aedo, S., Strynadka, N. C. J., Tomasz, A., Chatterjee, S. S., and Chambers, H. F. (2017) High-level resistance of staphylococcus aureus to β -Lactam antibiotics mediated by penicillin-binding protein 4 (PBP4). *Antimicrob. Agents Chemother.* **61**, AAC.02727-16.

I was responsible for cloning and recombinant protein expression as well as purification. I wrote all parts of this paper included in this chapter.

A version of chapter 3 has been published and includes work from a collaboration with the labs of Drs Som Chatterjee, Artem Cherkasov, Henry Chambers.

Alexander, J. A. N., Radaeva, M. King, D.T., Chambers, H. F., Cherkasov, A., Chatterjee, S. S., and Strynadka, N. C. J. (2020). Structural analysis of avibactam mediated activation of the bla and mec divergons in methicillin-resistant *Staphylococcus aureus*. *J. Biol. Chem.* In press.

With supervision from Dr Strynadka, I was responsible for all cloning, protein expression, purification, crystallization, data analysis, and manuscript writing. Mariia Radaeva and Dr Artem Cherkasov performed the *in silico* docking and molecular dynamics simulations while Dr Dustin King found the initial crystallization conditions for the BlaR1-avibactam crystals. Drs Som Chatterjee and Henry Chambers were involved in the gene expression studies.

Table of contents

Abstract.....	iii
Lay summary.....	v
Preface.....	vi
Table of contents	viii
List of tables.....	x
List of figures.....	xi
List of abbreviations	xiv
Acknowledgements	xvi
.....	xviii
Chapter 1: Introduction	1
1.1 <i>Staphylococcus aureus</i>	1
1.2 <i>S. aureus</i> peptidoglycan.....	4
1.2.1 <i>S. aureus</i> peptidoglycan synthesis	5
1.2.1.1 <i>S. aureus</i> penicillin-binding proteins	9
1.3 Inhibition of peptidoglycan synthesis: β -lactam antibiotics	14
1.4 β -lactam resistance in <i>Staphylococcus aureus</i>	16
1.4.1 Conventional <i>S. aureus</i> β -lactam antibiotic resistance mediated by the bla and mec divergons	17
1.4.2 Non-canonical, PBP4-mediated β -lactam resistance	25
1.5 Objective of thesis.....	25
Chapter 2: Structural and kinetic analyses of penicillin-binding protein 4 (PBP4)-mediated antibiotic resistance in <i>Staphylococcus aureus</i>	28
2.1 Introduction.....	28
2.2 Methods.....	33
2.2.1 Cloning, expression, and purification of PBP4 and PBP4 ^{CRB}	33
2.2.2 Antibiotics.....	34
2.2.3 Crystallization, structure determination, and modelling of PBP4 and PBP4 ^{CRB} ..	34
2.2.4 Kinetic analysis of PBP4 and PBP4 ^{CRB}	36
2.3 Results.....	36
2.3.1 X-ray crystallographic analysis of ligand-free PBP4 and PBP4 ^{CRB} as well as acyl- enzyme intermediate structures with ceftobiprole, ceftaroline, and nafcillin.....	36
2.3.2 PBP4 structures with ceftobiprole	40
2.3.3 PBP4 structures with ceftaroline.....	43
2.3.4 PBP4 structures with nafcillin	45
2.3.5 Two loops bordering the PBP4 active site display alternate conformations	46
2.3.6 Steady-state kinetic analysis of PBP4 and PBP4 ^{CRB}	47
2.4 Discussion.....	47

Chapter 3: Structural analysis of avibactam-mediated activation of the bla and mec divergons in methicillin-resistant <i>Staphylococcus aureus</i>	55
3.1 Introduction.....	55
3.2 Methods.....	59
3.2.1 Expression and purification of BlaR1 ^{SD} and MecR1 ^{SD}	59
3.2.2 Crystallization of BlaR1 ^{SD} and MecR1 ^{SD}	61
3.2.3 Soaking and harvesting crystals.....	61
3.2.4 Data collection and processing	62
3.2.5 In silico ligand docking into BlaR1 ^{SD} and MecR1 ^{SD} avibactam structures	63
3.2.6 Molecular dynamic simulations of avibactam with BlaR1 ^{SD} and MecR1 ^{SD}	63
3.2.7 Size exclusion chromatography multi-angle light scattering.....	63
3.2.8 Thermal aggregation assays.....	64
3.2.9 Quantitative Real-Time PCR of <i>blaZ</i> and <i>pbp2a</i>	65
3.3 Results.....	65
3.3.1 Effect of avibactam on gene expression of <i>pbp2a</i> and <i>blaZ</i>	65
3.3.2 Thermal stability of BlaR1 ^{SD} and MecR1 ^{SD} with avibactam and β -lactam antibiotics.....	66
3.3.3 BlaR1 ^{SD} and MecR1 ^{SD} avibactam crystal structures.....	67
3.3.4 In silico docking of avibactam, nacubactam, and relebactam into BlaR1 ^{SD} and MecR1 ^{SD} avibactam crystal structures.....	73
3.3.5 Molecular dynamics simulations of BlaR1 ^{SD} and MecR1 ^{SD} interactions with avibactam	75
3.4 Discussion.....	75
Chapter 4: Conclusion and future directions	86
4.1 Summary and significant results.....	86
4.1.1 The mechanism of PBP4-mediated β -lactam resistance in <i>S. aureus</i>	86
4.1.2 The effect of avibactam on the bla and mec divergons in MRSA	88
References	90
Appendices	106
Appendix A – Research publications.....	106
Appendix B – Chapter 2 supplementary information	108
Appendix C – Chapter 3 supplementary information	117

List of tables

Table 1.1: Antibiotics and β-lactamase inhibitors that were analysed in complex with proteins by x-ray crystallography in this thesis.	26
Table 2.1: Data collection and structure refinement statistics for PBP4	41
Table 2.2: Data collection and structure refinement statistics for PBP4^{CRB}	42
Table 2.3: Cα RMSD values for PBP4 structures	44
^aTable 2.4: Steady-state kinetic parameters for PBP4 and PBP4^{CRB}	47
Table 2.5: Distances between the β-lactam leaving	51
Table 2.6: Number of hydrogen bonds to each ligand in PBP4 and PBP4^{CRB} structures	52
Table 3.1: Data collection and structure refinement statistics for the BlaR1^{SD} and MecR1^{SD} in covalent complex with avibactam	68
Table 3.2: Cα RMSD values for existing MecR1^{SD} structures compared with the MecR1^{SD} structure with avibactam (PDB ID: 6o9s)	72
Table 3.3: Number of hydrogen bonds between the active site and avibactam in BlaR1^{SD}, MecR1^{SD}, and OXA-10 (PDB-ID: 4s2o) structures	72
Table 3.4: Cα RMSD values for existing BlaR1^{SD} structures (from <i>S. aureus</i> unless otherwise noted) compared with the BlaR1^{SD} structure with avibactam (PDB ID: 6o9w) ..	72
Table 3.5: Top predicted binding energies of various diazabicyclooctane β-lactamase inhibitors to BlaR1^{SD} and MecR1^{SD} (kcal/mol)	74
Table C1: Primers used for qRT-PCR	117

List of figures

Figure 1.1: An overview of some the main antibiotic resistance mechanisms in <i>S. aureus</i> . ..	2
Figure 1.2: The transpeptidase reaction in <i>S. aureus</i> . A)	6
Figure 1.3: A schematic of <i>S. aureus</i> PG synthesis starting with the reaction of uridine diphosphate- <i>N</i> -acetylglucosamine and phosphoenolpyruvate in the cytoplasm and terminating with the addition of nascent PG to the existing PG sacculus.	7
Figure 1.4: The β -lactam antibiotic mechanism of action.	8
Figure 1.5: Reaction scheme for the penicillin-binding protein transpeptidase reaction or the reaction with β -lactams.	10
Figure 1.6: The similarity of A) the D-Ala-D-Ala terminus of the PG stem peptide, B) the β -lactam core of the penicillin scaffold, and C) the diazabicyclooctane scaffold.	15
Figure 1.7 Mechanisms of β -lactam resistance in MRSA.	16
Figure 1.8: An overview of the <i>bla</i> and <i>mec</i> pathways in MRSA.	18
Figure 1.9: Amino acid sequence alignment of <i>Homo sapiens</i> ZMPSTE24 (UniProt ID: O75844), <i>Saccharomyces mikatae</i> Ste24p (UniProt ID: M4GGS2), <i>S. aureus</i> BlaR1 (UniProt ID: Q00419), <i>S. aureus</i> MecR1 (UniProt ID: P0A0B1).	20
Figure 2.1: PBP4 structure and protein sequence alignment of PBP4 and PBP4 ^{CRB} from <i>S. aureus</i>	30
Figure 2.2: <i>S. aureus</i> peptidoglycan monomer structure.	31
Figure 2.3: Separate structural alignments of A) PBP4 structures and B) PBP4 ^{CRB} structures.	37
Figure 2.4: PBP4 and PBP4 ^{CRB} active site residues in complex with ceftobiprole, ceftaroline, and nafcillin.	39
Figure 2.5: α alignment of PBP4 from <i>S. aureus</i> , PBP3 from <i>Streptococcus pneumoniae</i> (1xp4) and PBP5 from <i>E. coli</i> (3mze) shown in light brown, blue, and green respectively.	49
Figure 3.1: A schematic of the <i>bla</i> and <i>mec</i> divergons and their associated proteins.	56
Figure 3.2: Structure of intact and carbamylated avibactam.	58
Figure 3.3: Avibactam upregulates <i>blaZ</i> and <i>pbp2a</i> transcripts in <i>S. aureus</i> SF8300.	66
Figure 3.4: Thermal stabilization of the A) BlaR1 and B) MecR1 sensor domains with ampicillin, avibactam, nafcillin, and kanamycin.	67
Figure 3.5: Active site of BlaR1 ^{SD} and MecR1 ^{SD} in complex with avibactam.	70
Figure 3.6: Structural alignment of A) BlaR1 ^{SD} and MecR1 ^{SD} , B) BlaR1 ^{SD} and OXA-10, or C) MecR1 ^{SD} and OXA-10 showing residues surrounding the carbamylated avibactam in each structure.	81
Figure 3.7: BlaR1 ^{SD} and MecR1 ^{SD} active sites clefts with and without ligands.	83
Figure B1: The active site of PBP4 in grey cartoon representation with the catalytic serine (S75) and residues mutated in PBP4 ^{CRB} shown in stick form.	108

Figure B2: The active site of PBP4^{CRB} in grey cartoon representation with the catalytic serine (S75) and residues mutated in PBP4^{CRB} shown in stick form.....	109
Figure B3: A) PBP4 and B) PBP4^{CRB} interactions with ceftobiprole are shown using LigPlot+.....	110
Figure B4: A) PBP4 and B) PBP4^{CRB} interactions with ceftaroline are shown using LigPlot+.....	111
Figure B5: A) PBP4 and B) PBP4^{CRB} interactions with nafcillin are shown using LigPlot+.....	112
Figure B6: Cartoon representation of the aligned active site clefts of PBP4 (shown in green) and PBP4^{CRB} (shown in orange) in A) the ligand-free form and in complex with B) ceftobiprole, C) ceftaroline, and D) nafcillin (ligands not shown for clarity).	113
Figure B7: Plots of initial reaction velocity versus substrate concentration for PBP4 and PBP4^{CRB}.	114
Figure B8: PBP4 and PBP4^{CRB} active site clefts coloured according to B-factor value and depicted as surfaces with ligands shown as sticks.....	115
Figure B9: PBP4 and PBP4^{CRB} active site clefts coloured according to B-factor value and depicted as putty cartoons with ligands shown as sticks.	116
Figure C1: Volume mF_o-DF_c omit maps around avibactam modelled into the active sites of A) BlaR1^{SD} and B) MecR1^{SD}.	118
Figure C2: BlaR1^{SD} interactions with avibactam in conformation A are shown using LigPlot+.....	119
Figure C3: BlaR1^{SD} interactions with avibactam in conformation B are shown using LigPlot+.....	120
Figure C4: MecR1^{SD} interactions with avibactam are depicted using LigPlot+.....	121
Figure C5: The BlaR1^{SD} chains A and B are shown in green and purple cartoons, respectively.	122
Figure C6: SEC-MALS of A) BlaR1^{SD}, B) BlaR1^{SD} with 5 mM avibactam, and C) MecR1^{SD}.	123
Figure C7: Structural alignment of BlaR1^{SD} in complex with avibactam and a previously solved representative BlaR1^{SD} structure.....	124
Figure C8: Structural alignments of A) the BlaR1^{SD} avibactam structures and existing BlaR1^{SD} structures in the PDB (PDB IDs: 1nrf, 1xkz, 1xa1, 1xa7, 3uy6, 3q7v, 3q7z, 3q81, 3q82) and B) MecR1^{SD} avibactam existing MecR1^{SD} structures in the PDB (PDB IDs: 2iwb, 2iwc, 2iwd).	125
Figure C9: Docking poses calculated for avibactam and BlaR1^{SD} and MecR1^{SD}.	126
Figure C10: Structures of A) nacubactam, B) relebactam and their docking poses calculated for C) BlaR1^{SD} and D) MecR1^{SD}.	127
Figure C11: Molecular dynamics simulations of avibactam bound to BlaR1^{SD} and MecR1^{SD} in poses A and B in panels A-C as labelled.....	129

Figure C12: Electrostatic surface of the catalytic binding cleft of A) BlaR1^{SD} and B) MecR1^{SD} in complex with avibactam.	130
Figure C13: BlaR1 and MecR1 structures coloured according to B-factor value and depicted as putty cartoons	131

List of abbreviations

ANOVA	Analysis of variance
ASU	Asymmetric unit
ATP	Adenosine triphosphate
C-terminal	carboxy terminal
CA-MRSA	Community-associated methicillin-resistant <i>Staphylococcus aureus</i>
cDNA	Complementary DNA
Cryo-EM	Cryogenic electron microscopy
Ca	α -carbon
DNA	Deoxyribonucleic acid
DSLS	Differential static light scattering
FTIR	Fourier-transform Infrared spectroscopy
GlcNAc	<i>N</i> -acetylglucosamine
HA-MRSA	Hospital-associated methicillin-resistant <i>Staphylococcus aureus</i>
HPLC	High-performance liquid chromatography
IPTG	Isopropyl β -D-1-thiogalactopyranoside
k_{cat}	Catalytic constant
K_{d}	Dissociation constant
kDa	Kilodaltons
K_{M}	Michaelis constant
LA-MRSA	Livestock-associated methicillin-resistant <i>Staphylococcus aureus</i>
MD	Molecular dynamics
MES	Morpholineethanesulfonic acid
MIC	Minimum inhibitory concentration
MRSA	Methicillin-resistant <i>Staphylococcus aureus</i>
MSSA	Methicillin-sensitive <i>Staphylococcus aureus</i>
MurNAc	<i>N</i> -acetylmuramic acid
N-terminal	Amino terminal
NADPH	Nicotinamide adenine dinucleotide phosphate
NMR	Nuclear magnetic resonance
PBP	Penicillin-binding protein
PDB	Protein data bank
PEP	Phosphoenolpyruvate
PG	Peptidoglycan
psi	Pounds per square inch

qRT-PCR	Quantitative real-time polymerase chain reaction
RMSD	Root mean squared deviation
RNA	Ribonucleic acid
rpm	Revolutions per minute
SDS-PAGE	Sodium dodecyl sulfate polyacrylamide gel electrophoresis
SEC	Size-exclusion chromatography
SEC-MALS	Size-exclusion chromatography multiangle light scattering
SEDS	Shape, elongation, division, and sporulation
SMFM	Single-molecule force microscopy
Tagg	Temperature of aggregation
TEV	Tobacco etch virus
TP	Transpeptidase
UDP	Uridine diphosphate

Acknowledgements

My family has been instrumental in allowing me to dedicate so many years to my education. Thank you to my mother, Marcia Alexander, for her support which has allowed me to cultivate a love of learning and curiosity from an early age. Thanks to her I have always had someone to turn to, something for which I will be eternally grateful. I would also like to thank my uncle, Ralph Nelson, for his support and for taking the time to explain things to me from an early age. Your knowledge and willingness to explain things to be me as a child always left me with a desire and enthusiasm to better my understanding. My partner, Kelsey Huus, has been an inspiration and a source of support during the best and most difficult parts of my PhD. Thank you for your understanding and all our conversations.

I would like to thank my PhD supervisor, Professor Natalie Strynadka for taking a chance by taking me on as a PhD student despite my lack of a biochemistry undergraduate degree or any knowledge of structural biology or protein purification. I will always be grateful for her support and guidance as I have developed into a scientist. I am particularly appreciative of the time she has generously dedicated to discussing science and giving me guidance on my career, in addition to supporting me to attend workshops and conferences during my time in the lab. Put simply, she has created an inspiring place to live, work, and do science; thank you for these formative years of learning and discovery.

I would like to thank Professors Lindsay Eltis and Robert Hancock for their questions, advice and guidance throughout my time at UBC as part of my doctoral committee. I particularly appreciated the advice Dr Eltis imparted on kinetics. Additionally, my PhD research was much improved through collaborations with the labs of Professors Henry Chambers, Som Chatterjee,

Jean-Pierre Simorre, and Artem Cherkasov. I am indebted to them for the expertise and resources they freely provided.

I will always remember and appreciate the support, guidance, and mentorship of Professor Lucy Lee during my undergraduate degree. The opportunity to work in her lab helped steer me towards graduate school and her belief in me and consistent support were instrumental in making it happen.

Without the support of my lab mates my science and I would have suffered. Thank you to all the Strynadka lab members who have helped me; I hope I returned the favour. A particular thanks to Marija Vuckovic for her unlimited patience, help with cloning, and for keeping the lab working so well. Thanks to Dr Federico Rosell for his infectious mirth and for keeping me on my toes with conversation on all subjects. Thank you for time you devoted to my many questions, your help and advice with so many of my projects, and most of all for your camaraderie.

The community of Green College on the UBC campus was a constant source of emotional and physical nourishment during my time at UBC, without which everything would have been much more difficult. I would like to thank everyone in the Green College community who made the time during my PhD so incredible. Thank you to those who inspired, supported, challenged, agreed and disagreed with me; you have all taught me so much and immeasurably enriched my time at UBC.

I am most grateful for scholarship support from the Canadian Institutes of Health Research, the Natural Sciences and Engineering Research Council of Canada, and The Killam Trusts for their generous financial support during my graduate studies.

To family, friends, and the moments of discovery that make everything worthwhile.

Chapter 1: Introduction

1.1 *Staphylococcus aureus*

Staphylococcus aureus has been recognized as an important human pathogen since it was taken from a purulent leg wound and studied by Alexander Ogston in the 1870's (1–4). This Gram positive, coccoid bacterium is a common human commensal found in the nares of approximately 30% of individuals (5). Outside of its commensal habitat in the nasal passages and axillae, *S. aureus* is able to grow nearly everywhere in the body, where it is a primary cause of bacteraemia, skin and soft tissue infections, osteoarticular and device-associated infections as well as endocarditis (4, 6). Particularly troubling has been the rise of methicillin-resistant *S. aureus* (MRSA), a highly drug-resistant set of strains that have broad-spectrum resistance to many classes of antibiotics. The widespread presence of *S. aureus* and MRSA in the community has made it impossible to eradicate, making it essential that good treatment options are available, especially for immunocompromised individuals.

MRSA is resistant to many classes of antibiotics, including those of the β -lactam class targeting the cellular envelope, glycopeptides such as vancomycin also targeting the cell wall and cell membrane integrity, antibiotics targeting protein synthesis such as tetracycline, and antibiotics from the fluoroquinolone class of antibiotics that target DNA synthesis (Fig. 1.1) (7). While vancomycin has been a standard treatment for MRSA infections, newer lipopeptide antibiotics are now being recommended, such as daptomycin, a membrane disruptor and linezolid, a protein synthesis inhibitor (8). While vancomycin resistance, mediated by alteration of the terminal residue of the peptidoglycan (PG) stem peptide, remains relatively rare in MRSA, vancomycin can cause nephrotoxicity issues in patients and some MRSA strains have reduced susceptibility (8). The low incidence of vancomycin resistance, despite it being used to treat

<u>Resistance to antibiotics targeting cell-wall synthesis and cell membrane integrity</u>		
Peptidoglycan	Alternative penicillin binding protein <ul style="list-style-type: none"> • PBP2a (10) • Most β-lactam antibiotics 	Mutation of target <ul style="list-style-type: none"> • PBP4 mutations (11) • Selected β-lactam resistance
		Antibiotic modification <ul style="list-style-type: none"> • PC1 β-lactamase (9) • Penicillin resistance
	<u>Resistance to antibiotics targeting DNA synthesis</u>	<u>Resistance to antibiotics targeting protein synthesis</u>
Membrane		Alter membrane charge <ul style="list-style-type: none"> • MprF (13) • Daptomycin resistance
Cytosol	Efflux pumps <ul style="list-style-type: none"> • NorA/NorB/NorC (19) • Fluorquinolone resistance 	Alter lipid II structure <ul style="list-style-type: none"> • Proteins encoded by the <i>van</i> operons (some proteins are extracellular others are intracellular) (12) • Vancomycin and teicoplanin resistance
	Mutation of target <ul style="list-style-type: none"> • Topoisomerase mutations (19) • Fluorquinolone resistance 	Antibiotic modification <ul style="list-style-type: none"> • Acetyltransferase-phosphotransferase (<i>aacA-aphD</i>) (7,16) • Neomycin and gentamicin resistance • Phosphotransferase (<i>aphA</i>) or adenylyltransferase (<i>aaaD</i>) (7,16) • Neomycin resistance
	Ribosomal protection <ul style="list-style-type: none"> • TetO/M (15) • Tetracycline resistance 	Mutation of target <ul style="list-style-type: none"> • Ribosomal mutations (18) • Linezolid resistance
	Target modification <ul style="list-style-type: none"> • Modification of ribosome by Cfr (17) • Linezolid, chloramphenicol resistance 	

Figure 1.1: An overview of some the main antibiotic resistance mechanisms in *S. aureus*. References are indicated in the figure.

MRSA infections for more than 50 years, is attributed to the increased susceptibility to β -lactam antibiotics and slower growth rates of vancomycin resistant MRSA strains (7). Recently, the lipopeptides oritavancin and telavancin, which inhibit synthesis of the PG sacculus as well increasing the permeability of bacterial membranes (20, 21), have been approved for use in patients (7). Additionally, the late generation cephalosporin antibiotics, ceftaroline and

ceftobiprole, have been approved to treat MRSA infections (4). While a range of treatment options for MRSA do exist for some strains, evolving and rising antibiotic resistance to these compounds makes it prudent to have many different treatment options available (4, 22). While β -lactams are typically well tolerated by patients, they are currently almost all impotent against MRSA due to resistance. Improvements in patient safety could be made if β -lactam antibiotics were re-potentiated, preventing the need to prescribe antibiotics with increased side-effects. Thus, there is a need to develop new antibiotics that pathogens such as MRSA are sensitive to and that are well tolerated by patients.

Since the initial discovery of penicillin-resistant *S. aureus* in 1942 (23) and methicillin-resistant strains in 1961 (24), understanding and combating antibiotic resistance in *S. aureus* has been a priority public health initiative. While MRSA infections were initially mostly found in nosocomial environments, this started to change in the 1990s, with the rise of community-associated MRSA (CA-MRSA) (4). CA-MRSA prevalence continued to rise through the '90s and '00s before plateauing and even declining in some regions (25). However, surveys show MRSA remains common in both community and healthcare associated environments throughout the world (26). Livestock-associated MRSA (LA-MRSA) is also widespread, further increasing the burden of disease to agriculture and agricultural communities (4). There is considerable variation in the proportion of *S. aureus* infections caused by MRSA (from <1% of infections in some northern European countries to more than 50% in countries such as Portugal), (26, 27). Given the threat to public health, new ways to treat MRSA β -lactam resistance are urgently needed.

MRSA infections have been shown in several studies to have a significantly higher mortality rate compared to methicillin sensitive *S. aureus* strains (28). Even with the advances of

modern-day healthcare, in 2017 there were approximately 120,000 cases of *S. aureus* bloodstream infections and 20,000 associated deaths in the US alone (29). Furthermore, despite considerable effort and several clinical trials, no vaccine has been approved to prevent *S. aureus* infection, making it all the more essential that a broad range of treatment options exist (4, 30). Again, even with modern healthcare, *S. aureus* bloodstream infections have unacceptable mortality rates as high as 50% in some populations (28). The significant mortality and morbidity associated with MRSA is caused by a combination of its formidable array of virulence factors and its resistance to a wide range of antibiotic classes (4). This deadly combination of traits has earned MRSA a “high priority” listing on the recent World Health Organisation’s list of pathogens for which treatments are most urgently needed (31).

This thesis focuses on improving the understanding of MRSA resistance to the β -lactam class of antibiotics. The introductory chapter will begin by introducing synthesis of the PG cell wall in *S. aureus* with a focus on the terminal transpeptidation step, the target of β -lactam antibiotics. Following sections will review resistance mechanisms by which MRSA evades the action of β -lactam antibiotics.

1.2 *S. aureus* peptidoglycan

PG forms the main scaffold of the bacterial cell wall and is nearly ubiquitous in bacteria. In *S. aureus*, PG forms a continuous layer 20-40 nm thick around the bacterial cell and plays a pivotal role in determining their morphology, survival, and virulence, in addition to influencing the immune system of the host (32–34). It is essential PG surrounds the bacterial cell as a continuous net to counteract the effects of turgor pressure against the bacterial membrane. The PG sacculus consists of glycan strands made up of alternating, β -1-4 linked, *N*-acetylglucosamine (GlcNAc) and *N*-acetylmuramic acid (MurNAc) subunits that are crosslinked

with stem peptides bound to the MurNAc D-lactoyl moiety as shown in figure 1.2 (33). In *S. aureus* PG stem peptides consist of the penta-peptide L-Ala- γ -D-Glu-L-Lys-D-Ala-D-Ala with a penta-glycine chain bound to the ζ -nitrogen of the L-Lys in the stem peptide (Fig. 1.2A) (35).

1.2.1 *S. aureus* peptidoglycan synthesis

PG precursors are synthesized in the cytosol by the Mur-ligase enzymes to eventually form uridine diphosphate (UDP) MurNAc pentapeptide (33, 36). An overview of PG synthesis in *S. aureus* is shown in figure 1.3. The membrane-embedded enzyme MraY then transfers the UDP-MurNAc pentapeptide to a C55-P lipid carrier, forming a lipid linked oligosaccharide known as Lipid I that is embedded in the inner leaflet of the cell membrane (37, 38). The transglycosylase MurG, another polytopic membrane protein, then catalyses a β -1-4 linkage between Lipid I and UDP-GlcNAc to form Lipid II, the lipid anchored monomer of PG (39). In *S. aureus* the membrane-linked FemXAB peptidyl transferases catalyse the addition of five glycine residues to the ζ -N of the L-lysine in the stem peptide (40) before the completed Lipid II molecule is flipped to the outer leaflet of the cell membrane by MurJ for polymerization into the existing PG sacculus (41, 42). In *S. aureus*, the bifunctional penicillin-binding protein (PBP), PBP2, some dedicated monofunctional enzymes such as MGT, and RodA and FtsW (both members of the shape, elongation, division, and sporulation (SEDS) protein family) have glycopolymerase activity which catalyse the formation of β -1,4 bonds between the C1 carbon of the growing chain (donor strand) and the hydroxyl bound to the C4 carbon of lipid II (acceptor strand) (39, 43–45). Following polymerisation, the glycan chains must be crosslinked into the PG sacculus to ensure a reinforced net of PG surrounds the entire bacterium, protecting it from the environment and cellular turgor pressure (46). The transpeptidase (TP) domain of PBPs catalyse this peptide crosslinking reaction. In *S. aureus*, peptide crosslinking involves the formation of a

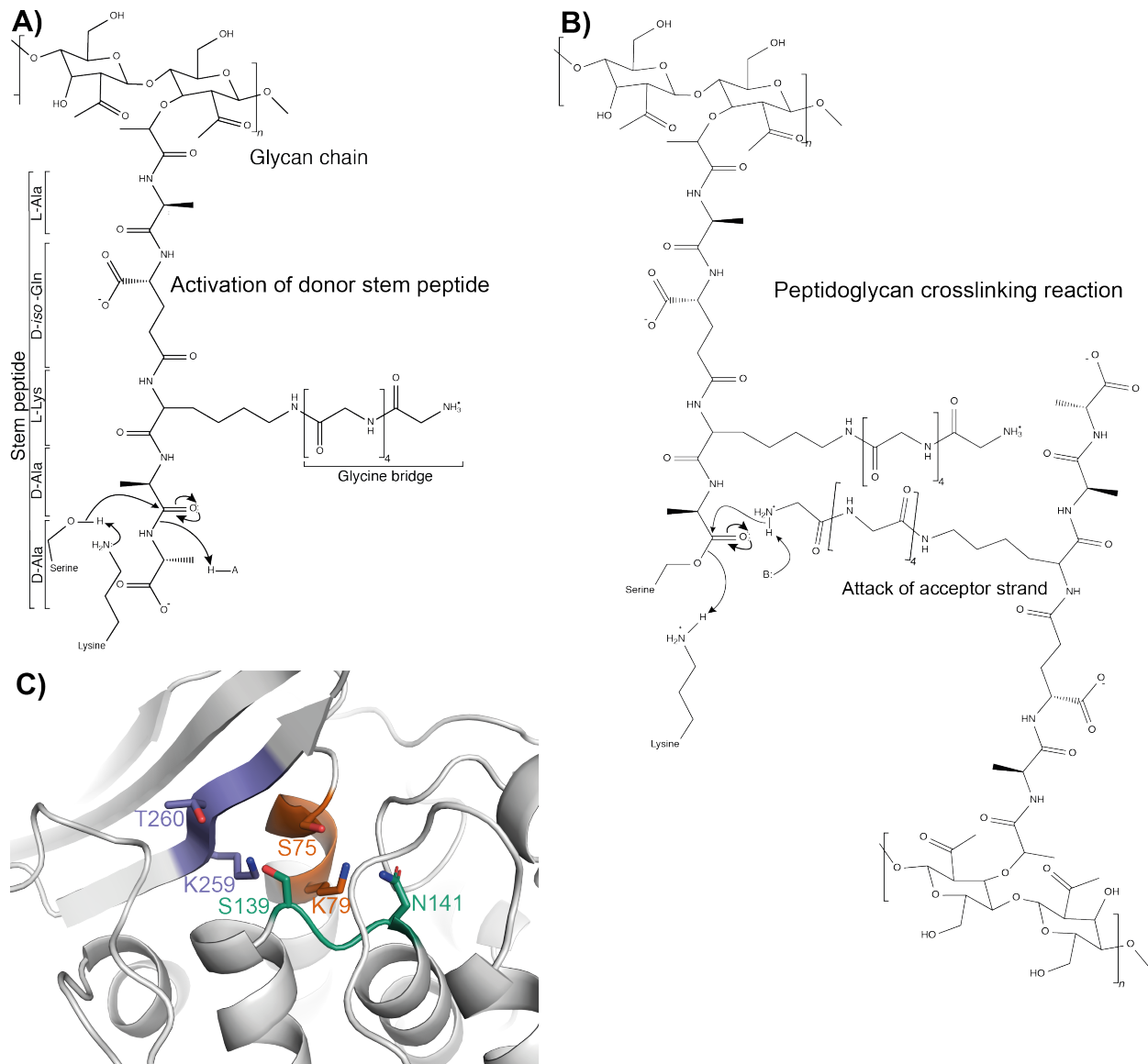


Figure 1.2: The transpeptidase reaction in *S. aureus*. A) The PG monomer in *S. aureus* is shown during activation of a donor strand by residues of the SXXK motif. B) Crosslinking of the acceptor strand and the acyl enzyme donor strand complex. C) View of the transpeptidase active site of PBP4 (PDB ID 6c39) from *S. aureus* shown in cartoon with residues from the three key PBP catalytic motifs shown as sticks. The SXXK motif residues are shown in orange, the SXN motif residues are shown in green, and the KTG motif residues are shown in purple.

peptide link between the terminal glycine of the pentaglycine chain, bound to the third amino acid of the acceptor stem peptide, and the fourth amino acid of the donor stem peptide, creating 3,4 crosslinked PG (Fig. 1.2B) (33). This last step in PG synthesis has long been the subject of

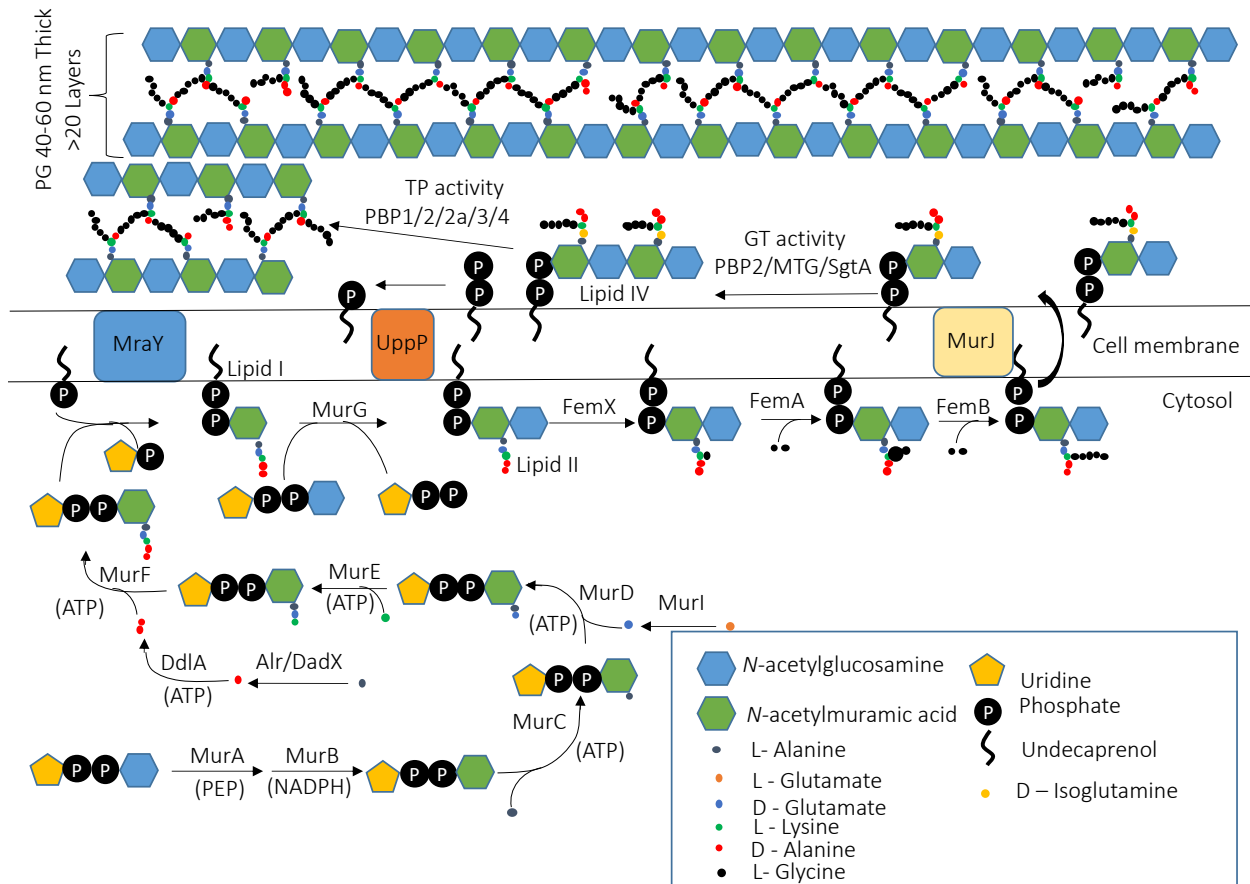


Figure 1.3: A schematic of *S. aureus* PG synthesis starting with the reaction of uridine diphosphate-*N*-acetylglucosamine and phosphoenolpyruvate in the cytoplasm and terminating with the addition of nascent PG to the existing PG sacculus. Phosphoenolpyruvate, adenosine triphosphate, and nicotinamide adenine dinucleotide phosphate are abbreviated as PEP, ATP, and NADPH respectively.

particular research interest as β -lactam antibiotics inhibit the PBPs catalysing this reaction (Fig. 1.4) (47).

PG synthesis is a highly dynamic process that is temporally and spatially regulated by protein complexes, allowing cell shape and integrity to be maintained (48). Two main protein complexes involved in PG synthesis, termed the divisome and the elongasome, are respectively responsible for coordinating cell division and elongation (49). In *E. coli*, the best characterised divisome system, it is thought there are over 30 components (50). In *S. aureus* these complexes are less well characterised, but both complexes typically contain at least a PBP, a SEDS protein,

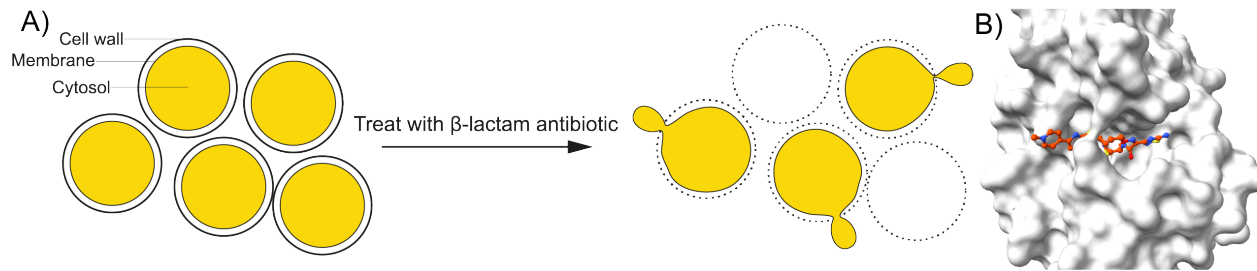


Figure 1.4: The β -lactam antibiotic mechanism of action. A) Cells that are sensitive to treatment with β -lactam lose the ability to build and maintain the peptidoglycan scaffold of the bacterial cell wall, leading to cell lysis. The β -lactam class of antibiotics inhibit catalysis of the peptidoglycan transpeptidase reaction through their action as essentially irreversible substrate analog inhibitors of the penicillin-binding proteins. B) Here the β -lactam, ceftaroline is shown in orange sticks, covalently bound state to the active site serine of PBP4 (PDB ID: 5tw8) from *S. aureus*.

and the scaffolding protein FtsZ (48). While *S. aureus* cells appear close to spherical, super-resolution microscopy experiments have shown the cells are elliptical (51). Despite the fact that *S. aureus* cells do elongate, they lack MreB, the scaffolding protein found in rod shaped bacteria and are thought to use FtsZ as a scaffold in both the elongasome and the divisome (52). A detailed understanding of how these proteins interact and regulate PG synthesis still remains to be understood in many instances. Structural characterisation of these complexes using X-ray crystallography has been frustrated by their often-transient, dynamic nature (50). Several factors are likely needed to stabilise these complexes, possibly including PG substrates, making it a challenge to find suitable conditions for analysis. Cryogenic electron microscopy (cryo-EM), possibly combined with crosslinking using the GraFix method (53), might allow insight into these fundamental bacterial processes.

PG recycling, where PG subunits are degraded and transported back into the cell to be used in the generation of new PG, was initially discovered in Gram negative bacteria (54). However, it has since been found to play an important role in providing precursors for the synthesis of nascent PG in *S. aureus* (55). *S. aureus* increases PG recycling during the transition from exponential to stationary phase. PG recycling does not sustain growth in *S. aureus*, but

rather serves to extend viability during nutrient limitation. Briefly, the PG autolysin, Atl cleaves assembled PG to produce free MurNAc-GlcNAc disaccharide (56). This disaccharide is then phosphorylated and transported back into the cytosol by MurP, a phosphotransferase system transporter (57). The 6-phospho-*N*-acetylmuramidase, MupG then cleaves the imported disaccharide and the etherase MurQ converts 6-phospho-MurNAc to 6-phospho-GlcNAc which is then eventually fed back into the Mur ligase pathway (56). While it appears PG recycling plays a smaller role in providing the materials for the construction of new PG in Gram positive bacteria compared to Gram negative species, this pathway could help Gram positive bacteria such as MRSA to maintain the cell wall in times of nutrient deprivation (55).

1.2.1.1 *S. aureus* penicillin-binding proteins

PBPs are anchored to the outer leaflet of the cytosolic membrane by a transmembrane domain and are traditionally classified into three broad categories based on their size and function. All PBPs have three catalytic sequence and structural motifs that facilitate transpeptidation: *SXXK*, *(S/Y)X(N/C)*, and *(K/H)(S/T)G* (Fig. 1.2C) (33). The TP reaction consists of two acylation steps catalysed by two serine-lysine catalytic dyads (33). The *SXXK* motif contains the serine nucleophile that is acylated by the donor stem peptide, or by β -lactam antibiotics if present. The lysine ζ -N of this *SXXK* motif serves as the general base to activate the serine hydroxyl of the same motif by extracting its proton and therefore increasing its nucleophilicity (33). The activated serine then attacks the electrophilic carbonyl carbon of the penultimate D-Ala residue in the donor PG stem peptide to form, via an oxyanion tetrahedral transition state, an acyl-enzyme intermediate with the associated loss of the terminal D-Ala residue (47). An oxyanion hole comprised of two main chain nitrogen atoms polarizes the substrate carbonyl, increasing electrophilicity and subsequently providing stabilization for the

oxyanion transition state. The SXN motif is thought to be involved in the acylation step with transfer of the proton from the SXXK motif lysine to the D-Ala peptide leaving group nitrogen, facilitating bond cleavage (58). The amino group of the terminal glycine of the acceptor stem peptide is then activated via abstraction of its proton by either the ζ -N lysine of the KTG motif directly or by the serine hydroxyl of the SXN motif after it has been activated by the ζ -N lysine of the KTG motif (58). The TP transfer reaction is then completed when the activated glycine amino nucleophile attacks the donor stem peptide at the carbonyl carbon of the covalent acyl-enzyme intermediate of the donor peptide and PBP, leading to the formation of a second oxyanion tetrahedral intermediate and subsequent regeneration of the enzyme.

PBPs catalyse TP reactions in a three-step process where the enzyme, denoted here as E , first forms a non-covalent interaction with S , the substrate or inhibitor in the case of PBP reaction with a β -lactam, to form the Michaelis complex, ES (Fig. 1.5) (59). This non-covalent complex can either disassociate or react to form an acyl-enzyme substrate/inhibitor complex shown here as ES^* . Finally, deacylation regenerates the enzyme and releases the product. Typically, the product is a crosslinked stem peptide if the native substrate is being processed or a hydrolysed inhibitor if a β -lactam antibiotic is being processed. Additionally, some low molecular weight PBPs catalyse a carboxypeptidase reaction where acylation of the donor stem peptide occurs as with transpeptidation, but instead of an acceptor peptide, water takes the role of

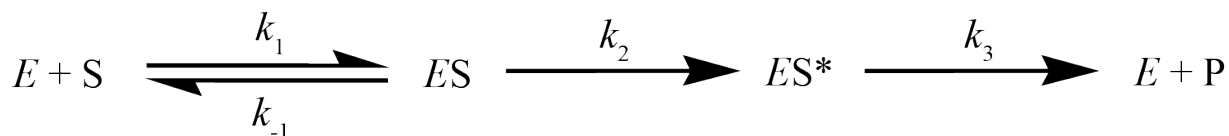


Figure 1.5: Reaction scheme for the penicillin-binding protein transpeptidase reaction or the reaction with β -lactams. E represents the enzyme, S the substrate or β -lactam, ES the Michaelis complex, ES^* the acyl-enzyme complex, and P the cross-linked stem peptide or hydrolysed β -lactam. The enzyme acylation rate follows a second order rate constant, k_2/K' where $K' = (k_{-1} + k_2)/k_1$. The rate of enzyme deacylation is characterised by the first order rate constant, k_3 . The equations for steady-state condition are defined as: the catalytic constant, $k_{cat} = k_2k_3/(k_2 + k_3)$ and the Michaelis constant, $K_M = k_3K'/(k_2 + k_3)$ (59).

the acceptor peptide (60). The β -lactam class of antibiotics are effective inhibitors as they function as de facto irreversible inhibitors within the timeframe of bacterial generation times due to a slow, rate-limiting deacylation step (61). In contrast, the rate limiting step of PBP mediated transpeptidation of stem peptides is acylation (59).

While this terminal step in PG synthesis has been thoroughly studied in the context of its inhibition by β -lactam antibiotics, from a structural perspective relatively little is known regarding the processing of the natural PG substrate. Since β -lactam antibiotics bind the donor site, the location of this site is well known from structures with β -lactam antibiotics, but the acceptor site location remains to be elucidated (62–64). Complexes of PBP and substrate have largely been recalcitrant to characterisation by x-ray crystallography, presumably due to the dynamic nature of their relatively weak association (65, 66). Furthermore, the challenge of obtaining a defined substrate suitable for analysis by x-ray crystallography due to the inherent heterogeneity of the PG polymer further complicates obtaining good occupancy of the substrate in the crystal structure. While efforts have been made to map the acceptor site of *S. aureus* PBP4 using NMR, there are still ambiguities over its location (65). Others have used synthetic peptide mimetics to probe PG binding to PBPs; while these have made important contributions to our understanding of catalysis of the natural substrate in the donor site, the acceptor site remains an enigma (60, 67, 68). The fact that we still lack structural and kinetic details of the TP reaction, despite the importance of β -lactam antibiotics in treating disease, is a testament to the challenging nature of research advances in this area. Recent progress with higher resolution analysis of proteins with cryo-EM may provide an avenue for exploration of substrate-PBP interactions with of the larger PBPs (69).

The PBPs of *S. aureus* are numbered according to size with the highest molecular weight PBP being PBP1, following longstanding tradition in the literature. The bifunctional class-A PBPs have both glycopolymerase and TP activity while the class-B PBPs act only as transpeptidases (70). The class-C PBPs are a lower molecular weight compared to classes A and B and typically act as carboxypeptidases, which serve to limit cell wall crosslinking as their preferred acceptor substrate is water instead of the acceptor stem peptide (70). However, in *S. aureus* the singular predicted class-C PBP4 acts primarily as a TP (71). Many bacterial species including the model Gram-negative, *Escherichia coli* and Gram-positive *Bacillus subtilis*, have more than 10 PBPs each with multiple functional, often redundant roles (58). As *S. aureus* only has four PBPs, with MRSA having a fifth PBP termed PBP2a (72, 73), it provides a simplified system to study the activity and regulation of PBPs, facilitating improved understanding of PG synthesis both in *S. aureus* and other organisms.

S. aureus PBP1 is an essential class-B PBP involved in cell division that interestingly appears to have little role in influencing PG crosslinking composition (73–75). Instead, PBP1 is hypothesized to have essential roles in coordinating cell division as a key member of the divisome complex and interacting with the glycopolymerase, FtsW (44, 52). Only PBP1 and PBP2, the latter a class-A bifunctional PBP (73), are essential for *S. aureus* viability *in vitro* (73). However, *S. aureus* strains with *pbp3* and *pbp4* deleted and only PBP1 and PBP2 present, show severe deficiencies in antibiotic resistance and virulence in the *Drosophila* infection model (73). While *S. aureus* PBP2 has been proposed to interact with PBP2a or PBP4 to allow for efficient glycopolymerase and TP activity, conclusive evidence of this interaction is lacking (76).

PBP2a is a class-B PBP present in MRSA strains with a single pass N-terminal transmembrane anchor, a TP domain, and a second domain of unknown function (62). PBP2a is

only essential in the presence of β -lactam antibiotics, and the gene encoding PBP2a is thought to have originated in the related organism, *Staphylococcus sciuri* (72, 77). X-ray crystallography has shown that the active site of PBP2a is protected from attack by β -lactams due to it being at the end of a deep cavity (78). This active site cavity opens when PG binds to its allosteric site approximately 60 Å away, but is otherwise normally closed (78). Ceftaroline, a late generation cephalosporin specifically developed to treat MRSA infections, inhibits PBP2a by first binding to its allosteric site which causes the active site to become exposed, allowing a second ceftaroline molecule to acylate the catalytic serine and preventing further transpeptidation reactions (78, 79). While the presence of PBP2a allows MRSA broad-spectrum resistance to nearly all β -lactams, there are notable exceptions including ceftobiprole and ceftaroline in most strains (80).

PBP3 is a non-essential class-B PBP composed of an N-terminal domain of unknown function and a poorly characterized C-terminal TP domain (81). Its precise role in PG synthesis remains unknown, but when *S. aureus* lacking functional PBP3 was grown in the presence of sub-MIC levels of methicillin, cell morphology was affected while wild type cells at the same concentration were unaffected (82). This non-functional PBP3 is a deletion mutant that only codes for 98 of 691 amino acids and does not bind radioactively labelled penicillin (82). Inactivation of *pbp3* does not appear to alter PG composition in *S. aureus*, nor does it appear to affect growth rates (82). However, PBP3 has recently been found to associate with RodA to form part of the *S. aureus* elongasome complex, which maintains the slightly ellipsoid shape of *S. aureus* cells (52).

PBP4 is a low molecular weight non-essential Class-C PBP with TP activity that is thought to provide additional crosslinking of existing PG as well as nascent PG (71). *S. aureus* cell morphology appears normal in the absence of PBP4 but PG crosslinking and virulence are

both reduced in *pbp4* knockouts (83). While β -lactam resistance in some strains of CA-MRSA have been found to be dependent on the presence of PBP4 (83), the presence of PBP4 has been found to have less effect on β -lactam resistance in the hospital-associated MRSA (HA-MRSA) strain, COL (84). In *pbp4* knockout strains of *S. aureus*, highly crosslinked PG (defined as more than 17 muropeptides as determined by reverse phase HPLC) is absent (85) and the PG sacculus is less stiff (86). Remarkably, despite these changes to the molecular structure of PG in the absence of PBP4, the PG sacculus morphology is largely maintained as in wild-type; however, the ordered ring of PG strands following cell division is denser in cells lacking *pbp4* (87). Structurally, PBP4 has the greatest structural similarity with carboxypeptidases rather than transpeptidases; however, *in vivo* and *in vitro* studies have shown that transpeptidation is clearly the dominant reaction (71). How TP activity is favoured in *S. aureus* PBP4 despite structural similarity (RMSD between PBP4, PDB ID: 6c39, and PBP5, PDB ID: 3mze, is 6.98 Å over 299 residues) to the carboxypeptidase PBP5 from *E. coli* is unknown.

1.3 Inhibition of peptidoglycan synthesis: β -lactam antibiotics

Following the serendipitous initial discovery that *Penicillium* mould can inhibit the growth of *S. aureus* by Sir Alexander Fleming in the 1920's (88) and the subsequent isolation and purification of penicillin, there has been much interest in developing the β -lactam scaffold for therapeutic purposes. This has led to the discovery and creation of several classes of β -lactam antibiotics, a collection of nearly miraculous drugs that have saved untold numbers of patients, have a generally favourable safety profile, and are the most prescribed class of antibiotics globally (89, 90).

β -lactam antibiotics work to inhibit the final transpeptidase step, discussed above, in the assembly of the bacterial cell wall peptidoglycan polymer (91). As initially suggested by Tipper

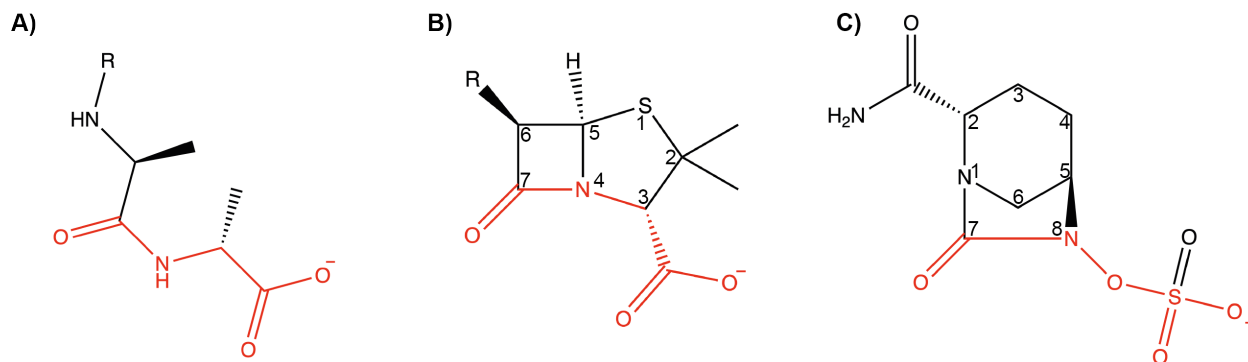


Figure 1.6: The similarity of A) the D-Ala-D-Ala terminus of the PG stem peptide, B) the β -lactam core of the penicillin scaffold, and C) the diazabicyclooctane scaffold. Atoms in similar key positions for binding to the TP domain of PBPs are shown in red.

and Strominger, β -lactam rings are substrate mimetics of the terminal D-Ala-D-Ala moiety of the PG stem peptide (Fig. 1.6) (91). More recently the diazabicyclooctane scaffold has also been found to be of sufficient similarity to inhibit PBPs (92) (Fig. 1.6). As PG is unique to bacteria, is partially synthesised on the extracellular face of the bacterial membrane, and is essential for bacterial growth in most environments, enzymes involved in the final stages of PG synthesis are excellent drug targets. In the case of β -lactam acylation, the activated serine nucleophile of the SXXK motif attacks the α -carbon of the β -lactam ring, causing ring opening. As discussed earlier in this chapter, in β -lactam-sensitive PBPs the slow deacylation rate of the β -lactam bound to the donor site effectively prevents further TP activity. TP reaction inhibition was initially thought to cause cell lysis due to a lack of balance between crosslinking and hydrolytic cell wall enzyme activities (93, 94). More recently it has been shown that β -lactams additionally cause a cascade of dysregulation including the depletion of lipid-linked PG precursors (95) and a futile cycle of cell wall anabolism and catabolism due to the disruption of the normally coupled glycopolymerase and TP activity, leading to the eventual exhaustion of resources and rupture of the cell wall (96).

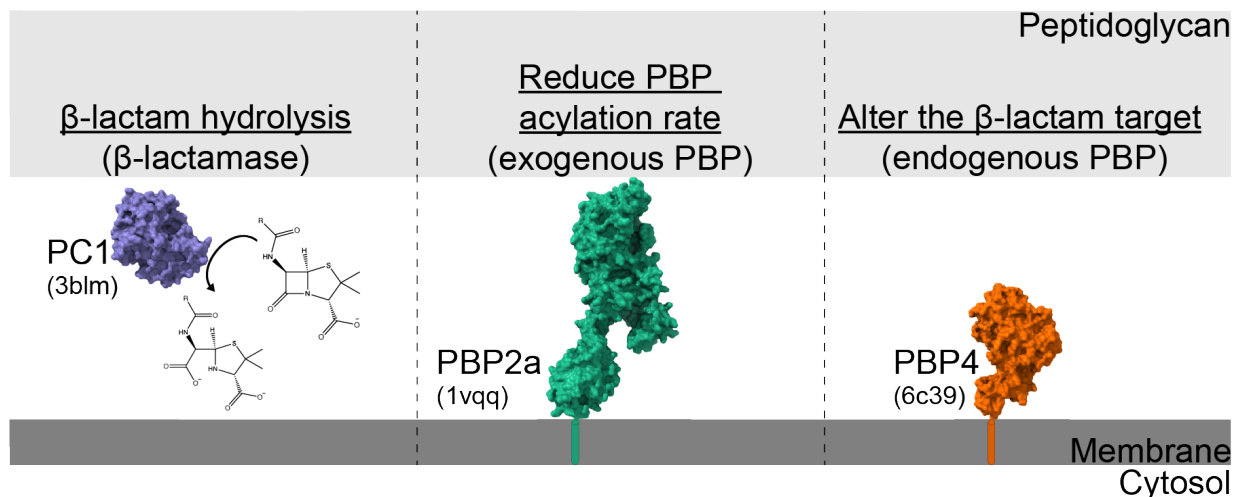


Figure 1.7 Mechanisms of β -lactam resistance in MRSA. PC1 levels are controlled by the *bla* divergon while the *mec* divergon controls levels of PBP2a. PBP4 can mediate β -lactam resistance through mutations or by increasing the amount present. The PDB codes for the x-ray crystal structures of PC1, PBP2a, and PBP4 are shown in brackets (11, 62, 97).

1.4 β -lactam resistance in *Staphylococcus aureus*

Ever since the first penicillin-resistant strains of *S. aureus* were detected in the 1940's it has demonstrated its ability to adapt to antimicrobial treatment (23). *S. aureus* employs three modes of β -lactam resistance: expression of β -lactamase, expression of PBPs that have poor sensitivity to inhibition by β -lactams, and resistance related to overexpression and mutation of PBP4 (Fig. 1.7). Initial resistance was due to the expression of the Class-A serine β -lactamase, PC1 (72), a highly efficient enzyme which hydrolyses the β -lactam bond to create now disarmed acid products. Research into making penicillin-based compounds resistant to destruction by β -lactamases led to the first wave of synthetic β -lactam drugs. Since the introduction of β -lactamase resistant β -lactams such as methicillin and later nafcillin, PC1 represents a decreased risk to public health. However, recently PC1 has been found to mediate borderline oxacillin resistance (98).

In 1959, methicillin, a β -lactamase resistant version of penicillin, was introduced to treat benzylpenicillin-resistant *S. aureus* infections; however, the respite from resistance was brief

(99). In 1961, in Colindale, UK the first strains of methicillin resistant *S. aureus* were recorded (24). This intrinsically resistant (i.e. the β -lactam was not being degraded as observed with PC1 mediated resistance) *S. aureus* strain was eventually found to have an extra PBP termed penicillin-binding protein 2a (PBP2a) that was responsible for the considerably broadened repertoire of resistance (100). As discussed above, the slow acylation rate and sterically hindered transpeptidase active site of PBP2a allow its TP activity to be resistant to most β -lactam antibiotics, enabling it to continue to crosslink PG stem peptides even in the presence of β -lactam antibiotics (62). The PBP2a and more recently, other proteins such as PBP4 have made treating *S. aureus* infections a moving target.

1.4.1 Conventional *S. aureus* β -lactam antibiotic resistance mediated by the bla and mec divergons

Conventional β -lactam resistance in *S. aureus* is regulated by two related divergons termed bla and mec as shown in figure 1.8. Here the focus will be on these two divergons from MRSA but there are also closely related divergons in *Bacillus licheniformis* (101) and *Clostridium botulinum* (102). The bla divergon is responsible for regulating the expression of *blaZ* which codes for PC1 and also *pbp2a* in the absence of a functional mec divergon (103). There are three key genes in both the bla and mec divergons. The bla divergon has the β -lactam sensing/activating integral membrane zinc metalloprotease, BlaR1; the transcriptional repressor, BlaI; and the β -lactamase, PC1 (104). PC1 is a class-A serine β -lactamase that is able to hydrolyse the penicillin class of β -lactams (9). The mec divergon is similarly structured with the respective proteins coded by the mec divergon termed MecR1, MecI, and the aforementioned PBP, PBP2a. The *blaR1/mecR1* and *blaI/mecI* genes are on one side of the operator while

blaZ/pbp2a are transcribed in the opposite direction on the other side of the operator sequence (105).

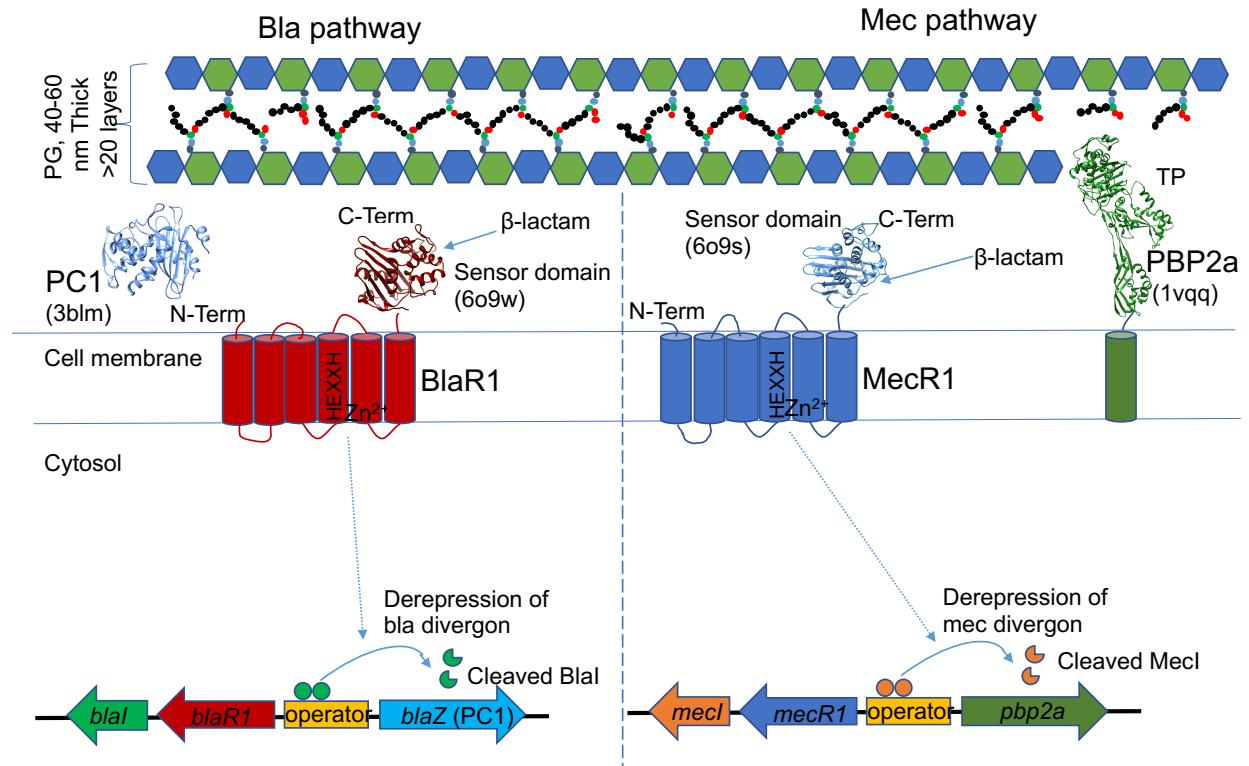


Figure 1.8: An overview of the *bla* and *mec* pathways in MRSA. Acylation of the BlaR1/MecR1 sensor domains by a β -lactam is thought to initiate *bla* pathway expression via activation of the BlaR1 zinc metalloprotease domain. The activated zinc metalloprotease domain is then hypothesised to cause cleavage of the *bla* divergon repressor, BlaI/MecI, lowering its affinity for the operator sequence. It is unclear how many other proteins are involved in derepression. Once the repressor has been removed from the operator sequence expression of the divergon, including *blaZ*, the gene coding for the β -lactamase PC1 can occur. The PDB codes for PC1 (97), BlaR1 sensor domain (this thesis), MecR1 sensor domain (this thesis), and PBP2a (62) are shown in cartoon representation.

BlaI and MecI are well-characterised, soluble, ~ 14 kDa, DNA-binding repressor proteins that prevent transcription of the *bla* and *mec* divergences when bound to the operator region. Both have two domains; an N-terminal DNA binding domain and a C-terminal dimerization domain (106, 107). Full-length BlaI and MecI each form dimers (BlaI dimer $K_d = 1.61 \mu\text{M}$ as measured by sedimentation equilibrium experiments) with approximately 2-fold symmetry (106–108). The DNA binding domain of BlaI alone has been found to have significantly reduced affinity for the palindromic operator DNA sequences compared to the full-length dimeric species (106).

BlaI/MecI oligomerization, and therefore the amount bound to operator DNA, can be tuned via cleavage between residues Asn-101 and Phe-102 (104). The cleavage of BlaI/MecI therefore serves to allow transcription of the divergon and the expression of antibiotic resistance genes in MRSA.

The discovery of *blaR1* and *mecR1* and their essential role in the regulation of β -lactam resistance in *S. aureus* in the 1980's and 1990's facilitated future research on these important pathways (109, 110). However, despite the importance of both BlaR1 and MecR1 in combating MRSA, a clear picture of their mechanism of action has remained largely elusive due to their extremely poor expression, autocleavage, and instability (111, 112). Both BlaR1 and MecR1 are composed of two domains, an N-terminal integral membrane zinc metalloprotease domain and a cytosolic C-terminal β -lactam sensing/binding domain.

While full-length constructs of BlaR1 and MecR1 have been recalcitrant to structural characterisation, some progress has been made by examining their N-terminal domain membrane topology with experimental and *in silico* methods. Initial attempts at the characterisation of the topology of BlaR1 from *Bacillus licheniformis* was made by Hardt and colleagues using the *E. coli* TEM- β -lactamase fusion method where a β -lactamase is fused to different length truncations of the protein and β -lactamase activity is assayed with intact cells to determine if the β -lactamase is facing the cytosol or outside the cell (113). These experiments suggested the transmembrane domain was composed of a four helix bundle (113). However, more recent analysis of MecR1 from *S. aureus* using *in silico* modelling with GFP truncation experiments has updated the predicated number of transmembrane helices to six for MecR1 and it is presumed for BlaR1 as well given their ~35% sequence identity and similar function (Fig. 1.9) (111). Based on *in silico* homology modelling, the sensor domain of BlaR1 and MecR1 is predicted to cap an α -helical

hydrophilic aqueous barrel that penetrates the membrane (111). The closest homologs of BlaR1 with solved structures are the zinc metalloproteases ZMPSTE24 from *Homo sapiens* (117) and Ste24p from *Saccharomyces mikatae* (118). The cytoplasmic side of the aqueous barrel is bordered by the zinc metalloprotease domain which is partially embedded into the membrane similar to the experimental structure of the human zinc metalloprotease ZMPSTE24 (117) which the model was based on (111).

The sensor domains of BlaR1 and MecR1 (BlaR1^{SD} and MecR1^{SD}) are structurally homologous to the class-D β -lactamases (e.g. OXA-10 and OXA-48) with a common SXXK motif and have been shown to covalently bind β -lactams and, as shown in chapter 3, the diazabicyclooctane avibactam (119, 120). It is thought the sensor domain of BlaR1/MecR1 is acylated by antibiotics in the environment which then elicits a conformational change and subsequent activation of the zinc metalloprotease domain (104). As neither sensor domain expressed alone significantly changes in conformation upon acylation with β -lactam antibiotics, as determined by high resolution x-ray crystallographic analysis of the two states, it remains unclear how the signal of acylation is relayed to the zinc metalloprotease domain on the other side of the membrane (119, 120). However, circular dichroism spectroscopy and Fourier-transform Infrared (FTIR) spectroscopy of the sensor domain do show some variation in secondary structure upon acylation with β -lactams in solution (121, 122). FTIR results suggest BlaR1 forms a more ordered, less dynamic sensor domain structure (121). Additionally, there is some evidence based on phage display, that the sensor domain of BlaR1 from *B. licheniformis* associates with a cytosolic loop of the N-terminal zinc metalloprotease domain in its ligand-free state but is released upon its acylation with a β -lactam antibiotic (123). According to this hypothesis by Hanique et al., when the sensor domain is no longer associated with the loop, the

zinc metalloprotease domain is activated (123). Later studies with NMR found evidence that a synthetic peptide composed of BlaR1 residues 73-105 binds to the BlaR1^{SD} with low mM affinity (124). However, the same study found little difference in binding affinity between this loop and ligand-free BlaR1^{SD} or β -lactam bound BlaR1^{SD}, casting doubt on this interaction being important for regulation of the BlaR1 zinc metalloprotease domain (124). Further NMR experimentation has identified residues Ile-531 to Lys-535 in the sensor domain as interacting with this cytoplasmic loop of the N-terminal domain; it is proposed sensor domain acylation affects how the two domains interact rather than preventing interaction altogether (125).

Using single-molecule force microscopy (SMFM) others have also found sensor domain acylation to influence the force needed to unfold BlaR1 from *B. licheniformis* (126). In the presence of β -lactam inducer, reduced affinity between the sensor domain and the zinc metalloprotease domain were recorded using SMFM (126). Specifically, the zinc metalloprotease domain was not able to be unravelled in the absence of penicillin using SMFM, but was sequentially unravelled when acylated, suggesting that acylation with penicillin relaxes the structure to allow for activation of the zinc metalloprotease domain, possibly exposing the active site to the cytosol (126).

While it makes sense that acylation of the sensor domain would signal the activation of the zinc metalloprotease domain, other mechanisms have been proffered. Most notably it has been shown that phosphorylation by the kinase Stk1 is needed for pathway activation *in vivo* (127). However, the phosphorylation sites have not yet been found to allow a more thorough analysis of possible mechanisms. Furthermore, it is unclear how Stk1 is activated in the presence of a β -lactam antibiotic threat. The lack of structural information for the full-length protein has

hindered a clear picture of how the BlaR1/MecR1 membrane proteins are activated and regulated.

Following activation, the zinc metalloprotease domain is then presumed to cause the cleavage of the repressor BlaI/MecI, allowing the *blaZ/pbp2a* expression. Both MecR1 and BlaR1 have the conserved HEXXH motif typical of the gluzincin class of zinc metalloproteases (128). In thermolysin-like enzymes and presumably in BlaR1/MecR1 the two histidine residues of this zinc metalloprotease motif coordinate a zinc(II) atom tetrahedrally, along with the hydrolytic water molecule as well as a glutamate (Glu-242 in BlaR1 and Glu-245 in MecR1) downstream of the HEXXH motif (129). Based on what has been observed with thermolysin, Glu-202 in BlaR1 and Glu-205 in MecR1 are proposed to be the catalytic glutamates. Mutation of these key motifs in the BlaR1 zinc metalloprotease domain has provided evidence that its activity is needed for the antibiotic resistant phenotype to occur in MRSA (130). There are two theories on how cleavage of the repressor is accomplished. Zhang et al. showed the HEXXH motif is needed and suggested that the zinc metalloprotease domain of *S. aureus* BlaR1 directly cleaves the repressor (104). Since BlaR1/MecR1 are embedded in the cell membrane, BlaI/MecI would have to diffuse to the cell membrane to be cleaved by BlaR1/MecR1. Others have suggested repressor cleavage is indirectly mediated by other proteins. One protein termed MecR2, located downstream of the *mec* divergon, has been found to be necessary for complete activation of the *mec* pathway (131). MecR2 binds MecI which reduces its affinity for the operator DNA and assists with its degradation (131). Additionally, in *B. licheniformis* there is some evidence that the PG fragments bind to BlaI and assist with its degradation (132). However, given that *E. coli* membranes containing BlaR1 can mediate the cleavage of BlaI while

membranes containing a catalytic mutant of BlaR1 cannot, suggests that direct cleavage is most likely the main cause of BlaI fragmentation (133).

As the BlaR1 zinc metalloprotease domain is closely localised within the cell membrane, if it is to cleave BlaI directly, BlaI must come to the inner surface of the cell membrane.

Conceivably, either operator bound BlaR1 could diffuse with the DNA strand to the BlaR1 zinc metalloprotease active site or free BlaI could be cleaved. Given the results of previous work finding the concentration of BlaI in the cell to be approximately equal to its dissociation constant for the operator DNA, it appears there may be sufficient populations of free and operator bound BlaI for either theory to be plausible (108). While the BlaI cleavage site is in the middle of an alpha helix, there is still the possibility that upon BlaI binding to the BlaR1 zinc metalloprotease active site there is a structural rearrangement that exposes the BlaI cleavage site, as has been previously suggested with the S2P zinc metalloprotease (106, 134).

Interestingly, BlaR1 and MecR1 both appear to readily undergo autocleavage under native expression conditions in *S. aureus* as well as heterologous expression in *E. coli* (104, 133). Autocleavage of BlaR1/MecR1 was initially thought to play a role in the activation of the zinc metalloprotease domain (104). However, it was later found in *S. aureus* that cleavage products of BlaR1 appeared in the presence and absence of antibiotics, suggesting that autocleavage probably does not play a role in regulation of the bla divergon (133). Instead, BlaR1 autocleavage has been proposed as a method of returning to a resting state following challenge by β -lactam antibiotics, such that activated, acylated BlaR1 can be removed from the membrane (135). Given the numbers of competing theories on BlaR1/MecR1 activation, it is clear additional insight is needed to fully comprehend these two key regulators of resistance in MRSA.

1.4.2 Non-canonical, PBP4-mediated β -lactam resistance

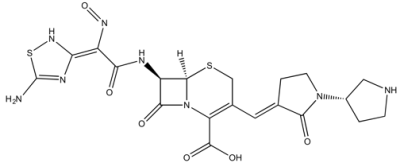
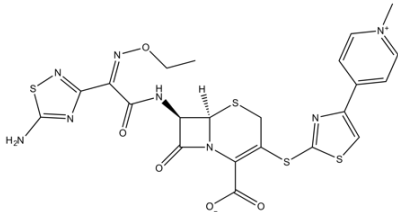
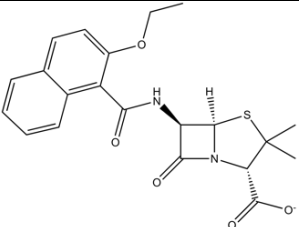
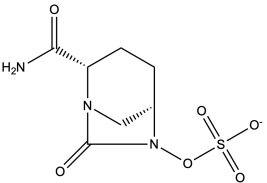
While the *bla* and *mec* controlled MRSA resistance mechanisms have been well documented, alternate forms of β -lactam resistance have been found involving penicillin-binding protein 4 (PBP4) (See section 1.2.1.1 for an introduction to PBP4). Initially, it was found that PBP4 could facilitate moderate levels of β -lactam resistance upon increased *pbp4* expression (136, 137). Worryingly, alternative mechanisms of resistance involving PBP4 have also been found to facilitate high-level β -lactam resistance independently of PBP2a (138–140). Banerjee et al. passaged several strains of *S. aureus* both with and without *pbp2a* in ceftobiprole, a late generation cephalosporin developed to treat MRSA (141), for 28 days (138). Surprisingly, this study showed the *pbp2a* negative strain gained the greatest resistance to ceftobiprole (138). Further work found mutations within the PBP4 gene could work in concert with *pbp4* promoter mutations to facilitate resistance (142–144). Surveys of clinically relevant strains of MRSA and methicillin sensitive *S. aureus* (MSSA) have found mutations in both the *pbp4* promoter as well as the *pbp4* gene, suggesting these alternative PBP4-mediated resistance mechanisms are already widespread outside the laboratory (145, 146).

1.5 Objective of thesis

This thesis aims to improve understanding of the mechanistic details of antibiotic resistance in *S. aureus* at a molecular level. Table 1.1 lists the antibiotics and β -lactamase inhibitor that were structurally characterised in complex with proteins in chapters 2 and 3 of this thesis. A greater understanding of the chemistry surrounding antibiotic resistance is needed if progress is to be made in finding new and improved treatments for MRSA infections.

Chapter 2 examines the mechanism of action of a new type of PBP2a independent β -lactam resistance in *S. aureus* involving PBP4. Using x-ray crystallography and Michealis-Menten kinetics, this work elucidates how *S. aureus* is able to survive treatment with β -lactam antibiotics. Particularly, this work shows that PBP4 from a resistant strain is able to mediate resistance in different ways depending on the β -lactam threat. Missense mutations in the gene were found to be important for resistance to the β -lactam ceftobiprole while mutations in the *pbp4* promoter causing increased *pbp4* expression were more important for ceftaroline

Table 1.1: Antibiotics and β -lactamase inhibitors that were analysed in complex with proteins by x-ray crystallography in this thesis.

Name	Class	Drug structure	Targets	Relevance
Ceftobiprole	β -lactam: cephalosporin		PBP1, PBP2, PBP2a, PBP3, and PBP4 from <i>S. aureus</i> and PBP's from other Gram-positive and -negative organisms (147)	Used clinically to treat MRSA infections
Ceftaroline	β -lactam: cephalosporin		PBP1, PBP2, PBP2a, PBP3, from <i>S. aureus</i> and PBP's from other Gram-positive and -negative organisms (79,148)	Used clinically to treat MRSA infections
Nafcillin	β -lactam: cephalosporin		PBP1, PBP2, PBP3, and PBP4 from <i>S. aureus</i> (149)	Used clinically to treat MSSA infections
Avibactam	Diazabicyclooctane		Class A, B, and D β -lactamases (150)	Avibactam is being considered as part of a broad-spectrum antibiotic for MRSA

resistance. A version of chapter 2 has been published in the *Journal of Biological Chemistry* and *Antimicrobial Agents and Chemotherapy*.

Chapter 3 investigates the effect of a new β -lactamase inhibitor, avibactam, on the *bla* and *mec* divergons in MRSA. This work demonstrates that the diazabicyclooctane, avibactam, is able to induce expression of *blaZ* and *pbp2a*, two genes important for β -lactam resistance in MRSA. Additionally, this chapter demonstrates the molecular basis of interaction between the sensor domains of BlaR1 and MecR1 and avibactam using x-ray crystallography. A version of chapter 3 has been published in the *Journal of Biological Chemistry*.

Chapter 2: Structural and kinetic analyses of penicillin-binding protein 4 (PBP4)-mediated antibiotic resistance in *Staphylococcus aureus*

2.1 Introduction

MRSA infections are a serious cause of both nosocomial and community-acquired infections, causing mortality and morbidity throughout the world. Indeed, the 2017 World Health Organization report, Priority Pathogens List for R&D of New Antibiotics, listed MRSA as a “high” priority pathogen for the development of new antimicrobials (31). Resistance to β -lactam antibiotics seen in MRSA is especially serious as they remain the most widely prescribed class globally, typically having a favourable safety profile and being relatively affordable and accessible. While broad spectrum MRSA resistance to β -lactam antibiotics has long been attributed to impaired acylation of the *mecA* gene product, penicillin-binding protein 2a (PBP2a) (151), recent evidence shows penicillin-binding protein 4 (PBP4), a low-molecular-weight monofunctional transpeptidase, can facilitate antibiotic resistance independently of PBP2a (85, 139, 140, 142–144, 152). It has been previously demonstrated that the only essential penicillin-binding proteins (PBPs) in *S. aureus* are the monofunctional high-molecular-weight transpeptidase, PBP1 and the bifunctional PBP2, (glycopolymerase/transpeptidase) (73). However, this strain expressing only the essential PBPs showed deficiencies in virulence and antibiotic resistance (73). Additionally, PBP4 has been shown to play an important role in mediating β -lactam resistance in some community acquired MRSA strains (83).

PBPs ensure the integrity of the peptidoglycan (PG) sacculus by catalysing peptide linkages between polymerized PG glycan chains, the hallmark transpeptidation reaction that β -lactam antibiotics such as penicillin and cephalosporins inhibit (39, 153). PBP4 is composed of

two domains, one more N-terminal composed of a classic α - β - α sandwich transpeptidase domain and a second C-terminal domain of unknown function and composed of seven β -strands (154). Near the end of the C-terminal domain there is a transmembrane segment, anchoring PBP4 to the cell membrane.

The transpeptidase reaction is facilitated by three highly conserved signature motifs in PBPs: *SXXK*, *(S/Y)X(N/C)*, and *(K/H)(S/T)G* (33). In *S. aureus* PBP4, these motifs are S75MTK, S139SN, K259TG (Fig. 2.1). The γ -O of Ser-75 is thought to be activated by the abstraction of the proton with Lys-78 serving in the general base role. The activated Ser-75 γ -O nucleophile then attacks the carbonyl carbon of the D-Ala-D-Ala bond in the donor PG stem peptide (Fig. 2.2), forming a tetrahedral oxyanion transition state before collapsing to an acyl-enzyme intermediate and releasing the leaving group terminal D-Ala from the stem peptide in the process (33). Deacylation follows when the amino terminal moiety of the acceptor strand pentaglycine bridge attacks, creating a stem peptide linkage between the two glycan chains and regenerating the resting state of the enzyme (33). The *SXN* motif has been proposed to have roles in enzyme acylation and deacylation in the transpeptidase reaction mechanism (58). It is thought the serine in the *SXN* motif may play a role in mediating the transfer of a proton from the lysine side chain N- ζ in the *SXXK* motif to the D-Ala leaving group nitrogen during acylation (58). The lysine of the *KTG* motif has been proposed to activate the serine of the *SXN* motif which then abstracts a proton from the attacking amino nitrogen of the PG acceptor strand, preparing it for nucleophilic attack of the α -carbon of the acyl-enzyme ester bond (58). The *KTG* residues also appear to play a role in orientating β -lactam antibiotics in the active site through hydrogen bonding with the carboxylate bound to the thiazolidine and dihydrothiazine ring in penicillin and cephalosporin antibiotics respectively (58).

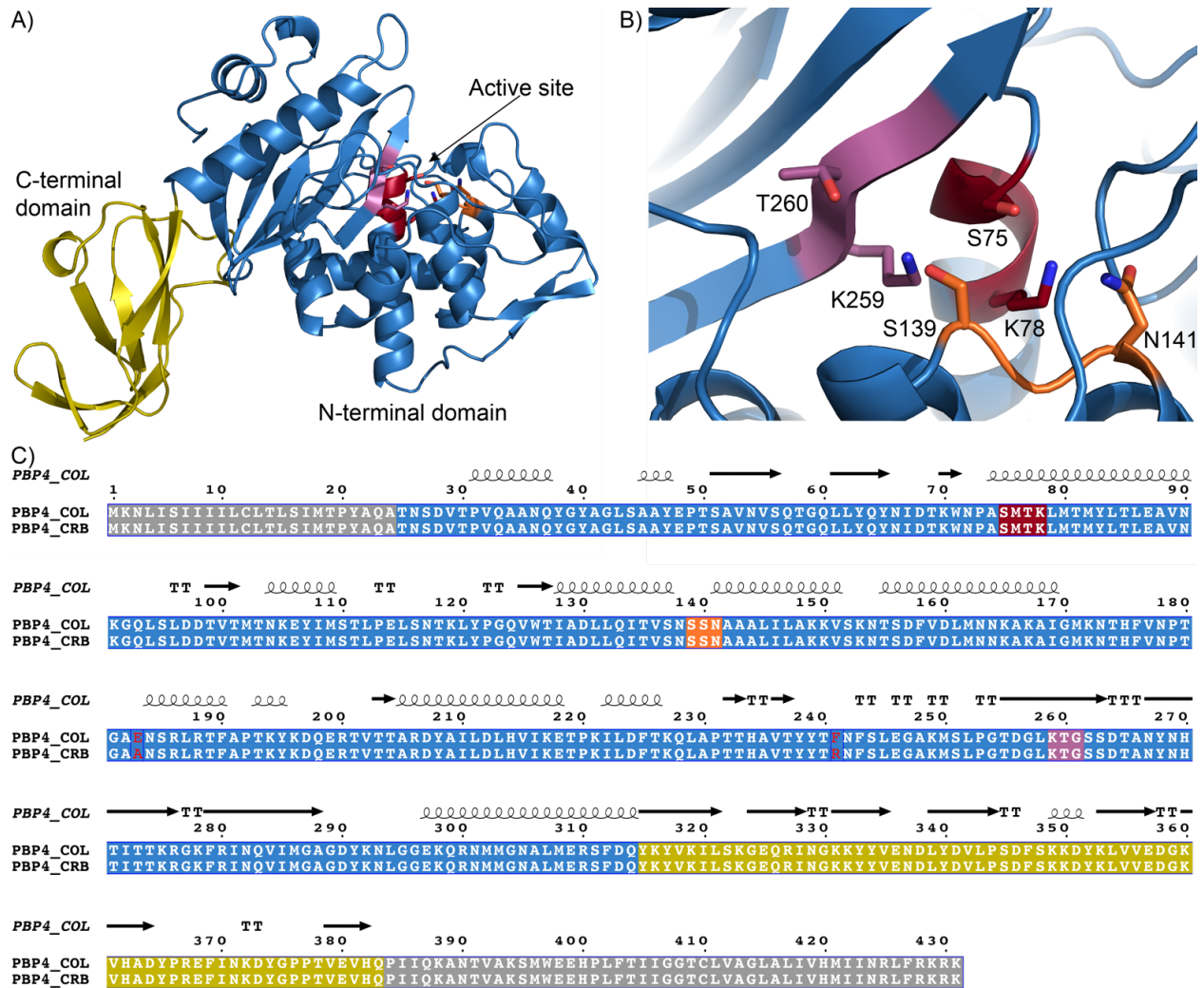


Figure 2.1: PBP4 structure and protein sequence alignment of PBP4 and PBP4^{CRB} from *S. aureus*. In each panel, the three conserved motifs in PBPs, SXXK, SXN, and KTG, are shown in red, orange and purple respectively. Panel A shows PBP4 in cartoon representation. Panel B depicts the PBP4 active site in cartoon representation with selected residues shown as sticks. A sequence alignment with PBP4 and PBP4^{CRB} sequences is shown in panel C. Areas with visible electron density are shown in colour (the N-terminal transpeptidase domain sequence is shown on a blue background while the C-terminal domain sequence is shown on a olive background) while areas with no density or not present in the construct crystallized are shown in grey. Areas of matching sequence are shown with white letters while mismatches are shown with red letters.

In an effort to better understand *S. aureus* β -lactam resistance, Chambers and colleagues took *S. aureus* COL, a strain initially isolated from a hospital in Colindale, England in the early 1960s (155) and excised the SCC*mec* cassette from a tetracycline-sensitive isolate creating the *mecA* (PBP2a) negative *S. aureus* COLnex strain (156). Following the creation of the *S. aureus*

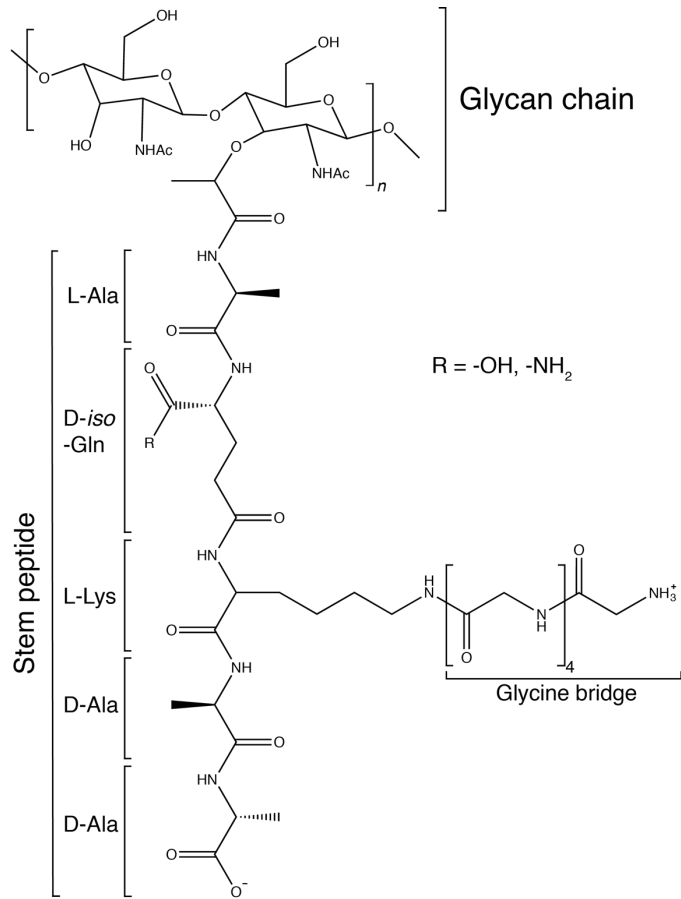


Figure 2.2: *S. aureus* peptidoglycan monomer structure. The PG glycan chain is characterized by repeating units of *N*-acetylglucosamine and *N*-acetylmuramic acid. The stem peptide allows the glycan strands to be crosslinked, creating an essential protective mesh around the bacterium. There is some variation in the *S. aureus* stem peptide between strains with the D-iso-Gln carboxyl group being converted to an amide group in some strains.

COLnex strain, researchers explored its ability to develop β -lactam resistance after serial passaging in increasing concentrations of ceftobiprole, a late-generation cephalosporin specifically developed to inhibit PBP2a in MRSA (138). This experiment created a new highly resistant strain, referred to as CRB, indicating PBP2a is not essential for β -lactam resistance (138). Genome sequencing of the *S. aureus* CRB strain revealed mutations in the cation efflux pump AcrB (I960V), the cyclic-di-AMP phosphodiesterase GdpP (N182K), the promoter of *pbp4* (denoted $P_{CRB} pbp4$), and the PBP4 gene product itself (E183A, F241R) (142, 144).

Although it is currently unknown what role AcrB might have in resistance, GdpP is thought to be

involved in the stress response (157) and $P_{\text{CRB}}pbp4$ leads to increased expression of PBP4 (85). While there are several mutations in the *S. aureus* CRB strain, those involving *pbp4* have recently been shown to play a central role in mediating high-level β -lactam resistance. When *S. aureus* COLnex and SF8300 strains were passaged in nafcillin, they attained high-level resistance within 18 days. By contrast, the isogenic strains lacking *pbp4* failed to display high-level β -lactam resistance even after 60 days of passaging (139).

Previously, we have shown that the *pbp4* promoter mutation ($P_{\text{CRB}}pbp4$) seen in *S. aureus* CRB does contribute to resistance; however it does not fully explain the increased resistance seen when the missense mutations in *pbp4* are also present (85, 152). Additionally, changes in peptidoglycan composition and thickening of the cell wall have been observed in the CRB strain, suggesting increased peptidoglycan cross-linking is occurring (85, 152). We set out to understand, therefore, how PBP4 could be facilitating high-level β -lactam resistance in notoriously drug-resistant *S. aureus* infections.

To probe the structural and mechanistic contributions of the enzyme to β -lactam resistance, we have determined and compared the ligand-free and acyl-enzyme intermediate X-ray crystallographic structures of *S. aureus* PBP4 with clinically relevant β -lactam antibiotics. Specifically, the atomic structures of PBP4 from both the COLnex strain (identical sequence to PBP4 from the parent COL strain) and PBP4^{CRB} from the CRB strain (substitutions E183A and F241A) were solved in complex with the late-generation cephalosporins ceftaroline and ceftobiprole (designed to specifically inhibit PBP2a and approved to treat MRSA) (79, 141, 158), as well as nafcillin (a penicillin used to treat methicillin-sensitive *S. aureus* infections) (159). We also show PBP4 and PBP4^{CRB} have differing kinetic behaviour, with PBP4 having higher kinetic efficiency with several β -lactam antibiotics compared to the PBP4^{CRB}.

2.2 Methods

2.2.1 Cloning, expression, and purification of PBP4 and PBP4^{CRB}

Genes coding for PBP4 and PBP4^{CRB} were cloned into pET-15b (Invitrogen) for protein expression and purification as previously described with the following modifications (26). Plasmids coding for wild-type PBP4 and PBP4^{CRB} were transformed into *E. coli* BL21(DE3) and were grown in Luria-Bertani broth (supplemented with 100 µg/ml ampicillin) at 37°C up to an OD_{600 nm} of 0.5 to 0.8. Cells were then cooled at 4°C for at least 30 min before the addition of IPTG to a final concentration of 0.1 mM. Protein was expressed overnight at 17°C with shaking before the cells were harvested by centrifugation and stored at -80°C. Cells from 4.5 L of culture were resuspended in buffer A (20 mM Tris, pH 7.5, 500 mM NaCl, 20 mM imidazole) containing DNase I (14 µg ml⁻¹; Roche) and a tablet containing EDTA-free protease inhibitor cocktail (Roche). Cells were lysed at 4°C with a homogenizer (Avestin). The cell lysate was centrifuged for 45 min at 45,000 rpm in a type 70 Ti rotor (Beckman Coulter) at 4°C. The supernatant was collected and filtered (pore size, 0.45 µm) before being loaded onto a 1-ml HisTrap HP (GE Lifesciences) nickel affinity column equilibrated in buffer A. The column was washed with at least 10 column volumes of buffer A before the protein of interest was eluted from the column with a gradient of from 0 to 50% buffer B (20 mM Tris, pH 7.5, 500 mM NaCl, 1.0 M imidazole) over 40 min at a flow rate of 1 ml/min. The recovered protein was dialyzed overnight in buffer A at 4°C, and 1 µl bovine α-thrombin (Hematologic Technologies Inc.) was added per ml of collected protein to cleave the polyhistidine tag. The dialyzed protein was again run through a 1-ml HisTrap HP column, and the flowthrough was collected and concentrated on a 30-kDa-molecular-mass-cutoff Centricon membrane (Amicon) before being loaded onto a Superdex 75 column (GE Life Sciences) equilibrated in buffer C (20 mM MES

[morpholineethanesulfonic acid], pH 6, 300 mM NaCl). Fractions were analysed via sodium dodecyl sulfate (SDS)-PAGE, and the fractions containing high-purity PBP4 were collected and concentrated to 25 to 30 mg/ml, as determined by measurement of the absorbance at 280 nm. The protein was cooled in liquid nitrogen before storage at -80°C .

2.2.2 Antibiotics

Antibiotics for crystallization and kinetic experiments were prepared as follows. Ceftobiprole (Basilea pharmaceutica), was dissolved in DMSO with 0.2% (v/v) trifluoroacetic acid. Ceftaroline (Forest labs) and nitrocefin (Toku-E) stocks were prepared in DMSO while nafcillin (Sigma) was dissolved in water.

2.2.3 Crystallization, structure determination, and modelling of PBP4 and PBP4^{CRB}

PBP4 crystals were obtained via the sitting drop vapor diffusion method in 24-well plates with streak seeding and incubation at 23°C . Streak seeding was performed by stroking PBP4 crystals in mother liquor with a housecat whisker before drawing the whisker through freshly set up drops. PBP4 in buffer C (20 mM MES pH 6, 300 mM sodium chloride) was crystallized in a 1:1 volume ratio of protein at 30 mg/mL and precipitant solution (8 mM zinc chloride, 80 mM sodium acetate pH 5, 400 mM dimethyl (2-hydroxyethyl) ammonium propane sulfonate, and 16% polyethylene glycol 6000), with a total drop volume of 2 μL . PBP4^{CRB} was crystallized in a 1:1 volume ratio of protein at 15-20 mg/mL and precipitant solution (8 mM zinc chloride, 80 mM sodium acetate pH 5, 100 mM sodium fluoride, and 16% polyethylene glycol 6000), with a total drop volume of 2 μL . Antibiotics were soaked into the crystals for 40-180 min at final concentrations of 2 mM for ceftaroline, 5 mM for nafcillin, and 0.75 mM for ceftobiprole. Cryoprotectant (1:1 precipitant solution and buffer C, with a final concentration of 15% glycerol,

and antibiotic at the soaking concentrations indicated above) was added to the crystals prior to looping, vitrification, and storage in liquid nitrogen.

Data were collected at the Canadian Light Source Synchrotron beam lines 08ID-1 and 08B1-1 under cryogenic conditions (100K). Data were processed using Xia2 (160) and XDS (161) with a space group of C121 and merged with Aimless (162) in the CCP4 software package (163). The structures were solved via molecular replacement using Phaser (164), with chain A of PDB ID: 1TVF as the starting model. Model building and refinement was conducted with the Phenix suite of programs (165). Particularly, AutoBuild (166) was used with iterative rounds of manipulating the model into the electron density with *Coot* (167), followed by refinement with Phenix.refine (168), with TLS being used in the later stages of refinement. The same set of R_{free} flags were used for cross-validation purposes in all eight structures. All structures were refined using isotropic B-factors. Ligand coordinates and restraints were generated using ACEDRG (distributed within the CCP4 package) and ligands were refined with an occupancy of 1 in all structures. Ions were included in the models based on the electron density, refined B factors and the surrounding chemical environment. Structures were validated with Molprobit (169) and PBD redo (170). The interfacial buried surface area PBP4^{COL} was calculated using PISA (171). Figs. 2.1, 2.3-2.5, and B1-B2, B6, and B8-B9 were generated using PyMOL (Schrödinger, LLC, New York) using chain B of the structures solved here. RMSD calculations comparing the C α alignment of the structures were performed in PyMOL (Schrödinger, LLC, New York) also using chain B. The sequence alignment in Fig. 2.1C was produced using the ESPript 3.0 server (116). Figures B3-B5 were generated using LigPlot+ (172). Coordinates and structure factors for PBP4-ligand-free, PBP4-ceftobiprole, PBP4-ceftaroline, PBP4-nafcillin, PBP4^{CRB}-ligand-free,

PBP4^{CRB}-ceftobiprole, PBP4^{CRB}-ceftaroline, PBP4^{CRB}-nafcillin, were deposited into the PDB with accession codes 6c39, 5txi, 5tw8, 5ty7, 6c3k, 5tx9, 5tw4, and 5ty2 respectively.

2.2.4 Kinetic analysis of PBP4 and PBP4^{CRB}

Protein was prepared as above and aliquots were thawed on ice as needed. PBP4 was used at a final concentration of 0.5 μM while PBP4^{CRB} was used at concentrations of 1 to 5 μM . Protein concentrations were measured via absorbance at 280 nm using an extinction coefficient of 45270 $\text{M}^{-1} \text{cm}^{-1}$ for PBP4 and PBP4^{CRB} calculated using ProtParam (173). All enzymatic reactions were carried out at 25°C using a plate reader (Bio-tek Synergy H4) in 384 well plates (Corning 3540). Enzyme assays were carried out in reaction buffer (40 mM 4-(2-hydroxyethyl)-1-piperazineethanesulfonic acid, 100 mM sodium chloride, pH 7.5) in a total volume of 20-30 μL . Hydrolysis of the β -lactam ring in ceftobiprole, ceftaroline, and nitrocefin was monitored as previously described by measuring absorbance at 290 ($\Delta\epsilon_{290} = 6,970 \text{ M}^{-1} \text{cm}^{-1}$), 306 ($\Delta\epsilon_{306} = 6,300 \text{ M}^{-1} \text{cm}^{-1}$), and 486 nm ($\Delta\epsilon_{486} = 14,600 \text{ M}^{-1} \text{cm}^{-1}$), respectively (174, 175). Steady-state kinetic parameters were calculated via non-linear least-squares regression to the Michaelis-Menten equation (GraphPad Prism7) with data from initial velocities. For each substrate concentration, data were collected using protein from two separate protein purifications.

2.3 Results

2.3.1 X-ray crystallographic analysis of ligand-free PBP4 and PBP4^{CRB} as well as acyl-enzyme intermediate structures with ceftobiprole, ceftaroline, and nafcillin

To investigate the structures of PBP4 and PBP4^{CRB} with and without β -lactam antibiotics we grew ligand-free crystals of both recombinantly produced variants and subsequently soaked in ceftobiprole, ceftaroline, and nafcillin to allow characterization of the generated covalent adducts. The eight resulting crystal structures (Figs. 2.1, 2.3-2.4), represent the highest resolution

S. aureus PBP4 structures published to date and the first characterizations of the ligand-free and acyl-enzyme intermediate forms. All structures were generated from isomorphous crystals in the space group C121, giving us confidence that any differences observed between the mutant and wild-type structures are due to mutations in PBP4 and conformational effects of the bound

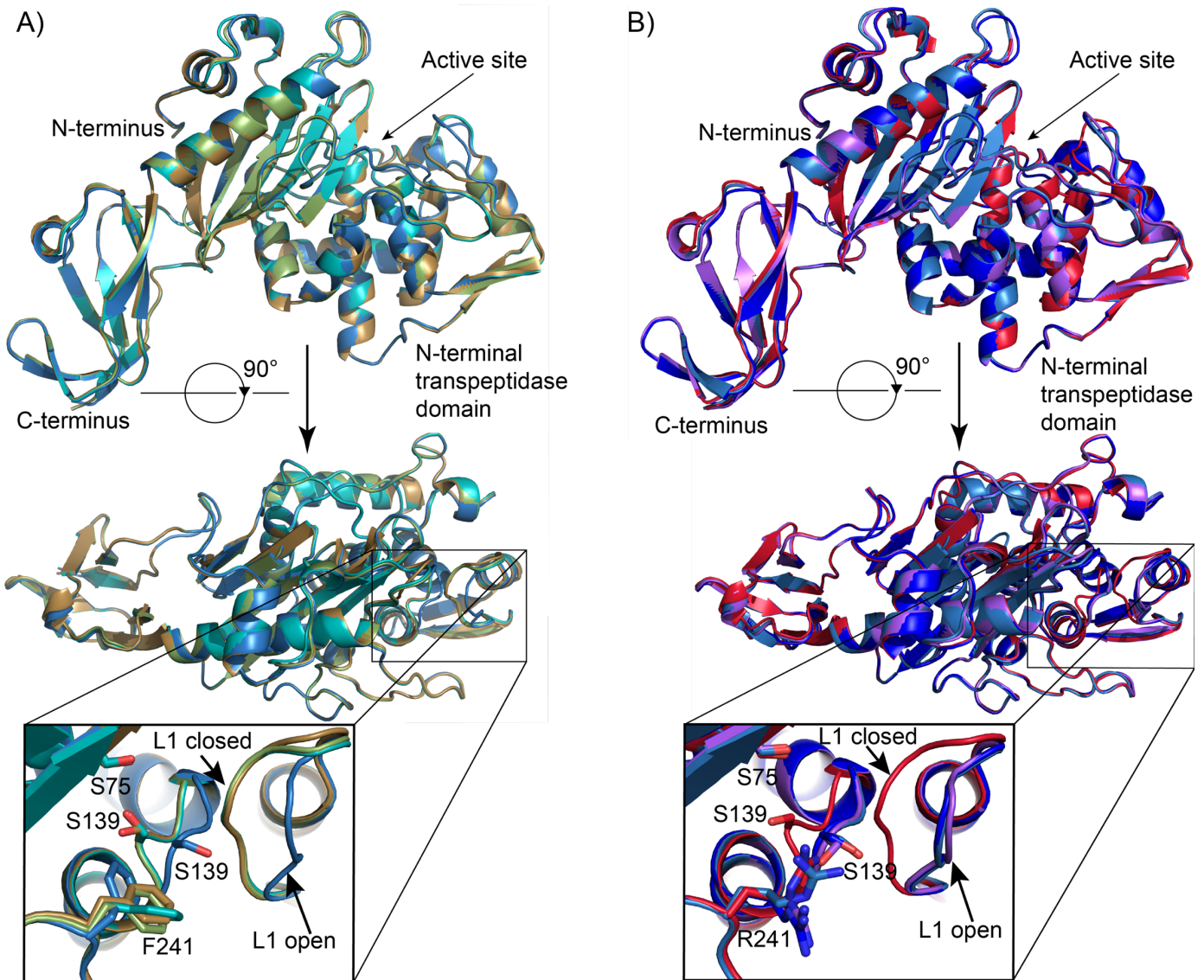


Figure 2.3: Separate structural alignments of A) PBP4 structures and B) PBP4^{CRB} structures. Ligand-free PBP4 and PBP4 acyl-enzyme intermediate structures in complex with ceftobiprole, ceftaroline, and nafcillin are shown in light brown, blue, green, and teal respectively. Ligand-free PBP4^{CRB} and PBP4^{CRB} acyl-enzyme intermediate structures in complex with ceftobiprole, ceftaroline, and nafcillin are shown in red, dark blue, purple, and light blue respectively. The structures are depicted as cartoons and the catalytic serine (Ser-75), Ser-139 of the *SXN* motif, and mutated residue in PBP4^{CRB} (F241R) are displayed as sticks in the bottom panel. Ligands are not shown for greater clarity.

ligands rather than differences in crystal packing. Additionally, comparison of existing PBP4 structures, all of which have been crystallized in space group P 21 21 21, show they closely align with the PBP4 ligand-free structure solved here, providing further support that the differences observed are not crystallization artefacts. The crystallographic data collection and refinement statistics for all structures described here can be found in Tables 2.1 and 2.2. The crystals have two highly similar monomers in the asymmetric unit (C α RMSD for chains A and B for the various structures are presented in Table 2.3) with no obvious physiological dimeric interface (interfacial buried surface of $\sim 580 \text{ \AA}^2$ in ligand-free PBP4 as calculated by PISA (171)). The uniformly excellent quality of crystals and data allowed us to obtain high-resolution structures at 1.7, 1.6, 1.7, 1.9, 1.6, 1.7, 1.6, and 1.7 \AA resolution for ligand-free PBP4, PBP4-ceftobiprole, PBP4-ceftaroline, PBP4-nafcillin, ligand-free PBP4^{CRB}, PBP4^{CRB}-ceftobiprole, PBP4^{CRB}-ceftaroline, and PBP4^{CRB}-nafcillin, respectively. Search of the Dali server (176) with chain B of ligand-free PBP4 suggests the PBP4 fold is most similar to the fold of several confirmed carboxypeptidases, PBPs which preferentially catalyse the trimming of terminal D-Ala residues from PG peptides rather than crosslinking transpeptidation. The closest matches between the PBP4 ligand-free structure solved here (residues 25-383) and other proteins in the PDB are PBP3 from *Streptococcus pneumoniae* and PBP5 and PBP6, both from *E. coli*, as measured by Dali Z-scores of 39.2, 34.5, and 34.5, respectively (177–179). A C α alignment of PBP3 from *Streptococcus pneumoniae* and PBP5 from *E. coli* show the N-terminal transpeptidase domains are broadly similar while the cylindrical C-terminal domains composed of several β -strands show more variation (Fig. 2.5). The closest matches to the PBP4 C-terminal domain (residues 315 to 383) using a Dali search (176) arise from the C-terminal domains of PBP3 from *Streptococcus pneumoniae*, a D-alanyl-D-alanine carboxypeptidase from *Bacillus subtilis* (unpublished, PDB

the O- γ of the Ser-75 serine nucleophile (2.9Å for both PBP4 and PBP4^{CRB}), presenting the optimal hydrogen bond distance and angle in the native enzyme for subsequent necessary deprotonation/activation of the serine hydroxyl during the acylation step.

In all acyl-enzyme intermediate structures, with the various substrates directly captured and observed, the 2mF_o-DF_c electron density maps clearly show the expected covalent linkage between the O- γ of the catalytic serine (Ser-75) and C8 of ceftobiprole and ceftaroline and C7 of nafcillin (Figs. B1 and B2), the first captured acyl-enzyme intermediates in this important MRSA antibiotic resistance mediator. Additionally, mF_o-DF_c volume omit maps provide unambiguous evidence for the presence of the well occupied ligand in the active site (Figs. B1 and B2) and supplemental figures 2.3-2.5 show detailed 2D depictions of ligand-protein interactions generated using LigPlot+ (172). The structures also show the backbone amide nitrogen of residues Ser-75 and Ser-262 in PBP4 form the oxyanion hole, allowing for highly similar and optimal coordination and polarization of the substrate carbonyl (distances and angles nearly identical amongst the various structures), an electrostatic feature which enhances electrophilicity at the carbon centre, and subsequent stabilization of the oxyanion tetrahedral transition state during acylation. Wild-type PBP4 and mutant PBP4^{CRB} structural differences of potential significance are depicted in figures 2.3, 2.4 and B6 while C α RMSD values comparing the structures and particular regions of the structures are listed in Table 2.3.

2.3.2 PBP4 structures with ceftobiprole

PBP4 and PBP4^{CRB} structures in complex with ceftobiprole, (141, 158) show antibiotic binding is stabilized via hydrogen bonds between the side chain O- γ of residue Ser-262 (2.6Å for

Table 2.1: Data collection and structure refinement statistics for PBP4

Ligand (PDB code)	Ligand-free (6c39)	Ceftaroline (5tw8)	Ceftobiprole (5txi)	Nafcillin (5ty7)
Data collection				
Beamline	CLS-08ID-1	CLS-08ID-1	CLS-08ID-1	CLS-08ID-1
Space group	C121	C121	C121	C121
Cell dimensions				
<i>a</i> , <i>b</i> , <i>c</i> (Å)	116.4, 92.4, 79.2	116.4, 92.2, 79.2	116.9, 92.3, 79.5	115.3, 92.2, 79.1
α , β , γ , (°)	90.0, 99.3, 90.0	90.0, 99.2, 90.0	90.0, 100.0, 90.0	90.0, 98.9, 90.0
Wavelength (Å)	0.9795	0.9795	0.9795	0.9795
Resolution (Å)	46.20-1.69 (1.75-1.69)	43.10-1.72 (1.78-1.72)	46.15-1.60 (1.66-1.60)	50.41-1.89 (1.96-1.89)
No. unique reflections	92121 (9120)	87245 (8633)	108425 (10241)	63836 (6053)
<i>R</i> _{merge}	0.087 (1.078)	0.110 (1.420)	0.098 (1.186)	0.066 (0.504)
<i>CC1/2</i>	0.998 (0.627)	0.997 (0.584)	0.998 (0.541)	0.999 (0.846)
<i>I</i> / σ <i>I</i>	10.0 (1.72)	9.40 (1.57)	9.33 (1.19)	12.19 (2.61)
Completeness (%)	99.1 (99.6)	99.7 (99.7)	98.2 (93.6)	97.5 (93.4)
Redundancy	3.8 (3.8)	3.8 (3.8)	3.7 (3.3)	3.8 (3.8)
Refinement				
Resolution (Å)	46.20-1.69	43.10-1.72	46.15-1.60	39.69-1.89
<i>R</i> _{work} / <i>R</i> _{free}	0.172/0.205	0.186/0.215	0.171/0.202	0.185/0.222
No. non-hydrogen atoms				
Protein	5672	5555	5687	5592
Ligand/ion	0/17	78/5	78/20	58/6
Water	667	481	580	388
B-factors (Å ²)				
Protein	26.8	32.2	23.0	37.8
Ligand	-	81.2	31.1	69.5
Ion	43.6	43.7	53.3	43.6
Water	37.8	38.5	36.6	39.3
RMSD				
Bond lengths (Å)	0.005	0.006	0.015	0.007
Bond angles (°)	1.15	0.86	1.42	0.78
Ramachandran favoured/allowed/disallowed (%)	98.0, 2.0, 0.0	97.6, 2.3, 0.1	98.3, 1.7, 0.0	97.7, 2.1, 0.1

Data corresponds to diffraction from a single crystal for each structure.

*Highest resolution shell is shown in parenthesis.

Table 2.2: Data collection and structure refinement statistics for PBP4^{CRB}

Ligand (PDB code)	Ligand-free (6c3k)	Ceftaroline (5tw4)	Ceftobiprole (5tx9)	Nafcillin (5ty2)
Data collection				
Beam line	CLS-08ID-1	CLS-08ID-1	CLS-08ID-1	CLS-08BM-1
Space group	C121	C121	C121	C121
Cell dimensions				
<i>a</i> , <i>b</i> , <i>c</i> (Å)	116.9, 92.6, 79.2	115.7, 92.6, 79.6	116.9, 92.3, 79.4	113.9, 92.2, 79.0
α , β , γ (°)	90.0, 99.3, 90.0	90.0, 99.8, 90.0	90.0, 100.2, 90.0	90.0, 98.4, 90.0
Wavelength (Å)	0.9795	0.9795	0.9795	1.1046
Resolution (Å)	43.19-1.60 (1.66-1.60)	46.28-1.57 (1.63-1.57)	32.84-1.68 (1.74-1.68)	42.80-1.70 (1.76-1.70)
No. unique reflections	108891 (10914)	114289 (11268)	93439 (9378)	85749 (7345)
<i>R</i> _{merge}	0.063 (1.158)	0.074 (0.937)	0.081 (0.731)	0.057 (0.851)
<i>CC1/2</i>	0.999 (0.498)	0.999 (0.654)	0.998 (0.768)	0.999 (0.630)
<i>I</i> / σ <i>I</i>	12.45 (1.26)	13.21 (1.66)	10.83 (1.88)	13.65 (1.54)
Completeness (%)	99.1 (99.8)	99.3 (98.3)	97.8 (99.7)	96.7 (83.4)
Redundancy	3.7 (3.7)	3.8 (3.8)	3.7 (3.8)	3.8 (3.4)
Refinement				
Resolution (Å)	43.19-1.60	46.28-1.57	32.84-1.68	42.80-1.70
<i>R</i> _{work} / <i>R</i> _{free}	0.176/0.204	0.156/0.177	0.208/0.242	0.169/0.205
No. non-hydrogen atoms				
Protein	5652	5633	5620	5618
Ligand/ion	0/9	84/9	72/8	58/7
Water	717	820	711	609
B-factors (Å ²)				
Protein	28.4	21.0	21.0	30.9
Ligand	-	30.0	22.7	34.7
Ion	27.8	23.5	35.0	42.3
Water	38.5	33.4	32.4	38.3
RMSD				
Bond lengths (Å)	0.007	0.008	0.007	0.007
Bond angles (°)	1.20	1.00	0.96	0.84
Ramachandran favoured/allowed/disallowed (%)	97.9, 2.1, 0.0	98.6, 1.3, 0.1	98.6, 1.4, 0.0	98.0, 2.0, 0.0

Data corresponds to diffraction from a single crystal for each structure.

*Highest resolution shell is shown in parenthesis.

PBP4 and 2.4Å for PBP4^{CRB}) as well as the side chain O-γ of Thr-260 (3.0Å for PBP4 and 3.3Å for PBP4^{CRB}) and the carboxyl group attached to C4 on the dihydrothiazine ring (Fig. 2.4A). Additionally, the side chain hydroxyl of Tyr-268 (3.1Å for PBP4 and 3.0Å for PBP4^{CRB}) is hydrogen bonded to the carbonyl oxygen in the R2 motif of ceftobiprole (Fig. 2.4A). The carboxyl group bonded to the C4 of the dihydrothiazine ring of ceftobiprole contributes to water-mediated hydrogen bond interactions via water W1 with the side chain N-η of Arg-300 and the nitrogen of the oxime group in ceftobiprole similarly interacts via water-mediated hydrogen bonds with the backbone amides of Glu-183 and Ala-183 (via waters W2 and W3 respectively) in PBP4 and PBP4^{CRB}. In both structures, there is an additional water-mediated hydrogen bond between the R1 carbonyl oxygen at C8 and the backbone amide of L115 (not shown in Fig. 2.4A for clarity) which could be contributing to the L1 loop adopting the closed position in both structures (Fig. 2.3). We also note a hydrogen bond between N1 of the ceftobiprole pyrrolidinyll group and the sidechain carboxyl group of Asp-351 (2.7Å for PBP4 and 2.8Å for PBP4^{CRB}) in the neighbouring monomer of the asymmetric unit in both PBP4 and PBP4^{CRB} complexes, potentially influencing the positioning of the ligand we observe. Furthermore, a sulfate and chloride ion (average B-factors = 79.5 and 21.5 Å² respectively at full occupancy) were modelled (see methods) into the active site cleft in the PBP4 ceftobiprole structure whereas interestingly the PBP4^{CRB} ceftobiprole structure appeared to lack both ions despite similar crystallization conditions.

2.3.3 PBP4 structures with ceftaroline

In both PBP4 and PBP4^{CRB} ceftaroline structures, a carboxyl group protruding from C4 of the dihydrothiazine ring of ceftaroline is hydrogen bonded with the O-γ on T260 (2.6Å for PBP4 and 2.9Å for PBP4^{CRB}) (Fig. 2.4B). This carboxyl group is also within hydrogen bonding

Table 2.3: Ca RMSD values for PBP4 structures

Structures or regions of structures compared		Ca RMSD (Å)	number of atoms aligned
Comparison of PBP4 and PBP4^{CRB} between structures			
PBP4 Ligand-free, Chain B	PBP4 ^{CRB} Ligand-free, Chain B	0.13	355
PBP4 Cefotaxime, Chain B	PBP4 ^{CRB} Cefotaxime, Chain B	0.14	356
PBP4 Ceftazidime, Chain B	PBP4 ^{CRB} Ceftazidime, Chain B	0.57	353
PBP4 Nafcillin, Chain B	PBP4 ^{CRB} Nafcillin, Chain B	0.54	356
Comparison of chain A and B within the same structure			
PBP4 Ligand-free, Chain A	PBP4 Ligand-free, Chain B	0.33	360
PBP4 ^{CRB} Ligand-free, Chain A	PBP4 ^{CRB} Ligand-free, Chain B	0.32	358
PBP4 Cefotaxime, Chain A	PBP4 Cefotaxime, Chain B	0.28	355
PBP4 ^{CRB} Cefotaxime, Chain A	PBP4 ^{CRB} Cefotaxime, Chain B	0.29	356
PBP4 Ceftazidime, Chain A	PBP4 Ceftazidime, Chain B	0.22	355
PBP4 ^{CRB} Ceftazidime, Chain A	PBP4 ^{CRB} Ceftazidime, Chain B	0.33	350
PBP4 Nafcillin, Chain A	PBP4 Nafcillin, Chain B	0.25	353
PBP4 ^{CRB} Nafcillin, Chain A	PBP4 ^{CRB} Nafcillin, Chain B	0.28	357
Comparison of loops 1 and 2 between different structures			
PBP4 Ligand-free, Chain B, loop 1 (residues 112-122)	PBP4 ^{CRB} Ligand-free, Chain B, (residues 112-122)	0.13	11
PBP4 Ligand-free, Chain B, loop 2 (residues 138-140)	PBP4 ^{CRB} Ligand-free, Chain B, loop 2 (residues 138-140)	0.08	3
PBP4 Cefotaxime, Chain B, loop 1 (residues 112-122)	PBP4 ^{CRB} Cefotaxime, Chain B, (residues 112-122)	0.25	11
PBP4 Cefotaxime, Chain B, loop 2 (residues 138-140)	PBP4 ^{CRB} Cefotaxime, Chain B, loop 2 (residues 138-140)	0.27	3
PBP4 Ceftazidime, Chain B, loop 1 (residues 112-122)	PBP4 ^{CRB} Ceftazidime, Chain B, (residues 112-122)	2.59	11
PBP4 Ceftazidime, Chain B, loop 2 (residues 138-140)	PBP4 ^{CRB} Ceftazidime, Chain B, loop 2 (residues 138-140)	2.44	3
PBP4 Nafcillin, Chain B, loop 1 (residues 112-118)	PBP4 ^{CRB} Nafcillin, Chain B, (residues 112-118)	2.59	11
PBP4 Nafcillin, Chain B, loop 2 (residues 138-140)	PBP4 ^{CRB} Nafcillin, Chain B, loop 2 (residues 138-140)	2.41	3

distance of the O- γ S262 in PBP4^{CRB} but long in PBP4 (2.6Å vs 3.5Å, respectively). The R2 group of ceftaroline in PBP4 engages in a π -stacking interaction between F241 and the 1,3-thiazole ring (4.0Å distance). In contrast, the R2 group of ceftaroline in PBP4^{CRB} is somewhat displaced out of the active site, such that the O- ϵ of E297 is 4.8Å away from N3 of the 1,3-thiazole ring in the PBP4^{CRB} structure compared to only 3.5Å away in the PBP4 structure. This shift in ligand position is likely due to the introduction of a repulsive positive charge in the F241R mutation with the inherent positive charge on the 1-methylpyridinium nitrogen of ceftaroline (~4.8Å away) and in parallel the abrogation of the π -stacking interaction between the 1,3-thiazole ring and Phe-241. In the PBP4 ceftaroline structure there are hydrogen bond (2.7 Å) contacts between the amine at C5 of the 1,2,4-thiadiazole ring and the O- ϵ of E183. In contrast, the Glu-183A mutation in PBP4^{CRB} eliminates this possibility. Instead it is replaced by a water (W4) mediated interaction between the C5 amine substituent and the side chain amide N- ϵ of Asn-72. A chloride ion (average B-factor = 18.0Å²) was modelled 3.2 Å and 3.1Å away from the ζ -N of Lys-78 and Lys-259 respectively in the PBP4^{CRB} ceftaroline structure (see methods) while the PBP4 structure appeared to lack this ion.

2.3.4 PBP4 structures with nafcillin

The PBP4 and PBP4^{CRB} nafcillin complexes superpose closely excepting substantial local variation in loops L1 and L2 (Table 2.3; Fig. B6D). PBP4 and PBP4^{CRB} both show analogous interactions between the carboxyl group bonded to the thiazolidine ring of nafcillin and the O- γ of Thr-260 (2.6Å for PBP4 and 2.8Å for PBP4^{CRB}) and Ser-262 (2.8Å for PBP4 and 2.7Å for PBP4^{CRB}). Similarly, the carboxyl group thiazolidine ring interacts via water (W1) with N- η on R300 in both nafcillin structures. The backbone carbonyl of Ser-262 is hydrogen bonding distance from the nitrogen of the R1 group (3.0Å for PBP4 and 2.9Å for PBP4^{CRB}). As a

consequence of the differing L1, the proximity between the amide oxygen linking the nafcillin R1 group and the backbone amide of S116 is markedly different in PBP4 and PBP4^{CRB} (3.9 Å for PBP4 and 7.1Å for PBP4^{CRB}). Further, a chloride ion (average B-factor = 37.2Å²) was modelled in the PBP4^{CRB} nafcillin active site structure (see methods) coordinated between the side chain ammonium atoms of Lys-78 and Lys-258 at a distance of 3.0 and 2.8Å respectively. In the PBP4 structure with nafcillin, the chloride ion position is occupied by the side chain hydroxyl of Ser-139 due to variation in the position of the L2 loop.

2.3.5 Two loops bordering the PBP4 active site display alternate conformations

Although all PBP4 and PBP4^{CRB} structures shown here have similar overall architecture, there are differences in two loops bordering the active site. Loop 1 (L1; ordered residues 112-122 in ligand-free, ceftaroline, and ceftobiprole bound structures and ordered residues 112-118 in the nafcillin bound structures) appears to adopt either an “open” or “closed” conformation that differs by 5.0-5.6Å when comparing the positions of the Leu-115 C α for PBP4 or PBP4^{CRB} structures (Fig. 2.3 and Table 2.3). Interestingly, of the PBP4 structures, only the ceftobiprole acyl-enzyme intermediate structure appears to adopt the open position while the ligand-free, ceftaroline and nafcillin structures all adopt the closed position. In contrast, only in ligand-free PBP4^{CRB} does the L1 loop adopt the closed position while PBP4^{CRB} in complex with ceftobiprole, ceftaroline, and nafcillin all adopt the open position of the L1 loop. Loop 2 (L2; residues 138-140) which contains the SXN motif, also displays a similar pattern of differences in position between PBP4 or PBP4^{CRB} structures as shown in (Fig. 2.3 and Table 2.3). In both PBP4 and PBP4^{CRB} structures displaying the open conformation, the perturbation of L2 causes a radical repositioning of the SXN motif serine hydroxyl such that it points away from the active site (Fig. 2.3).

2.3.6 Steady-state kinetic analysis of PBP4 and PBP4^{CRB}

Steady-state kinetic parameters for each of ceftaroline, ceftobiprole, and nitrocefin were calculated from plots of initial velocity versus substrate concentration (Fig. B7). All three β -lactams were poorly hydrolysed by PBP4 and PBP4^{CRB}, with k_{cat} values of less than 0.008 s^{-1} (Table 2.4), presumably reflecting slow deacylation rates previously observed for PBP4 (181). While k_{cat} values were similar (<4-fold difference) between PBP4 and PBP4^{CRB} for each of the three drugs, the K_M and k_{cat}/K_M values differed between the two enzymes. More specifically, the K_M for PBP4^{CRB} with ceftobiprole and nitrocefin was 150- and 48-fold the K_M for PBP4 with ceftobiprole and nitrocefin respectively (Table 2.4). Similarly, the catalytic efficiency (k_{cat}/K_M) was substantially decreased in PBP4^{CRB} compared to PBP4 (>45-fold reduction) with ceftobiprole and nitrocefin (Table 2.4). In contrast, the catalytic efficiency of PBP4^{CRB} for ceftaroline was only 2-fold lesser as compared to PBP4 and the K_M value was essentially unchanged.

^aTable 2.4: Steady-state kinetic parameters for PBP4 and PBP4^{CRB}

β -lactam	PBP4			PBP4 ^{CRB}		
	$k_{cat} (\text{s}^{-1}) \times 10^{-3}$	$K_M (\mu\text{M})$	$k_{cat}/K_M (\text{M}^{-1} \text{s}^{-1})$	$k_{cat} (\text{s}^{-1}) \times 10^{-3}$	$K_M (\mu\text{M})$	$k_{cat}/K_M (\text{M}^{-1} \text{s}^{-1})$
BPR	1.9 ± 0.2	1.1 ± 0.7	2000 ± 1000	7.2 ± 0.4	170 ± 20	43 ± 6
CPT	2.50 ± 0.06	27 ± 2	91 ± 8	1.10 ± 0.07	21 ± 6	50 ± 10
NCF	5.1 ± 0.3	2.1 ± 0.4	2500 ± 500	5.3 ± 0.1	100 ± 6	53 ± 3

^a Steady-state kinetic parameters were calculated using data from two different protein purifications and reported as means \pm standard deviations. BPR=ceftobiprole; CPT = ceftaroline; NCF=nitrocefin.

2.4 Discussion

An improved understanding of *S. aureus* antibiotic resistance is needed to develop new antimicrobials and reduce patient mortality. Here we shed light on the mechanisms of PBP4-mediated β -lactam resistance using X-ray crystallography to characterize ligand-free and acyl-

enzyme intermediate complexes of native PBP4 and PBP4^{CRB} from the drug resistant CRB MRSA strain with three clinically relevant β -lactam antibiotics: ceftobiprole, ceftaroline and nafcillin. Additionally, we collected steady-state kinetic parameters for PBP4 and PBP4^{CRB} with ceftobiprole, ceftaroline, and nitrocefin. Together, these data advance our understanding of PBP4 mediated β -lactam resistance in *S. aureus*.

Despite differences in the positioning of loops bordering the active site in the PBP4 and PBP4^{CRB} structures, the overall fold is preserved (Figs. 2.3 and B6; Table 2.3). In general, we observe the PBP4^{CRB} active site cleft to be more closed and with lower B-factors for both the ligand and the surrounding residues compared to the PBP4 active site cleft (Fig. B8 and B9). Given the isomorphous nature of the crystal structures determined here, one might suggest this apparent thermal order of a more closed state may facilitate less promiscuous interaction of this enzyme variant with antibiotics; whether this translates to heightened resistance *in vivo* remains to be verified.

Our data show the PBP4 structure aligns most closely to structures of known carboxypeptidases (Fig. 2.5), enzymes which trim rather than crosslink PG stem peptides. This is interesting as earlier *in vivo* experiments showed PBP4 acts to increase PG crosslinking and stiffness (86, 182), corroborating *in vitro* experiments suggesting transpeptidation rather than terminating carboxypeptidation is the primary action of PBP4 (71). It has been hypothesized that the C-terminal domains of *S. aureus* PBP4 and *E. coli* PBP5 may play a role in determining the preference for transpeptidase or carboxypeptidase activity (183). The *S. aureus* PBP4 C-terminal domain, annotated as DUF1958 (Pfam, PF09211), is distinct from the *E. coli* PBP5 C-terminal domain (Pfam, PF07943) and appears to be associated with transpeptidase activity in contrast to the carboxypeptidase activity of the latter (183). Interestingly, the *E. coli* PBP5 is N-terminally

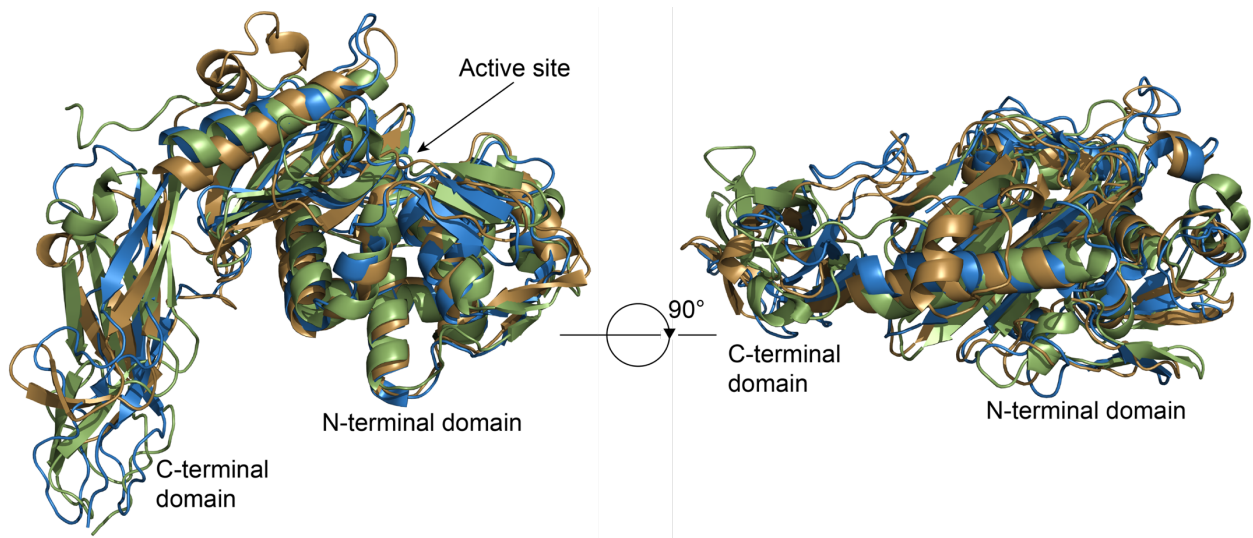


Figure 2.5: *Ca* alignment of PBP4 from *S. aureus*, PBP3 from *Streptococcus pneumoniae* (1xp4) and PBP5 from *E. coli* (3mze) shown in light brown, blue, and green respectively.

anchored to the membrane while *S. aureus* PBP4 is C-terminally anchored. As shown in figure 2.5, the C-terminal domain has the most structural variation between *S. aureus* PBP4 and closely related PBPs in the PDB. The implications of structural variations in these potentially dynamic accessory domains are currently not fully understood in terms of ultimate enzymatic specificity and activity, hindered by the hurdle of isolating homogenous PG substrates for atomic resolution analysis. Future experiments identifying and structurally characterizing the binding site of the PG acceptor strand in transpeptidases will help elucidate the mechanism by which the PG acceptor strand is selected to participate in deacylation over water, as is used in carboxypeptidases.

Movement of two loops (L1 and L2) bordering the active site causes reorientation of the serine hydroxyl of the *SXN* motif in PBP4^{CRB} structures (Figs. 2.3 and B6). L1 includes residues which directly interact with the *SXN* motif, while L2 includes the *SXN* motif, common to PBPs and containing key mechanistic residues as described above (33, 58, 60, 180, 184). It is intriguing to note that in all the ligand bound PBP4^{CRB} structures, the open conformation of L1

and L2 is adopted with the SXN motif serine (Ser-139) hydroxyl pointing away from the active site. In PBPs the SXN motif serine hydroxyl is typically positioned between the serine of the SXXK and lysine of the KTG motifs. This provides the hydrogen bonding and electrostatic environment for catalysis allowing the necessary serine hydroxyl mediated protonation of the leaving group nitrogen of the D-Ala-D-Ala peptide substrate or alternatively of the β -lactam antibiotic ring (substrate analogs). Indeed, the PBP4^{CRB} structures with ceftaroline and nafcillin both indicate significant displacement of the SXN motif located in L2, compared to the PBP4 structure with the same ligands (Figs. 2.3 and B6C-D). While the sequence is not conserved, analogous structures to the L1 loop can be found in Class A, B, and C PBPs and perturbation of this loop has been shown to play a role in β -lactam resistance (63, 180, 185). Notably, PBP2x from a highly mutated, penicillin-resistant strain of *Streptococcus pneumoniae* PBP2x, was also found to have variation in positioning of the SXN motif with the serine hydroxyl displaced away from the active site when compared to penicillin-sensitive PBP2x variants (186). In contrast, with PBP4 and PBP4^{CRB} the movements of the SXN motif appear to be mediated by a combination of the particular drug bound to the catalytic serine and the presence of the missense mutations in PBP4^{CRB}, underlining the complexity of predicting resistance patterns in these variants.

The similar catalytic constants (k_{cat} values) of PBP4 and PBP4^{CRB} for the three tested β -lactam antibiotics (Table 2.4) suggests that the two substitutions in PBP4^{CRB} do not affect the rate-limiting step of β -lactam hydrolysis. Previous studies have established that deacylation is rate-limiting in PBP4 (181) with rate constants for deacylation (k_3) of penicillin from several penicillin-sensitive and -resistant strains ranging from 0.4 to $3.4 \times 10^{-3} \text{ s}^{-1}$ (181). These values are very similar to the k_{cat} values of PBP4 and PBP4^{CRB} found here, suggesting that deacylation is

also rate-limiting in the turnover of ceftaroline, ceftobiprole, and nitrocefin. Despite the variation in the positioning of the *SXN* motif in the eight crystal structures presented here, and the overall higher B-factors suggesting potential dynamic motion (Fig. B9), we do not observe significant changes in deacylation rates of the associated variants. It therefore follows that the *S. aureus* PBP4 *SXN* motif may primarily be involved in acylation. In the structures presented here the distances between the *SXN* serine (Ser-139) and the leaving group β -lactam nitrogen ranges from 3.5 – 5.7 Å, suggesting that it is in a position to take part in catalysis when loops L1 and L2 are in the closed conformation but not when they are in the open conformation (Table 2.5; Fig. 2.3). While it has been suggested that this motif plays a role in deacylation in the structurally similar PBP5 of *E. coli* (60, 180, 184), perturbation of the *SXN* motif in PBP2, a transpeptidase from *Neisseria gonorrhoeae*, has been previously shown to reduce penicillin acylation rates (185). Future work is needed to determine the individual rate constants of acylation and deacylation in PBP4 and PBP4^{CRB} to better understand the role of the displaced and/or dynamic motion of the *SXN* motif in *S. aureus* PBP4 and the general resistance phenomenon it mediates.

Table 2.5: Distances between the β -lactam leaving group nitrogen and the S139 hydroxyl (Å)

β-lactam	PBP4	PBP4^{CRB}
Ceftobiprole	5.3	5.1
Ceftaroline	3.5	4.8
Nafcillin	3.6	5.7

Our 8 isomorphous high-resolution structures allow comparison of hydrogen bonding between the ligand and protein or solvent in the PBP4 and PBP4^{CRB} structures, as summarized in Table 2.6. Interestingly, in the PBP4^{CRB} structures all three ligands examined here appear to have

additional hydrogen bonds to water compared to ligands in the PBP4 structures. While the number of hydrogen bonds between the ligand and protein residues are relatively similar there are differences in the ligand hydrogen bonding networks to water and protein that may facilitate resistance.

Table 2.6: Number of hydrogen bonds to each ligand in PBP4 and PBP4^{CRB} structures

β-lactam	Number of hydrogen bonds to protein		Number of hydrogen bonds to water	
	PBP4	PBP4^{CRB}	PBP4	PBP4^{CRB}
Ceftobiprole	7	7	5	8
Ceftaroline	4	5	6	7
Nafcillin	5	5	1	2

The steady-state kinetic parameters we determined for PBP4^{CRB} and ceftobiprole are consistent with the *S. aureus* CRB resistance phenotype for this β-lactam drug. The lower catalytic efficiency of PBP4^{CRB} for ceftobiprole suggests it does not compete as effectively with the enzyme's physiological substrate and further supports the important role of the *pbp4* missense mutations (E183A and F241R) in our proposed mode of ceftobiprole resistance. Given this, we note, the K_M values of PBP4 and PBP4^{CRB} with ceftobiprole determined here ($1.1 \pm 0.7 \mu\text{M}$ and $170 \pm 20 \mu\text{M}$, respectively) agree remarkably well with the minimum inhibitory concentrations (MIC) of *S. aureus* COLnex and *S. aureus* CRB, ($1 \mu\text{g/mL}$ ($2 \mu\text{M}$) and $128 \mu\text{g/mL}$ ($239 \mu\text{M}$) respectively) (182). Furthermore, the MIC for *S. aureus* COLnex P_{CRB} *pbp4* (a COLnex strain with the same *pbp4* promoter mutation found in *S. aureus* CRB) was $4 \mu\text{g/mL}$ for ceftobiprole (182) suggesting this promoter mutation only plays a minor role in *S. aureus* CRB ceftobiprole resistance.

Our data also indicate the mechanisms of PBP4 mediated resistance in *S. aureus* may differ depending on the β -lactam antibiotic challenge. The similar kinetic parameters of PBP4 and PBP4^{CRB} for ceftaroline may indicate that the missense mutations in PBP4^{CRB} may not be the sole determinant of resistance to this drug. Instead, the previously described *S. aureus* CRB *pbp4* promoter mutation (P_{CRB}*pbp4*) may play a more pivotal role in this case (182). The ceftaroline MICs were 64 and 32 μ g/ml for *S. aureus* CRB and *S. aureus* COLnex P_{CRB}*pbp4* (182), supporting the significance of P_{CRB}*pbp4* in ceftaroline resistance. As *S. aureus* COLnex was passaged in ceftobiprole to generate the CRB strain (138), the mutations in PBP4^{CRB} may not be optimal for ceftaroline resistance, particularly considering that passaging *S. aureus* in ceftaroline resulted in different *pbp4* mutations than those seen for *S. aureus* CRB (144).

Collectively, we provide evidence *S. aureus* CRB employs at least two different PBP4-mediated mechanisms of resistance. High-level ceftobiprole resistance in this strain is heavily reliant on two PBP4 missense mutations, E183A and F241R. In contrast, the CRB strain resistance to ceftaroline appears less influenced by PBP4^{CRB} mutations and is instead at least partially conferred by increased expression of PBP4. These results have implications for screening and diagnostics of *S. aureus* infections as well as monitoring programs. As neither of these resistance mechanisms utilize PBP2a, even advanced PCR screening for *mecA*, *mecC*, or the staphylococcal cassette chromosome *mec* element as has previously been used (187) may not identify *S. aureus* infections with high-level β -lactam resistance. Indeed, *mecA* negative strains with high-level β -lactam resistance have already been observed in the clinic (145). Thus, our studies here recommend a more thorough investigation of potential resistance genes rather than simply looking for the presence of PBP2a when screening for MRSA. This work also emphasises the importance of PBP4 in *S. aureus* high-level β -lactam resistance and indicates the potential of

combination therapies targeting PBP4 and other PBPs as noted previously (83). Additionally, our high-resolution acyl-enzyme intermediate structures of PBP4 and PBP4^{CRB} provide a starting point for structure-aided drug design of improved PBP4 inhibitors.

Chapter 3: Structural analysis of avibactam-mediated activation of the *bla* and *mec* divergons in methicillin-resistant *Staphylococcus aureus*

3.1 Introduction

Staphylococcus aureus is an important Gram-positive pathogen infecting humans and livestock around the world (188). While *S. aureus* commonly forms part of the human microbiome as a commensal species, it also causes serious disease as an opportunistic pathogen in both nosocomial and community settings (189). Methicillin resistant *S. aureus* (MRSA) strains cause particularly notorious infections, due to their virulence and the reduced treatment options available (188).

While the β -lactam class of antibiotics has long been successfully used to inhibit penicillin-binding proteins (PBPs) and continues to be the most commonly prescribed class of antibiotics (190), this antibiotic class is now frequently ineffective in treating MRSA infections. *S. aureus* resistance to β -lactam antibiotics is facilitated by the β -lactamase PC1 (9, 72) and penicillin-binding protein 2a (PBP2a) (62, 72). PC1 is a Class-A β -lactamase which protects the bacterium by catalyzing the hydrolysis of the β -lactam ring, thereby preventing inhibition of PBPs (9). Expression of *pbp2a* enables broad-spectrum β -lactam antibiotic resistance via its sterically hindered active site (62) which is proposed to open when peptidoglycan (PG) binds to its allosteric site (78). Expression of *blaZ* (the gene coding for PC1) and *pbp2* are encoded and regulated by the *bla* and *mec* divergons in MRSA with similar pathways existing in *Bacillus licheniformis* (101) and the pathogen *Clostridium botulinum* (102).

A schematic of the *bla* and *mec* pathways is shown in figure 3.1. Expression of *blaZ* is regulated by two proteins: BlaR1 and BlaI. BlaR1 is a 69.3 kDa polytopic α -helical membrane

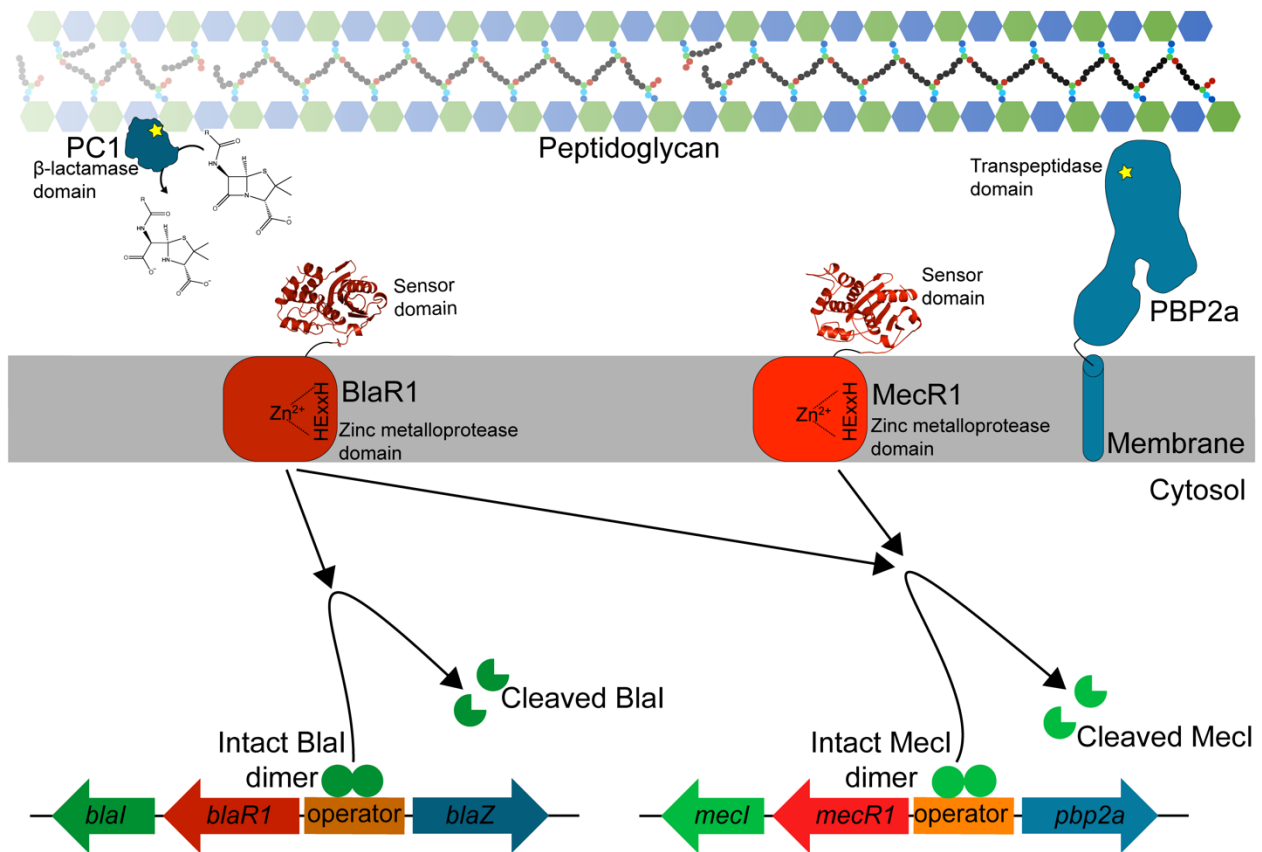


Figure 3.1: A schematic of the *bla* and *mec* divergents and their associated proteins. Upon acylation of the BlaR1 and MecR1 sensor domains with β -lactam antibiotic, BlaI and MecI are cleaved leading to derepression of the divergents. The β -lactamase PC1 is then expressed and transported across the cell membrane while PBP2a is tethered to the extra-cellular side of the membrane by its single transmembrane helix.

protein with a predicted amino-terminal zinc-metalloprotease domain and carboxy-terminal penicilloyl serine transferase extracellular domain that functions as a β -lactam sensor. BlaI is a transcriptional repressor that regulates the expression of *blaI*, *blaR1*, and *blaZ* by binding to the operator and restricting transcription of the divergon (104). The *mec* divergon is closely analogous to the *bla* divergon with a sensor/transducer protein, MecR1, and a repressor protein MecI, both regulating the expression of *pbp2a* (191). The close protein sequence identities of the corresponding proteins in the pathway (MecR1/BlaR1, 35%; MecI/BlaI, 61%) suggests the *mec* and *bla* pathways are similarly regulated and indeed, BlaR1 can regulate the *mec* pathway in the absence of MecR1 (103). Acylation of BlaR1/MecR1 sensor domains (here denoted BlaR1^{SD} and

MecR1^{SD} respectively) by a β -lactam antibiotic is hypothesized to activate the zinc metalloprotease domain of both proteins, leading to the cleavage of the repressor (BlaI/MecI).

Searches of the PDB using the Dali server reveal BlaR1^{SD}/MecR1^{SD} most closely resemble the Ambler class-D β -lactamases (176). The top match for both sensor domains is the Class-D β -lactamase, YbxI, from *Bacillus subtilis* (PDB ID: 5e2f) (Dali Z scores of 30.5/34 and C α RMSD of 3.7/3.0Å over 212/216 atoms for BlaR1^{SD} and MecR1^{SD} respectively).

BlaR1^{SD}/MecR1^{SD} are also structurally very similar to the Gram-negative class-D β -lactamases, OXA-10 from *Pseudomonas aeruginosa* (e.g. PDB ID: 4s2o) and OXA-48 from *Klebsiella pneumoniae* (e.g. PDB ID: 4s2k).

Both sensor domains have the three canonical catalytic motifs found in all penicillin-binding proteins and β -lactamases: SXXK, (S/Y/F)X(N/C), and (K/H)(S/T)G (33, 192). Despite close structural similarity to OXA-10/48 both the sensor domains have an SXN motif instead of (Y/F)XN common in the class-D β -lactamases (192).

The sole function of a β -lactamase is to hydrolyse β -lactam antibiotics as efficiently as possible, affording drug resistance to the pathogen. In contrast, BlaR1 and MecR1 function as receptors and therefore it is presumably advantageous to have a slow deacylation rate to allow signal propagation even in the presence of low concentrations of β -lactams. While both class-D β -lactamases and the sensor domains described here bind β -lactams, a key difference between the BlaR1/MecR1 sensor domains and β -lactamases is their deacylation rates. Deacylation in class-D β -lactamases is thought to occur when the carboxy-lysine of the SXXK motif abstracts a proton from the hydrolytic water (193). This activated nucleophile then attacks the α -carbon of the acyl-enzyme intermediate, causing the enzyme to be regenerated (193). The BlaR1 sensor domain has also been found to have a carboxylated SXXK motif lysine in the ligand-free form

(194). However, lysine carboxylation is lost upon acylation of the BlaR1 SXXK motif serine (121). The sensor domains are thought to retard the regeneration of the carboxy-lysine via hydrogen bonding between the N- ζ of the lysine and a nearby asparagine side chain (Asn-339 in BlaR1 and Asn-341 in MecR1) (194, 195).

Efforts to re-potentiate β -lactams rendered ineffective by the presence of the Class-A serine β -lactamases have been made using a combination therapy of β -lactam antibiotic and β -lactam based β -lactamase inhibitor (196). Further research with diazabicyclooctane based inhibitors led to the development of the first clinically used non- β -lactam β -lactamase inhibitor, avibactam. Once avibactam is carbamylated to the β -lactamase active site serine it has a very slow rate of decarbamylation. Further, upon eventual processing, intact avibactam is produced instead of a hydrolysed product as is found with conventional β -lactam based β -lactamase inhibitors (Fig. 3.2) (197, 198).

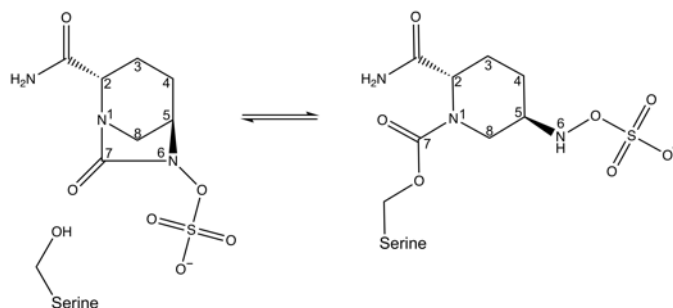


Figure 3.2: Structure of intact and carbamylated avibactam.

New broad-spectrum antibiotics are critically needed to allow treatment prior to the identification of the bacterial species causing the infection. Avibactam in combination with the β -lactam ceftazidime has since been approved in the US by the FDA to treat complicated urinary tract infections, intra-abdominal infections, hospital-acquired bacterial pneumonia, and ventilator-associated bacterial pneumonia (199). While ceftazidime/avibactam combination

therapy is currently indicated in the treatment of Gram-negative organisms, studies have shown that combination therapy with ceftaroline and avibactam is additionally effective against clinical isolates of MRSA and pathogenic Gram-negative bacteria such as *Enterobacteriaceae*, *Pseudomonas aeruginosa*, and *Acinetobacter* spp. suggesting avibactam could be useful in treating infections where the causative pathogen has yet to be identified or where a broad-spectrum antibiotic is needed (200–202).

While avibactam has shown promise as a β -lactamase inhibitor, it has also been shown to influence transcription of the β -lactamase gene *ampC* found in *Enterobacter cloacae* with effects ranging from strong upregulation of *ampC* transcription to no detectable upregulation in other strains (203, 204). For these reasons we are interested as to whether avibactam, a non- β -lactam, can also activate the *bla* and *mec* pathways of MRSA in a similar way as for conventional β -lactam antibiotics or whether it inhibits these pathways by preventing β -lactams from binding. In this paper we show evidence that avibactam binds to the BlaR1^{SD} and MecR1^{SD} and upregulates *blaZ* and *pbp2a* expression in the *S. aureus* SF8300, a USA300 clone. The USA300 MRSA clone is a leading cause of MRSA infections in the USA (205, 206). Additionally, we use X-ray crystallography to visualize the molecular interactions between avibactam and the sensor domains of BlaR1 and MecR1. While avibactam adopts a single conformation in MecR1^{SD}, it is oriented in two, approximately equally occupied, conformations in the BlaR1^{SD} active site. These findings have potential relevance for drug discovery efforts and MRSA treatment.

3.2 Methods

3.2.1 Expression and purification of BlaR1^{SD} and MecR1^{SD}

The sensor domains of *S. aureus mecR1* (coding for residues Ser-334 – Ile-585) (UniProt ID: P0A0B0) and *S. aureus blaR1* (coding for residues Met-330 – Gln-585) (UniProt ID:

P18357) were expressed from a pET28a vector with a cleavable N-terminal deca-histidine tag in *Escherichia coli* BL21 (DE3). Cells were grown in LB media supplemented with 50 $\mu\text{g mL}^{-1}$ kanamycin at 37°C to $\text{OD}_{600} = 0.5-0.8$ with 225 rpm shaking before being cooled at 4°C for 30-60 minutes and induced with a final concentration of 100 mM isopropyl β -D-1-thiogalactopyranoside (IPTG). Cells were incubated at 17°C overnight with shaking before being harvested by centrifugation and stored at -80°C.

Cell pellets from 4.5-9 L were thawed and resuspended in buffer A (20 mM Tris, pH 7.5; 20 mM imidazole; 500 mM sodium chloride) with either cOmplete, EDTA-free protease inhibitor cocktail tablet (Roche) or Protease Inhibitor Cocktail Set II, EDTA free (Calbiochem) and Bovine DNase Type I (Roche) to a final concentration of $\sim 10 \text{ ng mL}^{-1}$. Future steps were carried out at 4°C unless noted otherwise. Cells were lysed in a homogenizer (Avestin) followed by centrifugation at 45,000 rpm for 45 minutes in a Type 70Ti rotor (Beckman Coulter). The supernatant was filtered through a 0.45 μm membrane and loaded onto a 1 mL HisTrap HP column (GE Healthcare Life Sciences) pre-equilibrated with buffer A. The column was washed with buffer A until the flow-through absorbance at 280 nm stabilized and the protein was eluted with a linear gradient of buffer B (20 mM Tris, pH 7.5; 1 M imidazole; 500 mM sodium chloride) to 500 mM imidazole over 40 minutes at a flow rate of 1 mL min^{-1} . Fractions were analyzed via SDS-PAGE and those containing high-levels of the protein of interest were pooled. The polyhistidine tag on MecR1^{SD} was removed with a 40:1 (mol:mol) protein to TEV protease ratio before while being dialyzed in buffer A overnight. This produced protein with an amino terminus Gly-His-Met sequence before the MecR1^{SD} protein sequence. The polyhistidine tag on the BlaR1 construct was cleaved overnight with a 1:1000 (v/v) ratio of bovine α -thrombin (Hematologic Technologies Inc.) to protein ratio following desalting of the sample into buffer C

(20 mM Tris, pH 8; 200 mM NaCl). This produced BlaR1^{SD} protein with an amino terminus sequence starting with GSH followed by the BlaR1^{SD} protein. The sample was then concentrated on a 10 kDa molecular weight cut off Centricon (Amicon) and imidazole was added to 20 mM if necessary, before being run on a 1 mL HisTrap HP column (GE Healthcare Life Sciences) pre-equilibrated with buffer A. The flow-through was collected and concentrated as above before being loaded on a Superdex 75 10/300 column (GE Healthcare Life Sciences) pre-equilibrated with buffer C. Fractions with purified protein were pooled, concentrated as above, flash frozen in liquid nitrogen, and stored at -80°C.

3.2.2 Crystallization of BlaR1^{SD} and MecR1^{SD}

Avibactam bound BlaR1^{SD} crystals were grown using the sitting drop vapor diffusion method at 23 °C in 24 well plates. Drops contained 1 µL of 20 mg mL⁻¹ protein preincubated with 4 mM avibactam and an equal volume of precipitant (200 mM tri-potassium citrate, 20% PEG3350). The BlaR1^{SD} precipitant solution was made without addition of acid or base, but the final pH was ~8.1. Crystals were seeded by twirling a housecat whisker in a drop containing avibactam bound BlaR1^{SD} crystals and then moving the whisker through the freshly set up drop.

MecR1^{SD} was crystalized in a 1:1 volume ratio of MecR1 protein at 7.5 mg mL⁻¹ preincubated with 1 mM oxacillin and precipitant solution (2.5 M ammonium sulphate, 50 mM HEPES pH 7.5) producing a total drop volume of 2 µL. Drops were set up in 24 well sitting drop plates and incubated at 23°C.

3.2.3 Soaking and harvesting crystals

Avibactam (Fedora Pharmaceuticals or Cayman Chemical Company) stock solution was made in DMSO. Avibactam was soaked into MecR1^{SD} crystals by adding 3 µL avibactam soaking solution (9 mM avibactam diluted in an equivolume ratio of Buffer C and precipitant

solution) to the 2 μ L crystallization drop. The crystals were soaked for 2 to 40 minutes before the crystals were looped and passed through cryo protectant solution (3 mM avibactam and 20% glycerol diluted in a 1:1 ratio of crystal buffer and precipitant solution) before vitrification in liquid nitrogen. This avibactam concentration and soaking time was sufficient to outcompete the existing oxacillin in the crystallization drop.

BlaR1^{SD} avibactam co-crystals were cryo protected by adding 10 μ L of cryo protectant solution (30% glycerol and 5 mM avibactam diluted in mother liquor) directly to the 2 μ L crystallization drop before looping and vitrification in liquid nitrogen.

3.2.4 Data collection and processing

All X-ray diffraction data were collected at the Canadian Light Source, beamline ID-08. Data were processed with Xia2 (160) using XDS (161), and Aimless (162) from the CCP4 (163) program suite. The avibactam bound BlaR1^{SD} and MecR1^{SD} structures were solved by molecular replacement using Phaser (164), with chain A of PDB ID: 1xa1 and 2iwb respectively. The Phenix program suite (165) was used for model building and refinement with AutoBuild (166) initially being used. Models were built with several cycles of manual rebuilding in *Coot* (167), followed by refinement using phenix.refine (168). TLS groups determined using the TLS Motion Determination server (207, 208) were used later in refinement. Avibactam was added manually after several rounds of refinement by examination of the $F_o - F_c$ and $2F_o - F_c$ electron density maps. Coordinates and structure factors were deposited to the PDB with accession codes (6o9w) and (6o9s) for BlaR1^{SD} and MecR1^{SD} avibactam structures respectively. Figures 3.5-7 and figures in the appendix C, C1, C5, C7-C10, and C12-C13 were designed using PyMol (Schrödinger, LLC, New York) while C3 – C5 were created using LIGPLOT⁺ (172). Electrostatic potential surfaces

in figure C10 were calculated using PDB2PQR (209) and APBS (210) plugins in PyMol. Chain B of the BlaR1^{SD} avibactam structure was used for all analysis.

3.2.5 In silico ligand docking into BlaR1^{SD} and MecR1^{SD} avibactam structures

All preparation and covalent docking calculations were performed in the Molecular Operating Environment (MOE, version 2009, Chemical Computing Group Inc., Canada). Covalent docking was performed using atomic contact count, force field-based, and shape-based scoring functions (211). For all in silico docking calculations, chain B of the BlaR1^{SD} avibactam structure and chain A of the MecR1^{SD} avibactam structure were used. Protein modules were prepared for docking by including any missing sidechains, removing the avibactam ligand, and protonating the model. The catalytic serine (Ser-389 in BlaR1 and Ser-391 in MecR1) sidechain was restored to its unreacted form for docking with the unhydrolysed form of the ligand and MOE was used to create a reaction file for the β -lactam ring opening.

3.2.6 Molecular dynamic simulations of avibactam with BlaR1^{SD} and MecR1^{SD}

Protein models were prepared as described for the *in silico* docking. Molecular dynamics (MD) simulations were performed using Desmond package from Schrödinger (212). The setting for each simulation: an SPC water solvent model; orthorhombic simulation box shape; NPT ensemble with a pressure of 1.01325 bar and temperature 300 K. The simulations were run for 40 nanoseconds with approximately 1000 frames. Figure 11 in appendix C was created with output from the Desmond package and edited to show all residues interacting with avibactam for at least 20% of the duration of the simulation.

3.2.7 Size exclusion chromatography multi-angle light scattering

Purified *S. aureus* BlaR1^{SD}, with or without 5 mM avibactam, or MecR1^{SD} applied to a size exclusion column (Superdex 75 10/300 column (GE Healthcare) for BlaR1^{SD} and Superdex

200 10/300 column (GE Healthcare) for MecR1^{SD} using an Agilent 1100 series HPLC (Agilent Technologies), that was coupled in-line to a Dawn® HeleosTMII 18-angle MALS light scattering detector, and Optilab® T-rEXTM differential refractometer protein detector (both from Wyatt Technology). The light scattering detectors were first normalized using monomeric bovine serum albumin (Sigma-Aldrich). A total of 100 µg of purified protein sample was injected on the column, pre-equilibrated in running buffer (20 mM Tris pH 7.5 or 8, 150 mM NaCl). Data were collected and analysed using the Astra 6 software. The protein absolute molecular weight was calculated assuming a dn/dc value of 0.185 mL/g and a theoretical extinction coefficient of 2.04 ml (mg cm)⁻¹ for BlaR1^{SD} and 1.94 mL (mg cm)⁻¹ for MecR1^{SD}.

3.2.8 Thermal aggregation assays

BlaR1 and MecR1 sensor domain protein was thawed on ice and diluted in assay buffer (100 mM sodium phosphate, pH 7.0) to a final concentration of 0.5 mg ml⁻¹. Ampicillin (Fisher), avibactam (Cayman Chemical), nafcillin (Sigma), and kanamycin (Gold-Bio) were serially diluted in assay buffer and mixed with the protein samples. 9 µL of sample was added to each well of a 384 well plate (Corning, 3540). The four replicates of each condition were pipetted into the plate, the plate was briefly centrifuged, 11 µL mineral oil was added to overlay the samples, and the plate was centrifuged again. The plate was then assayed with differential static light scattering (Stargazer2, Epiphyte Three Inc.) while increasing the temperature at 1°C min⁻¹ from 25-85°C. The data were analysed using Stargazer AIR (Epiphyte3) software and the temperature of aggregation (Tagg) was found using Boltzmann regression. By subtracting the Tagg at a given drug concentration from the Tagg in the absence of drug the ΔTagg was calculated to give an idea of the stability gained or lost with a particular compound.

3.2.9 Quantitative Real-Time PCR of *blaZ* and *pbp2a*

Quantitative Real-Time PCR (qRT-PCR) was carried out as before (143) with a few modifications. Briefly, overnight culture of *S. aureus* SF8300 strain was sub-cultured in TSB media and grown for 2 hours at 37°C with constant shaking. 10 ml of the bacterial culture was aliquoted in 50 ml conical tubes and antibiotics were added to attain the desired condition. The resultant bacterial cultures were incubated for an additional 1 hour and approximately 10^9 bacterial cells were harvested for RNA isolation. Bacterial total RNA was isolated using Qiagen RNeasy Mini kit and following treatment of the RNA with DNase (Ambion), cDNA was synthesized using Superscript IV (Thermo Fischer Scientific). Absolute quantification of genes was carried out using SYBR Green qRT-PCR master mix (Thermo Fischer Scientific) and the primers indicated in table 1C. Each experiment was carried out in triplicate and *gyrB* gene was used as housekeeping control. Groups given avibactam or nafcillin were compared to the DMSO control using a one-way ANOVA with the Dunnett multiple comparison test in GraphPad Prism version 8.3.1.

3.3 Results

3.3.1 Effect of avibactam on gene expression of *pbp2a* and *blaZ*

Avibactam activates expression of the *bla* and *mec* divergons in *S. aureus* SF8300, a USA300 clone of MRSA (Fig. 3.3). *S. aureus* SF8300 lacks MecR1 from the *mec* divergon so *pbp2a* expression is under the control of BlaR1. Both *pbp2a* and *blaZ* mRNA transcripts were upregulated by avibactam at concentrations of $\geq 8 \mu\text{g mL}^{-1}$ with further increased expression at 16, 32, and $64 \mu\text{g mL}^{-1}$. Expression levels of *pbp2a* and *blaZ* mRNA transcripts at $2 \mu\text{g mL}^{-1}$ were comparable with the DMSO control used.

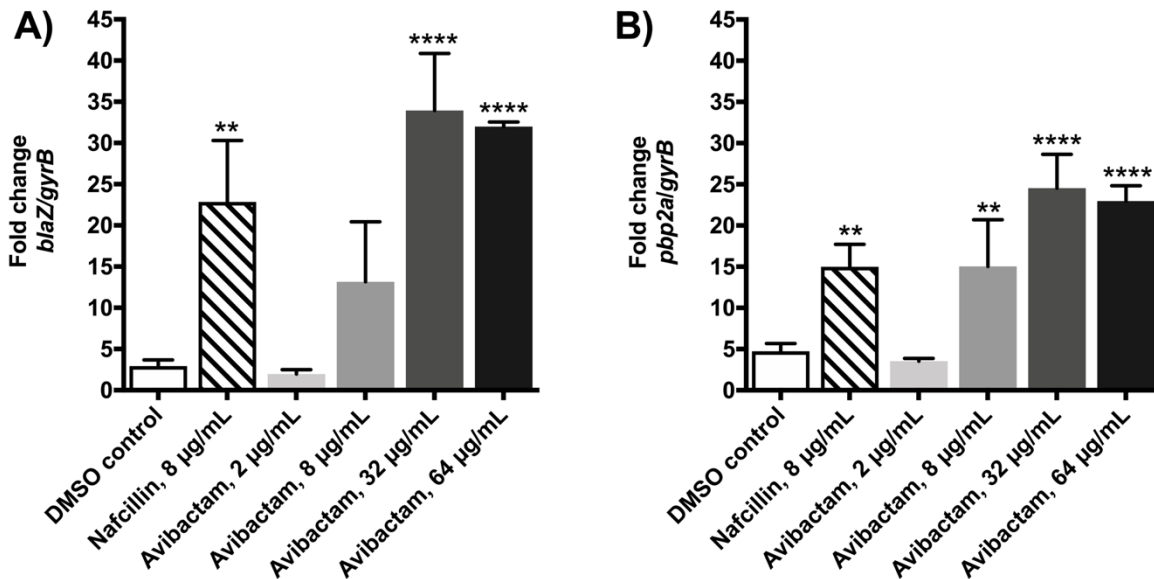


Figure 3.3: Avibactam upregulates *blaZ* and *pbp2a* transcripts in *S. aureus* SF8300. qRT-PCR analysis of A) *blaZ* and B) *pbp2a* gene expression relative to *gyrB* expression upon exposure to the indicated chemicals. Values shown reflect the mean with error bars displaying standard deviation (n=3). **, $p < 0.01$; ****, $p < 0.0001$

3.3.2 Thermal stability of BlaR1^{SD} and MecR1^{SD} with avibactam and β -lactam antibiotics

Avibactam binding to the BlaR1^{SD} and MecR1^{SD} affects their thermal stability differently. The thermal stability of the sensor domains was measured in the presence of a range of concentrations of different β -lactam antibiotics and avibactam using differential static light scattering. Avibactam appears to increase the thermal stability of MecR1^{SD} by 2.6°C, while minimally affecting BlaR1^{SD} thermal stability (0.4°C of stabilization) (Fig. 3.4). Similarly, nafcillin also appears to confer different effects on the two proteins, but with the opposite effect, stabilizing BlaR1^{SD} but having little effect on MecR1^{SD}. As expected, both sensor domains show an increase in ΔT_{agg} when acylated by ampicillin and were not affected by the control antibiotic kanamycin for which they are not a target.

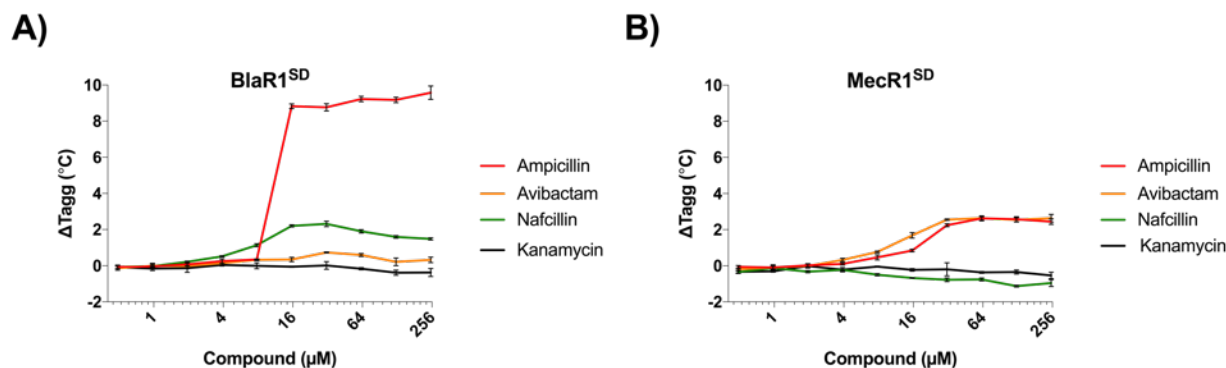


Figure 3.4: Thermal stabilization of the A) BlaR1 and B) MecR1 sensor domains with ampicillin, avibactam, nafcillin, and kanamycin. ΔTagg was calculated by subtracting the Tagg for ligand-free protein from the Tagg for a particular ligand and concentration. Four replicates were conducted for each condition and concentration while the error bars display standard deviation.

3.3.3 BlaR1^{SD} and MecR1^{SD} avibactam crystal structures

BlaR1^{SD} and MecR1^{SD} avibactam X-ray crystallographic co-structures were solved to 2.0 and 1.6 Å resolution respectively with excellent statistics and no Ramachandran outliers (full data collection and refinement statistics shown in Table 3.1). BlaR1^{SD} crystals were obtained in potassium citrate and PEG3350 at pH 8.1 while MecR1^{SD} crystals formed in ammonium sulfate at pH 7.5. Avibactam was modelled with a total occupancy of 1 in both structures with clear electron density supporting modelled positions as shown by $2mF_o-DF_c$ maps (Fig. 3.5) and mF_o-DF_c volume omit maps (Fig. C1). In both structures avibactam is covalently bound to the catalytic serine of BlaR1 (Ser-389) or MecR1 (Ser-391) SXXK motifs with the C7 carbonyl group coordinated in the oxyanion hole by the backbone nitrogen atoms of Ser-389 and Thr-529 in BlaR1 (Ser-391 and Thr-531 in MecR1) (Fig. 3.5). Interactions between avibactam and BlaR1^{SD} or MecR1^{SD} are also depicted in figures created with LigPlot⁺ (Figs. C2-C4). Remarkably, avibactam is observed covalently bound in two alternate orientations to BlaR1^{SD} while in MecR1^{SD} it is only present in one orientation (Fig. 3.5). Despite MecR1^{SD} being co-crystallized initially with oxacillin (oxacillin was included to aid in the initial formation of

Table 3.1: Data collection and structure refinement statistics for the BlaR1^{SD} and MecR1^{SD} in covalent complex with avibactam

Data collection		
Structure	BlaR1 ^{SD} -avibactam	MecR1 ^{SD} -avibactam
PDB ID	6o9w	6o9s
Beamline	CLS-08ID-1	CLS-08ID-1
Space group	P12 ₁ 1	P4 ₁ 2 ₁ 2
Cell dimensions		
<i>a</i> , <i>b</i> , <i>c</i> (Å)	53.4, 92.6, 56.5	58.7, 58.7, 147.6
α, β, γ, (°)	90.0, 104.6, 90.0	90.0, 90.0, 90.0
Wavelength (Å)	0.9793	0.9794
Resolution (Å)	46.32-1.95 (2.02-1.95)	45.93-1.59 (1.65-1.59)
<i>R</i> _{merge}	0.094 (0.915)	0.049 (0.502)
<i>CC1/2</i>	0.997 (0.639)	0.999 (0.812)
<i>I</i> / <i>σI</i>	10.05 (1.31)	21.73 (2.59)
Completeness (%)	99.58 (99.51)	99.1 (92.9)
Redundancy	3.4 (3.4)	6.7 (4.4)
Refinement		
Resolution (Å)	2.0	1.6
No. reflections	38592 (3840)	35297 (3214)
<i>R</i> _{work} / <i>R</i> _{free}	0.185/0.225	0.158/0.197
No. non-hydrogen atoms		
Macromolecules	3984	2290
Ligand/ion	34/0	17/5
Water	168	159
B-factors (Å ²)		
Protein	39.8	27.2
Ligand	32.4	33.2
Ion	-	105.9
Water	41.3	38.3
RMSD		
Bond lengths (Å)	0.010	0.007
Bond angles (°)	1.02	0.95
Favoured/allowed/disallowed (%)	97.4/2.6/0.0	98.0/2.1/0.0

Data corresponds to diffraction from a single crystal for each structure.

*Highest resolution shell is shown in parenthesis.

crystals), the resulting electron density shows unequivocally that soaking with high concentrations of avibactam post crystallization successfully displaced the oxacillin. Although backsoaking is a commonly used technique for hard to crystallize proteins, there is always the possibility that this method prevented a second conformation of avibactam binding. However, we do point out the close similarity of the MecR1^{SD} ligand-free structure determined in a different space group, the prior oxacillin structure, and our avibactam structure here (Table 3.2) would suggest the latter's conformation is not being influenced or modulated by the initially present oxacillin.

The two conformations of avibactam in the BlaR1^{SD} structure are orientated approximately 180° to the other (Fig. 3.5A-C). The occupancy of the two avibactam conformations was allowed to float during refinement in Phenix.refine (168) resulting in occupancies of 0.58 and 0.42 for conformation A (Fig. 3.5A) and conformation B (Fig. 3.5B) respectively. Thr-529 forms hydrogen bonds with both conformations but at opposite termini of avibactam, interacting with the sulfate of conformation A and the C2 carboxamide of conformation B. The avibactam sulfate in conformation A, in keeping with the electronegative carboxylate of typical β -lactam substrates, projects toward an electropositive pocket formed by Lys-526 and Thr-527 of the KTG motif as well as Thr-529. The sulfate in conformation B on the other hand, is coordinated by hydrogen bonds to the δ -N of Asn-388, the backbone nitrogen of Ile-531, and via a water coordinated by the backbone carbonyl of Ile-531 (Figs. 3.5B-C). Avibactam is bound to MecR1^{SD} in a similar orientation as conformation A in the BlaR1^{SD} structure with analogous conserved residues Ser-439, Thr-529, Thr-531, and Lys-528 forming hydrogen-bonds with the sulfate moiety of avibactam, while the C2 carboxamide at the opposite

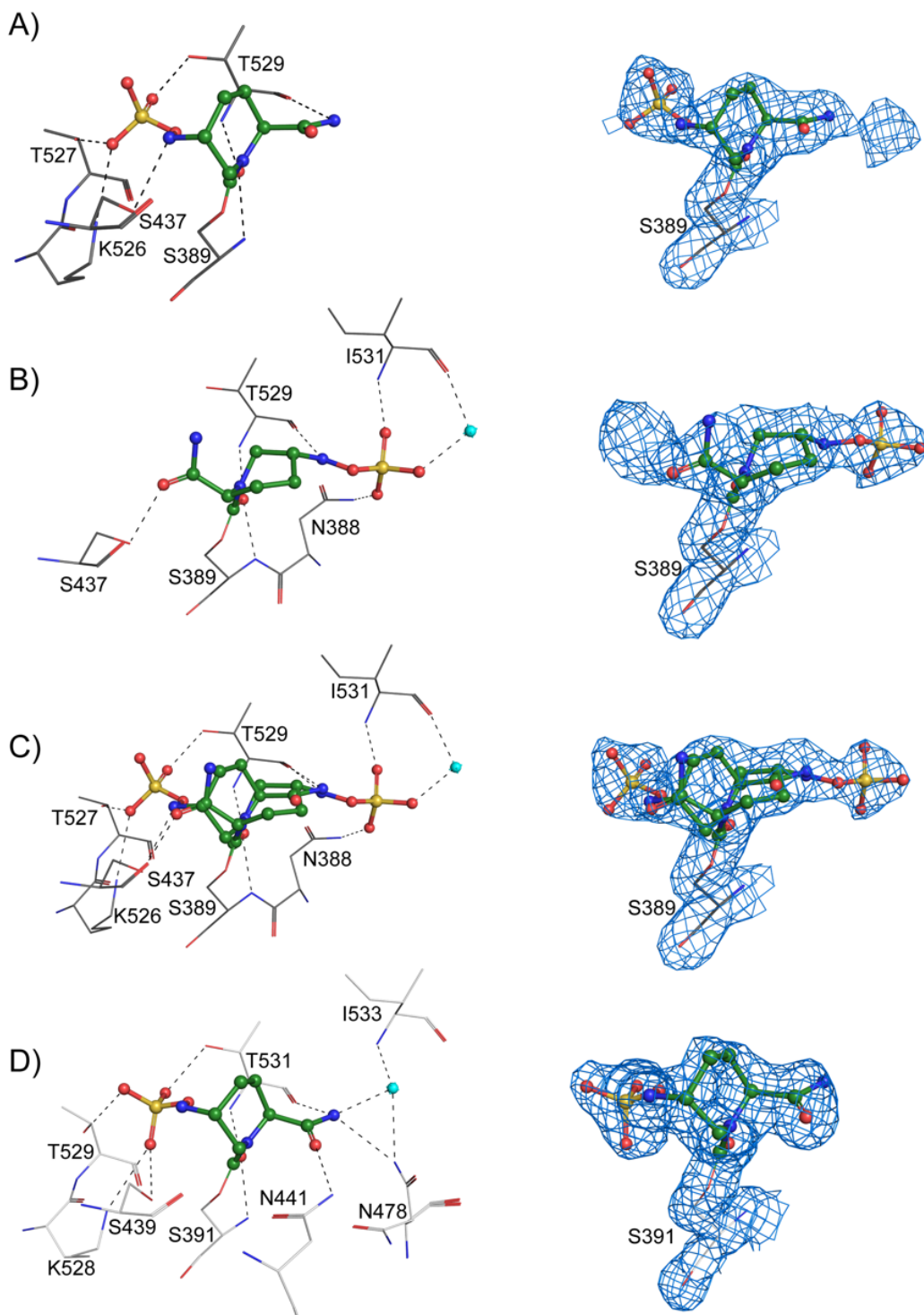


Figure 3.5: Active site of BlaR1^{SD} and MecR1^{SD} in complex with avibactam. Avibactam is shown in the active site of BlaR1^{SD} in either A) conformation A, B) conformation B, C) conformation A and B together, or D) in the MecR1^{SD} active site. Selected residues from BlaR1^{SD} and MecR1^{SD} are depicted in grey and white wire respectively on the left while the 2mF_o-DF_c map around avibactam is shown in blue mesh and contoured at 1 σ on the right. Avibactam is shown in ball and stick form with carbon atoms shown in green, water molecules are shown in cyan, and other atoms with conventional colouring.

termini hydrogen-bonds with a water, Asn-441, Asn-478, and Thr-531 (Fig. 3.5D). There is unambiguously no evidence of a secondary orientation of avibactam in the active site of MecR1^{SD} that we see in BlaR1^{SD} (Figs. 3.5D and C1).

Due to the orientation of the two BlaR1^{SD} molecules in the ASU, the avibactam ligands are in close proximity to residues of the opposite chain (Fig. C5). This juxtaposition allows the formation of the inter-chain hydrogen bonds to the avibactam sulfate oxygen and C2 carboxamide nitrogen (Fig. C5). However, as suggested by the *in silico* docking and molecular dynamics simulations discussed below, we believe these inter-chain hydrogen bonds are not necessary for the observed dual orientation of avibactam in the BlaR1^{SD} active site.

Size-exclusion chromatography multi-angle light scattering (SEC-MALS) of both BlaR1^{SD} and MecR1^{SD} show both constructs are monomeric in solution and provide molecular weights that reflect theoretical predictions (Fig. C6). Additionally, as the N-terminus of BlaR1^{SD} is located on opposite sides of the ASU dimer, it suggests this interaction would not be topologically possible when the sensor domain is expressed as a full-length protein along with the N-terminal zinc-metalloprotease domain in the cell membrane (Fig. C5). The most significant buried interface between the two monomers in the BlaR1 crystal ASU as calculated using PISA (171) is 979 Å², also supporting the observed pair as not reflective of a physiological interaction.

The BlaR1^{SD} and MecR1^{SD} active sites are clearly similar but do display differences in hydrogen bonding between the general base lysine and nucleophilic serine of the SXXK motif (Fig. 3.6A). The number of hydrogen-bonds between avibactam and the active site is listed for each structure in table 3.3. Briefly, MecR1 appears to have more hydrogen bonding with avibactam than BlaR1 does in either conformation of avibactam. In the BlaR1^{SD} avibactam structure, the N-ζ of the lysine is far (3.9Å) from the O-γ of the serine for hydrogen bonding and

Table 3.2: C α RMSD values for existing MecR1^{SD} structures compared with the MecR1^{SD} structure with avibactam (PDB ID: 6o9s)

PDB ID	Ligand present	C α RMSD (Å)	Number of atoms aligned	Reference
2iwb	Ligand-free	0.56	246	(120)
2iwc	Benzylpenicillin	0.31	246	(120)
2iwd	Oxacillin	0.37	246	(120)

Table 3.3: Number of hydrogen bonds between the active site and avibactam in BlaR1^{SD}, MecR1^{SD}, and OXA-10 (PDB-ID: 4s2o) structures

Complex and conformation	Number of hydrogen bonds to protein in the same chain		Number of hydrogen bonds to the active site via a water	
	Conformation A	Conformation B	Conformation A	Conformation B
	BlaR1 ^{SD} – avibactam	7	6	0
MecR1 ^{SD} – avibactam	9	-	1	-
OXA-10 – avibactam	6	-	2	-

Table 3.4: C α RMSD values for existing BlaR1^{SD} structures (from *S. aureus* unless otherwise noted) compared with the BlaR1^{SD} structure with avibactam (PDB ID: 6o9w)

PDB ID	Ligand	C α RMSD (Å)	Number of atoms aligned	Notes	Reference
1nrf	Ligand-free	4.45	232	<i>BlaR1</i> from <i>Bacillus licheniformis</i>	(101)
1xkz	Ceftazidime	2.44	242		(213)
1xa1	Ligand-free	2.28	242		(119)
1xa7	Benzylpenicillin	2.48	237		(119)
3uy6	Ligand-free	2.39	245	with N439V mutation	(195)
3q7v	Ligand-free	2.40	245	with carboxylated Lys-392	(194)
3q7z	2-(2'-carboxyphenyl)-benzoyl-6-aminopenicillanic acid	2.45	245		(194)
3q81	Imipenem	2.41	245		(194)
3q82	Meropenem	2.42	245		(194)

base mediated extraction of the serine O- γ bound hydrogen in the decarbamylated state. In contrast, the same residues in MecR1^{SD} are only 3.1Å away and in a position to facilitate both hydrogen bonding and extraction of the aforementioned hydrogen in the decarbamylated state. Additionally, the distance between the δ -N of the asparagine (Asn-439 in BlaR1 and Asn-441 in MecR1) and the C2 carboxamide oxygen of avibactam in the MecR1 structure is 3.0Å while it is 3.7Å in the BlaR1 structure.

The BlaR1^{SD} and MecR1^{SD} avibactam structures closely align (C α RMSD: 3.5Å over 321 common residues), excepting the same loop (residues His-403 – Gln-428 in BlaR1 and residues Asn-405 – Gln-430 in MecR1). The loop formed by BlaR1 residues His-403 – Gln-428 in the avibactam structure is in a completely different orientation compared to previous BlaR1^{SD} structures (Figs. C7, C8) while the overall MecR1^{SD} avibactam complex structure is highly similar to existing MecR1^{SD} structures, (Tables 3.2-3.4 and Fig. C8). Residues 408 – 427 were not modelled in chain A of the BlaR1^{SD} avibactam structure due to disorder/poor electron density while more defined electron density in chain B allowed the majority of the loop to be modelled excepting residues 413 – 414.

3.3.4 In silico docking of avibactam, nacubactam, and relebactam into BlaR1^{SD} and MecR1^{SD} avibactam crystal structures

We also performed *in silico* docking to further our understanding of the binding energies associated with each avibactam conformation in the BlaR1^{SD} and MecR1^{SD} structures (Table 3.5). Covalent docking was performed in the Molecular Operating Environment (MOE, version 2009; Chemical Computer Group Inc.). For all *in silico* modelling described here, three different docking algorithms were used based on the active-site-ligand shape, atomic contact count, and force field (211). The calculated energies of binding for avibactam to BlaR1 were the same for

conformation A and B using the Affinity dG and ASE docking algorithms (Table 3.5). However, for the GBVI/WSA dG, force field-based docking algorithm the calculated docking energy of avibactam to BlaR1 for conformation A (-4.7 kcal mol⁻¹) was slightly more favorable than for conformation B (-4.3 kcal mol⁻¹). The generally similar binding energies for avibactam in both conformations supports our observed dual orientation, ~equal occupancy of avibactam in the BlaR1^{SD} X-ray crystal structure and suggests crystal packing effects are likely not causing the

Table 3.5: Top predicted binding energies of various diazabicyclooctane β -lactamase inhibitors to BlaR1^{SD} and MecR1^{SD} (kcal/mol)

Docking algorithm	Compound	BlaR1 ^{SD}		MecR1 ^{SD}	
		Conformation A	Conformation B	Conformation A	Conformation B
Affinity dG (atomic contact count)	Avibactam	-3.8	-3.8	-3.7	-3.4
	Nacubactam	-6.4	-3.7	-3.7	-2.8
	Relebactam	-3.9	-2.8	-4.4	-3.7
GBVI/WSA dG (force field-based)	Avibactam	-4.7	-4.3	-4.6	-4.1
	Nacubactam	-5.1	-4.4	-5.4	-5.1
	Relebactam	-5.6	-4.2	-5.8	-5.3
ASE (shape-based)	Avibactam	-4.5	-4.5	-7.2	-4.7
	Nacubactam	-9.2	-4.6	-8.8	-7.0
	Relebactam	-10.1	-4.7	-9.5	-8.1

dual orientation of avibactam as only one of the two protein chains in the ASU were used in the docking calculation. Interestingly, in the docking trials for MecR1^{SD}, the energy of binding was reduced for avibactam in conformation B compared to conformation A which follows our observation that avibactam adopts only conformation A in the crystal structure. The reported docking poses closely match the avibactam crystal structure poses for MecR1^{SD} with avibactam in the A conformation and for both orientations of avibactam in BlaR1^{SD} (RMSD < 1Å over 17 atoms) (Fig. C9). Additionally, we docked two avibactam derivatives that are of clinical interest, nacubactam and relebactam, into the BlaR1^{SD} and MecR1^{SD} structures (214–217). Interestingly,

the *in silico* binding energies for both nacubactam and relebactam suggest conformation A is more favorable in both sensor domains (Fig. C10; Table 3.5).

3.3.5 Molecular dynamics simulations of BlaR1^{SD} and MecR1^{SD} interactions with avibactam

Molecular dynamics (MD) simulations over 40 nanoseconds were used to further explore the interactions between the BlaR1/MecR1 sensor domains and avibactam in poses A and B. As in the *in silico* docking experiments, the MD simulations were performed with a single protein monomer. In BlaR1 5 stable contacts (maintained for $\geq 30\%$ of the simulation) were observed between active site residues and the avibactam terminal sulfate and carboxamide moieties in either conformation (Fig. C11). In MecR1 there were 6 contacts between active site residues and avibactam terminal sulfate and carboxamide moieties in conformation A and 3 stable contacts with avibactam in the B conformation (Fig. C11). The interaction trajectories for residues interacting with avibactam are shown for each frame of the simulation in figure 11 of appendix C.

3.4 Discussion

While studies have shown that avibactam may be a suitable β -lactam inhibitor for use in new broad-spectrum treatments for Gram-positive and -negative infections (200–202), the effect of avibactam on the mec and bla resistance pathways in MRSA was previously unknown. Here we show avibactam induces upregulation of antibiotic resistance genes in a clinical strain of MRSA while our X-ray crystallographic models provide a molecular basis for avibactam binding to the BlaR1 and MecR1 sensor domains.

Gene expression studies performed here in *S. aureus* SF8300, a USA300 clone, suggest avibactam is able to trigger an antibiotic resistance phenotype by causing increased expression of

pbp2a and *blaZ* transcripts (Fig. 3.3). As this strain of *S. aureus* lacks a functional copy of *mecR1*, this also supports previous evidence that *pbp2a* expression can be controlled via BlaR1 and BlaI when MecR1 is not present (103). Cotreatment of MRSA infections with avibactam and ceftaroline, a late generation cephalosporin, has not been found to be inferior to treatment with ceftaroline alone (200); however, given that avibactam does trigger upregulation of MRSA resistance genes we provide evidence that caution should be exercised when using avibactam in combination with β -lactam antibiotics.

Following the initial evidence that avibactam binds the sensor domains of BlaR1^{SD} and MecR1^{SD} we became interested in the specific interactions mediating avibactam binding. The BlaR1^{SD} avibactam structure displays a novel, dual orientation of avibactam in the active site with both conformers forming a carbamoyl link with the catalytic serine (Ser-389) (Fig. 3.5 and C1). Given the structural and sequence similarity between BlaR1^{SD} and MecR1^{SD} it was surprising that the BlaR1^{SD} avibactam structure appears to have two orientations of avibactam while the MecR1^{SD} structure only has avibactam in a single orientation, similar to that observed in serine-based Class-A and -D β -lactamases. To our knowledge this dual orientation of avibactam binding has not been previously observed. Further work is needed to determine if one or both avibactam poses are responsible for activating BlaR1 as this could be important for guiding the development of future diazabicyclooctane β -lactam inhibitors and drugs to combat MRSA.

Avibactam co-structures typically have residues of the signature KTG motif coordinate the sulfate moiety of avibactam while the asparagine residue side chain from the SXN motif coordinates the C2 carboxamide group on the opposite side of the diazabicyclooctane scaffold (196). Avibactam in conformation A of the BlaR1^{SD} structure presented here partially follows

this trend with Lys-526 and Thr-527 of the KTG motif coordinating the avibactam sulfate moiety but lacks SXN motif coordination of the C2 carboxamide (Fig. 3.5A). Instead, the γ -O of Ser-437 of the SXN motif forms a hydrogen bond with N6 of avibactam. Predictably, avibactam in the B conformation, orientated approximately 180° to conformation A, does not have the canonical conformation either. Instead, Ser-437 of the SXN motif coordinates the carboxamide and Asn-388 and Ile-531 coordinates the sulfate (Fig. 3.5B). The MecR1^{SD} structure shows typical avibactam coordination with Asn-441 of the SXN motif coordinating the carboxamide and Lys-528 and Thr-529 of the KTG motif forming electrostatic contacts with the sulfate (Fig. 5D).

Equivalent residues, Asn-439 in BlaR1 and Asn-441 in MecR1 both hydrogen bond similarly with the lysine ζ -nitrogen of the SXXK motif but interact differently with the C2 carboxamide oxygen of avibactam. Residue Asn-439 of the SXN motif in BlaR1 has been shown to be instrumental in allowing the sensor domain of BlaR1 to function as a receptor rather than a β -lactamase (195). Hydrogen bond interactions between the Asn-439 δ -oxygen and the lysine ζ -nitrogen of the SXXK motif are thought to prevent the carboxylation of the same lysine when the catalytic serine is acylated by a β -lactam antibiotic, thereby inhibiting release of bound inhibitors (194, 195). We observe no evidence of SXXK lysine carboxylation in both avibactam co-structures described here, which follows given the observed hydrogen bonding between the asparagine and lysine of the aforementioned motifs. Additionally, as shown above, avibactam causes the upregulation of *pbp2a* and *blaZ* in *S. aureus*, suggesting the BlaR1 sensor domain is working as an avibactam receptor rather than a β -lactamase. Despite the similarity of Asn-439–Lys-392 (Asn-441–Lys-394 in MecR1) hydrogen bonding in both structures, in the MecR1^{SD} structure the avibactam C2 carboxamide oxygen hydrogen bonds (3.0Å) with the same

asparagine (Asn-441 in MecR1) δ -nitrogen while in the BlaR1 structure this interaction is long in avibactam conformation A (3.7Å) and not present with avibactam conformation B.

From our crystallographic analysis, and the very similar structures of ligand-free and avibactam forms, we surmise that crystal packing effects are not the underlying basis for our observations, although subtle or longer-range influences cannot be unequivocally ruled out. Following on this we wanted to better understand how the observed avibactam conformations might be predicted to behave in solution. As mentioned above, there are inter-chain interactions involving the avibactam ligands in the BlaR1^{SD} structure (Fig. C5). However, only a single protein chain of the BlaR1^{SD} structure was used in the *in silico* docking and MD experiments, allowing us to explore whether these inter-chain electrostatic interactions seen in the crystal structure were likely significantly perturbing the avibactam ligand position. The closely aligning poses for avibactam in the BlaR1^{SD} structure and the *in silico* docking experiments (Fig. C9) suggest the electrostatic interactions between avibactam from one chain and protein in the neighboring chain (Fig. C5) do not dramatically influence the binding of the avibactam in the crystal structure.

In silico docking and MD simulations hint as to why there are two main binding poses for avibactam in BlaR1 and only one in MecR1. The top two *in silico* predicted avibactam binding poses for BlaR1 show avibactam binding in conformations A and B as seen in the crystal structure with similar binding energies for both conformations (Table 3.5; Fig. C9). Additionally, MD simulations suggest there are an equal number of stable contacts (interactions maintained for $\geq 30\%$ of the simulation) between BlaR1 active site residues and both poses of avibactam terminal moieties, further supporting the presence of two avibactam binding sites in solvated BlaR1 (Fig. C11). In contrast, only half as many stable contacts were present in the MecR1 MD

simulation with avibactam terminal moieties in conformation B as compared to conformation A, providing support for the single observed conformation A in the crystal structure (Fig. C11).

While *in silico* docking and MD results were supportive of the crystallographic observations, it led us to consider the molecular basis for this finding. Upon alignment of the BlaR1^{SD} and MecR1^{SD} avibactam structures, we deduce MecR1 residues Asn-478 and Asn-390 (corresponding to residues Met-476 and Asn-388 in BlaR1) may play a role in favoring avibactam conformation A. In the MecR1^{SD} structure we modelled Asn-478 in two alternate orientations as supported by the electron density. However, conformation A of the Asn-478 side chain would clash with the sulfate moiety of avibactam if it were in the B conformation (Fig. 3.6A). Additionally, the position of Asn-478 influences the hydrogen bonding network such that the side chain of Asn-390 in MecR1 is flipped and would clash with avibactam sulfate in orientation B. Fewer hydrogen-bonds between the BlaR1^{SD} active site and both conformers of avibactam versus avibactam in the MecR1^{SD} structure may also facilitate the multiple orientations of avibactam in the BlaR1^{SD} structure (Table 3.3). Furthermore, BlaR1^{SD} has a more positively charged electrostatic surface in and surrounding the catalytic cleft than MecR1^{SD} which may contribute to accommodating the dual orientation of the avibactam ligand with its negatively charged sulfate moiety (Fig. C12).

While we do not eliminate the possibility that the dual orientation of avibactam in the BlaR1^{SD} structure or the singular pose of avibactam in the MecR1^{SD} structure, are influenced by crystal packing, we believe the *in silico* docking and MD simulations detailed above provide more likely explanations. Together, these experiments demonstrate the significant changes in ligand binding that can arise from subtle changes in hydrogen bonding networks and highlight the challenges of rational drug design.

To probe whether the dual orientation of avibactam observed with the BlaR1 structure is likely to be present with other clinically relevant diazabicyclooctane β -lactamase inhibitors, we also docked relebactam and nacubactam into the BlaR1^{SD} and MecR1^{SD} crystal structures. Relebactam and nacubactam are in current or recently completed clinical trials in combination with β -lactam antibiotics (215–217). Both relebactam and nacubactam are derivatized at the C2 carboxamide with the addition of a 2-aminoethoxy and piperidinium substituents respectively (Fig. C10). Interestingly, our *in silico* docking experiments show more favorable binding energies for the nacubactam and relebactam binding pose analogous to the A conformation seen with avibactam (Table 3.5; Fig. C10). This result is not entirely surprising given that binding in two orientations would cause the positively charged 2-aminoethoxy or piperidinium moieties to be in close proximity to the binding site of one of the two negatively charged avibactam sulfates.

While BlaR1^{SD} and MecR1^{SD} have closely analogous structures with the class-D β -lactamases (particularly OXA-10 and OXA-48 commonly found in *Pseudomonas aeruginosa* (218) and carbapenem-resistant Enterobacteriaceae (219) respectively), there are key differences in how the active sites coordinate avibactam. Here we compare the avibactam BlaR1/MecR1 sensor domain structures with the previously solved OXA-10-avibactam structure (PDB ID: 4s2o) (Fig. 3.6), but similar differences occur in the OXA-48-avibactam structure (PDB ID: 4s2k) (220). The two largest differences in avibactam binding between the two sensor domains and OXA-10 are the coordination of the avibactam sulfate and carboxamide. The guanidinium cation moiety of Arg-250 in OXA-10 directly coordinates the avibactam sulfate (2.7 and 3.1 Å away) in addition to the ζ -N of Lys-205 (3.2 Å away) (Fig 3.6B-3.6C). The two sensor domains examined here lack an arginine residue in this position and instead use a lysine-threonine cradle to stabilize the avibactam sulphate moiety in conformation A. The second, B conformation of

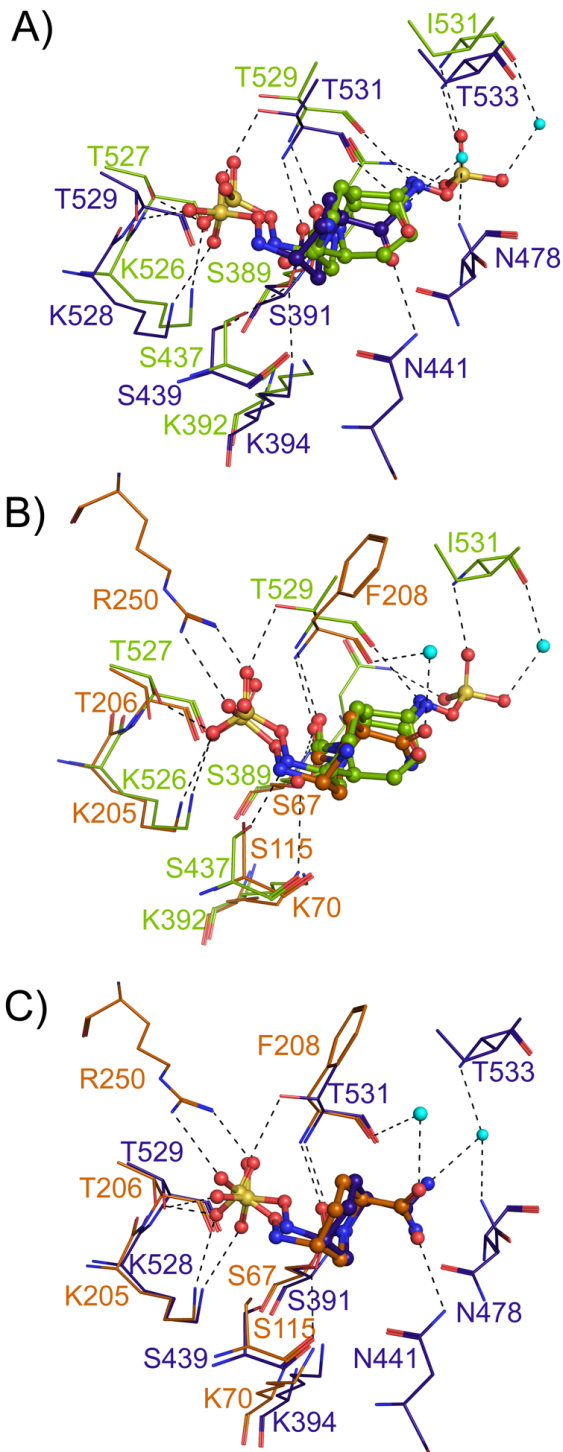


Figure 3.6: Structural alignment of A) BlaR1^{SD} and MecR1^{SD}, B) BlaR1^{SD} and OXA-10, or C) MecR1^{SD} and OXA-10 showing residues surrounding the carbamylated avibactam in each structure. The OXA-10 structure here has the PDB ID: 4s2o. Carbon atoms for BlaR1^{SD}, MecR1^{SD}, and OXA-10 are shown in green, blue, and orange respectively while other atoms are colored by type. In each panel, protein residues are shown in wire while avibactam is shown as a stick and ball structure. Residues are labeled in the identical color as the carbon atoms for that structure while waters are shown as cyan spheres.

avibactam seen in the BlaR1^{SD} structure is stabilized by an asparagine side chain nitrogen and the backbone nitrogen of an isoleucine residue as previously discussed. Notably, the C2 carboxamide at the opposite termini of the avibactam sulfate is coordinated directly by residues of the active site in the sensor domain structures while in the OXA-10 structure it is orientated toward solvent with only a single bridging water. The MecR1^{SD} structure appears to have the most contacts to avibactam, with BlaR1 and OXA-10 having fewer contacts (Table 3.3). While the BlaR1/MecR1 sensor domain, OXA-10, and OXA-48 active site cavities are closely similar, only BlaR1 has avibactam bound in two orientations. Further research is needed to determine if improved Class-D β -lactamase inhibitors can be developed to take advantage of this secondary sulfate binding site found in the BlaR1^{SD} active site.

As has been previously observed with the β -lactam class of inhibitors, there is no global change in either sensor domain structure following binding of avibactam compared to either inhibitor-free or β -lactam bound structures (Fig. C8; Tables 3.2 and 3.4) (119, 120). However, the BlaR1^{SD} avibactam structure has a loop consisting of residues His-403 – Asp-429 that adopts a radically different orientation than observed in all previous inhibitor-free and β -lactam acylated BlaR1^{SD} structures even when compared with crystals from the same space group and grown in similar, high molecular weight polyethylene glycol based, crystallization conditions (Figs. C7-C8). Given this, it is inferred that the binding of avibactam may be influencing the relative position of this loop. This loop showing considerable variation in position, borders the active site and is analogous to the P-loop found in class-D β -lactamases (221, 222). In some class-D β -lactamases, residues of the P-loop interact directly with covalently bound β -lactam (223) which is hypothesised to contribute to increased affinity for the ligand (224). In the BlaR1^{SD} avibactam structure described here, the analogous P-loop is retracted from the active site such that the

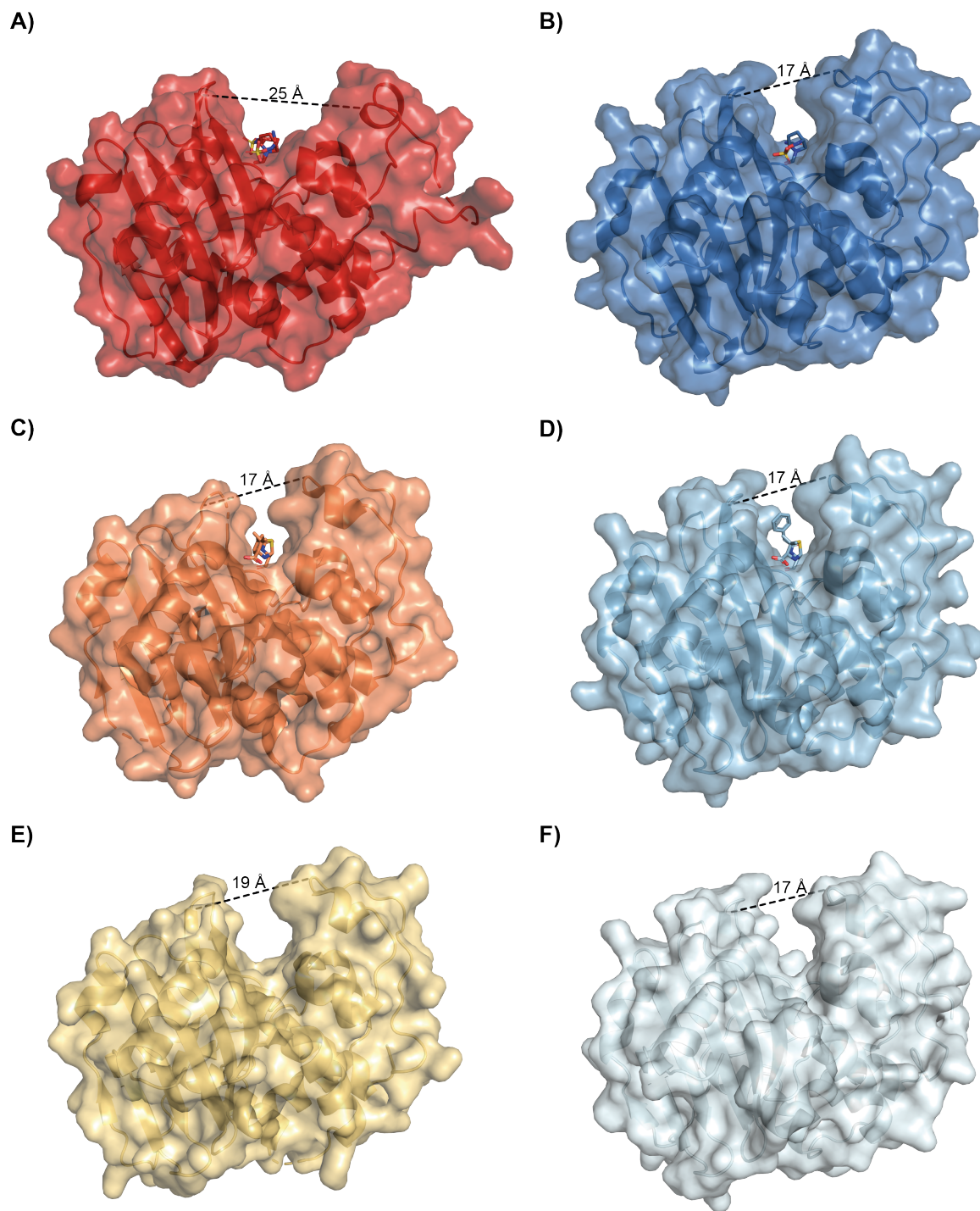


Figure 3.7: BlaR1^{SD} and MecR1^{SD} active sites clefts with and without ligands. BlaR1^{SD} structures are shown with A) avibactam, C) benzylpenicillin (PDB ID: 1xa7), and E) without ligand (PDB ID: 1xa1). MecR1^{SD} structures are shown with B) avibactam, D) benzylpenicillin (PDB ID: 2iwc), F) and without ligand (PDB ID: 2iwb). Distance between equivalent atoms on either side of the active site cleft in BlaR1 and MecR1 (distances measured between the C α of Pro-420 within the P-loop and the C α of Lys-535 of BlaR1 or the C α of Pro-422 and the C α of Lys-537 of MecR1) are shown in the figure.

catalytic groove is widened by 6-8 Å compared to other BlaR1^{SD} and MecR1^{SD} structures with and without ligand (Fig. 3.7). While only one conformation of the BlaR1 loop was observed and modelled, the B-factors of this loop are obviously higher than the corresponding residues in the MecR1^{SD} structure, suggesting that they may be more dynamic (Fig. C13). This is corroborated by previous research examining the ligand-free and acylated structures of BlaR1^{SD} using NMR which found the P-loop experienced local dynamic changes upon acylation (125). Finally, we note the P-loop has been predicted to pack against with the L2 loop of the closely related full-length MecR1 zinc metalloprotease domain (111) opening the possibility it may play a role in signal transduction between the sensor domain and the zinc metalloprotease domain.

The thermal stability of the sensor domains depends on the ligand added. While both sensor domains were stabilized by 2-9 °C by ampicillin, avibactam appeared to have little effect on the stability of BlaR1^{SD} while conferring stability at higher temperatures to MecR1^{SD}. While nafcillin provided a small increase in Δt_{agg} with BlaR1^{SD} it appeared to slightly destabilize MecR1^{SD}. It is not known how the alternate positioning of the analogous P-loop consisting of residues 403-439 would affect BlaR1 sensing or activation capability, but its position may contribute to the absence of thermal stability gained upon avibactam binding to BlaR1^{SD} (Fig. 3.4). The apparent dynamic nature of the avibactam ligand in the active site where more than one binding orientation is present could also be contributing to the lack of thermal stabilization effect on BlaR1^{SD} by avibactam. In contrast, the MecR1^{SD} structure with avibactam shows that one orientation of the ligand is preferred, which combined with the increased number of hydrogen bonds between the ligand and protein, may aid in providing the increase in thermal stability seen here.

Given avibactam is already used in the clinic, and the substantial investment in this drug by the pharmaceutical industry, a thorough examination of its off-target effects is needed. This research begins to address this unmet need by exploring the interaction between avibactam and a major determinant of drug resistance in Staphylococcal strains, BlaR1/MecR1. Additionally, work presented here could facilitate the development of inhibitors that do not activate and/or inhibit the bla/mec pathways. Developing an inhibitor that is still able to bind the sensor domain active site but at the same time blocks activation of the pathway could be a useful way to circumvent β -lactam resistance in MRSA. Finally, more research is needed to determine the structure of full-length BlaR1 and MecR1, with and without sensor domain inhibitors, to illuminate the mechanism of signal propagation from the sensor domain to the zinc metalloprotease domain.

Chapter 4: Conclusion and future directions

4.1 Summary and significant results

This thesis focused on contributing to the understanding of β -lactam resistance in MRSA in three areas: the mechanism of PBP4-mediated resistance; the effect of avibactam on β -lactam resistance pathways in MRSA; and the preliminary structural and kinetic analysis of BlaR1, an integral membrane protein responsible for regulating resistance in MRSA. Together these chapters contribute to our knowledge of MRSA β -lactam resistance and provide a foundation for the development of new treatments.

4.1.1 The mechanism of PBP4-mediated β -lactam resistance in *S. aureus*

PBP4-mediated β -lactam resistance is an emerging resistance mechanism in *S. aureus*. This work presents the first acyl-enzyme intermediate structures of PBP4 from wild type and mutant strains of *S. aureus*. These structures, together with kinetic analysis, show the mechanism of PBP4-mediated resistance is different depending on the β -lactam. For ceftobiprole, the mutations present in *pbp4* from the resistant *S. aureus* strain dramatically increased the catalytic efficacy (k_{cat}/K_M) and therefore prevented it from effectively competing with the physiological substrate for PBP4, PG. In contrast, ceftaroline resistance is likely mediated by increased expression of *pbp4* and not by the PBP4 mutations present in the mutant strain. The eight x-ray crystallographic structures solved in this chapter, including wild type PBP4 and the PBP4 from a mutant strain in ligand-free and as acyl-enzyme intermediates with nafcillin, ceftaroline, and ceftobiprole, provide a platform for rational PBP4 inhibitor development. Indeed, collaborators at the University of Washington are already using the coordinates of our PBP4 models to rationally design new inhibitors.

In spite of the structural insights in the work presented here, the transpeptidase activity of PBP4 remains curious. Structures of PBP4 from *S. aureus* and PBP5 from *E. coli* are very similar, but the former is primarily a transpeptidase while the latter is a carboxypeptidase. Indeed, most class-C PBPs have dominant carboxypeptidase activity. Enzyme substrate complexes may be useful for gaining insight into the catalytic mechanism, the acceptor binding site, and the regulation of transpeptidase versus carboxypeptidase activity in PBP4. Future experiments to understand why two such similar structures have such different enzymatic activity could also help further understanding of PG regulation in *S. aureus*.

Large multiprotein complexes are thought to be responsible for the maintenance and growth of PG as well as the coordination of PG remodelling to facilitate cell division (49). However, a clear understanding of how the components interact and are regulated is in many cases lacking. A major goal of future research should be to structurally characterise these interactions. To date this has been challenging to tackle with x-ray crystallography due to the large size and dynamic nature of these complexes (50). Additionally, the heterogeneous nature of the glycan substrates is inimical to crystal formation which has so far hindered a clear mechanistic understanding of PG transpeptidase and glycopolymerase reactions. Cryo-EM is uniquely well suited for large complexes, is better able to handle flexible substrates as no crystals are required, and large complexes are sometimes able to be stabilized with crosslinkers. Future analysis with cryo-EM could be helpful in providing a molecular of understanding of how PG synthesis occurs and is regulated.

Finally, while there are several efforts worldwide to monitor the spread of MRSA using PCR-based methods to detect the presence of *pbp2a*, this research suggests it would be prudent to include other genes in these tests. Screening strains for mutations in the *pbp4* promoter and

pbp4 gene might give a fuller picture of the scale of β -lactam resistance present by monitoring both PBP4- and PBP2a-mediated β -lactam resistance.

4.1.2 The effect of avibactam on the *bla* and *mec* divergons in MRSA

New broad-spectrum antibiotics are needed to tackle emerging antibiotic resistance. One potential broad-spectrum antibiotic combination is the cephalosporin, ceftaroline, plus the β -lactamase inhibitor, avibactam. It is thought that this combination would work well as the β -lactamase inhibitor would inhibit the β -lactamases of Gram-positive pathogens including those *Pseudomonas aeruginosa*, *Enterobacteriaceae*, and *Acinetobacter* spp. while the ceftaroline would inhibit the Gram-positive pathogens such as MRSA and *Streptococcus pneumoniae* (200–202). Unfortunately, we show avibactam can upregulate the expression of β -lactam antibiotic resistance genes, presumably via carbamylation of the BlaR1 sensor domain and activation of the zinc metalloprotease domain. While this does not necessarily make avibactam unsuitable for use, it does suggest caution and further research is needed before avibactam- β -lactam combinations are used to treat MRSA.

Two crystal structures of MecR1^{SD} and BlaR1^{SD} in complex with avibactam were solved here. While avibactam forms a complex with MecR1^{SD} similar to those observed with Class-D β -lactamases, it forms an additional, not previously observed pose in BlaR1^{SD}. Surprisingly, avibactam binds to the BlaR1 sensor domain in two orientations that are approximately 180° to each other.

The findings in this chapter lay the groundwork for future experiments to investigating avibactam binding to the BlaR1 and MecR1 sensor domains. Firstly, the dual conformation of avibactam seen in BlaR1 crystals needs to be confirmed in solution. Secondly, it would be very interesting to understand whether one or both poses of avibactam are responsible for activation

of BlaR1. The answer to this question could have ramifications for drug development as it could be useful clinically to find or design a ligand that would bind to the sensor domain active site and not elicit activation of the associated zinc metalloprotease domain. Such a compound could be co-administered with a β -lactam to prevent the β -lactam from acylating the sensor domain and activating antibiotic resistance genes. Thirdly, given the similarity of the BlaR1^{SD} to the Class-D β -lactamases, the structures presented here could aid the development of new inhibitors of both these sensor domains and Class-D β -lactamases. If the BlaR1^{SD} is able to bind avibactam sulfate moiety in two orientations perhaps there is an additional sulfate binding pocket in the Class-D β -lactamases that can be exploited.

Finally, future research efforts should be deployed to solve the full-length structure of BlaR1/MecR1. It would be especially interesting to compare BlaR1/MecR1 structures before and after acylation of the sensor domain, as this could provide insight into the mechanism of signal transduction across the cell membrane between the sensor domain and the zinc metalloprotease domain. Besides providing mechanistic insight to signal transduction across the bacterial membrane, a structure of BlaR1 could provide the starting information for the rational design of new inhibitors of the BlaR1 zinc metalloprotease domain.

References

1. Ogston, A. (1881) Report upon micro-organisms in surgical diseases. *Br. Med. J.* **1**, 369–377
2. Lakhundi, S., and Zhang, K. (2018) Methicillin-Resistant *Staphylococcus aureus*: Molecular Characterization, Evolution, and Epidemiology. *Clin. Microbiol. Rev.* 10.1128/CMR.00020-18
3. Newsom, S. W. B. (2008) Ogston's coccus. *J. Hosp. Infect.* **70**, 369–372
4. Turner, N. A., Sharma-Kuinkel, B. K., Maskarinec, S. A., Eichenberger, E. M., Shah, P. P., Carugati, M., Holland, T. L., and Fowler, V. G. (2019) Methicillin-resistant *Staphylococcus aureus*: an overview of basic and clinical research. *Nat. Rev. Microbiol.* **17**, 203–218
5. Gorwitz, R. J., Kruszon-Moran, D., McAllister, S. K., McQuillan, G., McDougal, L. K., Fosheim, G. E., Jensen, B. J., Killgore, G., Tenover, F. C., and Kuehnert, M. J. (2008) Changes in the Prevalence of Nasal Colonization with *Staphylococcus aureus* in the United States, 2001–2004. *J. Infect. Dis.* **197**, 1226–1234
6. Tong, S. Y. C., Davis, J. S., Eichenberger, E., Holland, T. L., and Fowler, V. G. (2015) *Staphylococcus aureus* infections: epidemiology, pathophysiology, clinical manifestations, and management. *Clin. Microbiol. Rev.* **28**, 603–61
7. Foster, T. J. (2017) Antibiotic resistance in *Staphylococcus aureus*. Current status and future prospects. *FEMS Microbiol. Rev.* 10.1093/femsre/fux007
8. Rodvold, K. a., and McConeghy, K. W. (2014) Methicillin-Resistant *Staphylococcus aureus* Therapy: Past, Present, and Future. *Clin. Infect. Dis.* **58**, S20–S27
9. Herzberg, O., and Moul, J. (1987) Bacterial resistance to beta-lactam antibiotics: crystal structure of beta-lactamase from *Staphylococcus aureus* PC1 at 2.5 Å resolution. *Science.* **236**, 694–701
10. Lim, D., and Strynadka, N. C. J. (2002) Structural basis for the β -lactam resistance of PBP2a from methicillin-resistant *Staphylococcus aureus*. *Nat. Struct. Biol.* **9**, 870–876
11. Alexander, J. A. N., Chatterjee, S. S., Hamilton, S. M., Eltis, L. D., Chambers, H. F., and Strynadka, N. C. J. (2018) Structural and kinetic analysis of penicillin-binding protein 4 (PBP4)-mediated antibiotic resistance in *Staphylococcus aureus*. *J. Biol. Chem.* **293**, 19854–19865
12. Courvalin, P. (2006) Vancomycin Resistance in Gram-Positive Cocci. *Clin. Infect. Dis.* **42**, S25–S34
13. Ernst, C. M., Staubitz, P., Mishra, N. N., Yang, S.-J., Hornig, G., Kalbacher, H., Bayer, A. S., Kraus, D., and Peschel, A. (2009) The Bacterial Defensin Resistance Protein MprF Consists of Separable Domains for Lipid Lysinylation and Antimicrobial Peptide Repulsion. *PLoS Pathog.* **5**, e1000660
14. Chopra, I., and Roberts, M. (2001) Tetracycline Antibiotics: Mode of Action, Applications, Molecular Biology, and Epidemiology of Bacterial Resistance. *Microbiol. Mol. Biol. Rev.* **65**, 232–260
15. Connell, S., Trieber, C., Dinos, G., Einfeldt, E., Taylor, D., and Nierhaus, K. (2003) Mechanism of Tet(O)-mediated tetracycline resistance. *EMBO J.* **22**, 945–953
16. Jensen, S. O., and Lyon, B. R. (2009) Genetics of antimicrobial resistance in *Staphylococcus aureus*. *Future Microbiol.* **4**, 565–582

17. Shore, A. C., Lazaris, A., Kinnevey, P. M., Brennan, O. M., Brennan, G. I., O'Connell, B., Feßler, A. T., Schwarz, S., and Coleman, D. C. (2016) First report of cfr-carrying plasmids in the pandemic sequence type 22 methicillin-resistant *Staphylococcus aureus* staphylococcal cassette chromosome mec type IV clone. *Antimicrob. Agents Chemother.* **60**, 3007–3015
18. Long, K. S., and Vester, B. (2012) Resistance to linezolid caused by modifications at its binding site on the ribosome. *Antimicrob. Agents Chemother.* **56**, 603–612
19. Hooper, D. C., and Jacoby, G. A. (2015) Mechanisms of drug resistance: Quinolone resistance. *Ann. N. Y. Acad. Sci.* **1354**, 12–31
20. Higgins, D. L., Chang, R., Debabov, D. V., Leung, J., Wu, T., Krause, K. M., Sandvik, E., Hubbard, J. M., Kaniga, K., Schmidt, D. E., Gao, Q., Cass, R. T., Karr, D. E., Benton, B. M., and Humphrey, P. P. (2005) Telavancin, a multifunctional lipoglycopeptide, disrupts both cell wall synthesis and cell membrane integrity in methicillin-resistant *Staphylococcus aureus*. *Antimicrob. Agents Chemother.* **49**, 1127–1134
21. Zhanel, G., Schweizer, F., and Karlowsky, J. (2012) Oritavancin: Mechanism of Action. *Clin. Infect. Dis.* 10.1093/cid/cir920
22. Long, S. W., Olsen, R. J., Mehta, S. C., Palzkill, T. G., Cernoch, P. L., Perez, K. K., Musick, W. L., Rosato, A. E., and Musser, J. M. (2014) PBP2a Mutations Causing High-Level Ceftaroline Resistance in Clinical Methicillin-resistant *Staphylococcus aureus* Isolates. *Antimicrob. Agents Chemother.* **58**, 6668–6674
23. Rammelkamp, C. H., and Maxon, T. (1942) Resistance of *Staphylococcus aureus* to the Action of Penicillin. *Exp. Biol. Med.* **51**, 386–389
24. Jevons, M. P. (1961) “*Celbenin*” -resistant *Staphylococci*, BMJ Publishing Group, **1**, 124–125
25. Planet, P. J. (2017) Life After USA300: The Rise and Fall of a Superbug. *J. Infect. Dis.* **215**, S71–S77
26. Hassoun, A., Linden, P. K., and Friedman, B. (2017) Incidence, prevalence, and management of MRSA bacteremia across patient populations-a review of recent developments in MRSA management and treatment. *Crit. Care.* **21**, 211
27. Köck, R., Becker, K., Cookson, B., van Gemert-Pijnen, J. E., Harbarth, S., Kluytmans, J., Mielke, M., Peters, G., Skov, R. L., Struelens, M. J., Tacconelli, E., Torné, A. N., Witte, W., and Friedrich, A. W. (2010) Methicillin-resistant *Staphylococcus aureus* (MRSA): Burden of disease and control challenges in Europe. *Eurosurveillance.* **15**, 1–9
28. van Hal, S. J., Jensen, S. O., Vaska, V. L., Espedido, B. A., Paterson, D. L., and Gosbell, I. B. (2012) Predictors of mortality in staphylococcus aureus bacteremia. *Clin. Microbiol. Rev.* **25**, 362–386
29. Kourtis, A. P., Hatfield, K., Baggs, J., Mu, Y., See, I., Epton, E., Nadle, J., Kainer, M. A., Dumyati, G., Petit, S., Ray, S. M., Ham, D., Capers, C., Ewing, H., Coffin, N., McDonald, L. C., Jernigan, J., and Cardo, D. (2019) Vital signs: Epidemiology and recent trends in methicillin-resistant and in methicillin-susceptible staphylococcus aureus bloodstream infections - United States. *Morb. Mortal. Wkly. Rep.* **68**, 214–219
30. Redi, D., Raffaelli, C. S., Rossetti, B., De Luca, A., and Montagnani, F. (2018) *Staphylococcus aureus* vaccine preclinical and clinical development: Current state of the art. *New Microbiol.* **41**, 208–213
31. World Health Organization (2017) *Global priority list of antibiotic-resistant bacteria to*

- guide research, discovery, and development of new antibiotics*
32. Wolf, A. J., and Underhill, D. M. (2018) Peptidoglycan recognition by the innate immune system. *Nat. Rev. Immunol.* **18**, 243–254
 33. Lovering, A. L., Safadi, S. S., and Strynadka, N. C. J. (2012) Structural perspective of peptidoglycan biosynthesis and assembly. *Annu. Rev. Biochem.* **81**, 451–78
 34. Giesbrecht, P., Kersten, T., Maidhof, H., and Wecke, J. (1998) Staphylococcal cell wall: morphogenesis and fatal variations in the presence of penicillin. *Microbiol. Mol. Biol. Rev.* **62**, 1371–414
 35. Sharif, S., Singh, M., Kim, S. J., and Schaefer, J. (2009) Staphylococcus aureus peptidoglycan tertiary structure from carbon-13 spin diffusion. *J. Am. Chem. Soc.* **131**, 7023–7030
 36. Typas, A., Banzhaf, M., Gross, C. a., and Vollmer, W. (2012) From the regulation of peptidoglycan synthesis to bacterial growth and morphology. *Nat. Rev. Microbiol.* **10**, 123–136
 37. Bouhss, A., Trunkfield, A. E., Bugg, T. D. H. H., and Mengin-Lecreulx, D. (2008) The biosynthesis of peptidoglycan lipid-linked intermediates. *FEMS Microbiol. Rev.* **32**, 208–233
 38. Chung, B. C., Zhao, J., Gillespie, R. A., Kwon, D. Y., Guan, Z., Hong, J., Zhou, P., and Lee, S. Y. (2013) Crystal structure of MraY, an essential membrane enzyme for bacterial cell wall synthesis. *Science (80-.).* **341**, 1012–1016
 39. Sobhanifar, S., King, D. T., and Strynadka, N. C. (2013) Fortifying the wall: Synthesis, regulation and degradation of bacterial peptidoglycan. *Curr. Opin. Struct. Biol.* **23**, 695–703
 40. Monteiro, J. M., Covas, G., Rausch, D., Filipe, S. R., Schneider, T., Sahl, H. G., and Pinho, M. G. (2019) The pentaglycine bridges of Staphylococcus aureus peptidoglycan are essential for cell integrity. *Sci. Rep.* **9**, 1–10
 41. Sham, L. T., Butler, E. K., Lebar, M. D., Kahne, D., Bernhardt, T. G., and Ruiz, N. (2014) MurJ is the flippase of lipid-linked precursors for peptidoglycan biogenesis. *Science (80-.).* **345**, 220–222
 42. Kuk, A. C. Y., Hao, A., Guan, Z., and Lee, S. Y. (2019) Visualizing conformation transitions of the Lipid II flippase MurJ. *Nat. Commun.* 10.1038/s41467-019-09658-0
 43. Reed, P., Veiga, H., Jorge, A. M., Terrak, M., and Pinho, M. G. (2011) Monofunctional transglycosylases are not essential for Staphylococcus aureus cell wall synthesis. *J. Bacteriol.* **193**, 2549–56
 44. Taguchi, A., Welsh, M. A., Marmont, L. S., Lee, W., Sjodt, M., Kruse, A. C., Kahne, D., Bernhardt, T. G., and Walker, S. (2019) FtsW is a peptidoglycan polymerase that is functional only in complex with its cognate penicillin-binding protein. *Nat. Microbiol.* **4**, 587–594
 45. Meeske, A. J., Riley, E. P., Robins, W. P., Uehara, T., Mekalanos, J. J., Kahne, D., Walker, S., Kruse, A. C., Bernhardt, T. G., and Rudner, D. Z. (2016) SEDS proteins are a widespread family of bacterial cell wall polymerases. *Nature.* **537**, 634–638
 46. Yao, Z., Kahne, D., and Kishony, R. (2012) Distinct Single-Cell Morphological Dynamics under Beta-Lactam Antibiotics. *Mol. Cell.* **48**, 705–712
 47. King, D. T., Sobhanifar, S., and Strynadka, N. C. J. (2016) One ring to rule them all: Current trends in combating bacterial resistance to the β -lactams. *Protein Sci.*

- 10.1002/pro.2889
48. Cabeen, M. T., and Jacobs-Wagner, C. (2005) Bacterial cell shape. *Nat. Rev. Microbiol.* **3**, 601–610
 49. Szwedziak, P., and Löwe, J. (2013) Do the divisome and elongasome share a common evolutionary past? *Curr. Opin. Microbiol.* **16**, 745–751
 50. Söderström, B., and Daley, D. O. (2017) The bacterial divisome: more than a ring? *Curr. Genet.* **63**, 161–164
 51. Monteiro, J. M., Fernandes, P. B., Vaz, F., Pereira, A. R., Tavares, A. C., Ferreira, M. T., Pereira, P. M., Veiga, H., Kuru, E., Vannieuwenhze, M. S., Brun, Y. V., Filipe, S. R., and Pinho, M. G. (2015) Cell shape dynamics during the staphylococcal cell cycle. *Nat. Commun.* 10.1038/ncomms9055
 52. Reichmann, N. T., Tavares, A. C., Saraiva, B. M., Jousselin, A., Reed, P., Pereira, A. R., Monteiro, J. M., Sobral, R. G., VanNieuwenhze, M. S., Fernandes, F., and Pinho, M. G. (2019) SEDS–bPBP pairs direct lateral and septal peptidoglycan synthesis in *Staphylococcus aureus*. *Nat. Microbiol.* **4**, 1368–1377
 53. Kastner, B., Fischer, N., Golas, M. M., Sander, B., Dube, P., Boehringer, D., Hartmuth, K., Deckert, J., Hauer, F., Wolf, E., Uchtenhagen, H., Urlaub, H., Herzog, F., Peters, J. M., Poerschke, D., Lührmann, R., and Stark, H. (2008) GraFix: Sample preparation for single-particle electron cryomicroscopy. *Nat. Methods.* **5**, 53–55
 54. Borisova, M., Gaupp, R., Duckworth, A., Schneider, A., Dalügge, D., Mühleck, M., Deubel, D., Unsleber, S., Yu, W., Muth, G., Bischoff, M., Götz, F., and Mayer, C. (2016) Peptidoglycan recycling in gram-positive bacteria is crucial for survival in stationary phase. *MBio.* 10.1128/mBio.00923-16
 55. Borisova, M., Gaupp, R., Duckworth, A., Schneider, A., Dalügge, D., Mühleck, M., Deubel, D., Unsleber, S., Yu, W., Muth, G., Bischoff, M., Götz, F., and Mayer, C. (2016) Peptidoglycan recycling in gram-positive bacteria is crucial for survival in stationary phase. *MBio.* **7**, e00923-16
 56. Kluj, R. M., Ebner, P., Adamek, M., Ziemert, N., Mayer, C., and Borisova, M. (2018) Recovery of the Peptidoglycan Turnover Product Released by the Autolysin Atl in *Staphylococcus aureus* Involves the Phosphotransferase System Transporter MurP and the Novel 6-phospho-N-acetylmuramidase MupG. *Front. Microbiol.* **9**, 2725
 57. Mayer, C., Kluj, R. M., Mühleck, M., Walter, A., Unsleber, S., Hottmann, I., and Borisova, M. (2019) Bacteria’s different ways to recycle their own cell wall. *Int. J. Med. Microbiol.* **309**, 151326
 58. Sauvage, E., Kerff, F., Terrak, M., Ayala, J. A., and Charlier, P. (2008) The penicillin-binding proteins: Structure and role in peptidoglycan biosynthesis. *FEMS Microbiol. Rev.* **32**, 234–258
 59. Galleni, M., and Frère, J. (2007) Kinetics of β -lactamases and penicillin-binding proteins. in *Enzyme-Mediated Resistance to Antibiotics: Kinetics of β -lactamases and penicillin-binding proteins: mechanisms, dissemination, and prospects for inhibition*, 1st Ed. (Bonomo, R., and Tolmasky, M. eds), ASM Press, Washington, D.C.
 60. Nicola, G., Peddi, S., Stefanova, M., Nicholas, R. A., Gutheil, W. G., and Davies, C. (2005) Crystal structure of *Escherichia coli* penicillin-binding protein 5 bound to a tripeptide boronic acid inhibitor: A role for Ser-110 in deacylation. *Biochemistry.* **44**, 8207–8217

61. Bush, K., and Bradford, P. A. (2019) Interplay between β -lactamases and new β -lactamase inhibitors. *Nat. Rev. Microbiol.* **17**, 295–306
62. Lim, D., and Strynadka, N. C. J. (2002) Structural basis for the beta lactam resistance of PBP2a from methicillin-resistant *Staphylococcus aureus*. *Nat. Struct. Biol.* **9**, 870–876
63. Lovering, A. L., Castro, L. H. de, Lim, D., and Strynadka, N. C. J. (2007) Structural Insight into the Transglycosylation Step of Bacterial Cell-Wall Biosynthesis. *Science (80-)*. **315**, 1402–1405
64. King, D. T., Wasney, G. A., Nosella, M., Fong, A., Strynadka, N. C. J., and Peter Guengerich, F. (2017) Structural insights into inhibition of *Escherichia coli* penicillin-binding protein 1B. *J. Biol. Chem.* **292**, 979–993
65. Maya-Martinez, R., Alexander, J. A. N., Otten, C. F., Ayala, I., Vollmer, D., Gray, J., Bougault, C. M., Burt, A., Laguri, C., Fonvielle, M., Arthur, M., Strynadka, N. C. J., Vollmer, W., and Simorre, J.-P. (2019) Recognition of peptidoglycan fragments by the transpeptidase PBP4 from *Staphylococcus aureus*. *Front. Microbiol.* **9**, 3223
66. Sauvage, E., and Terrak, M. (2016) Glycosyltransferases and transpeptidases/penicillin-binding proteins: Valuable targets for new antibacterials. *Antibiotics*. 10.3390/antibiotics5010012
67. Sauvage, E., Duez, C., Herman, R., Kerff, F., Petrella, S., Anderson, J. W., Adediran, S. A., Pratt, R. F., Frère, J. M., and Charlier, P. (2007) Crystal Structure of the *Bacillus subtilis* Penicillin-binding Protein 4a, and its Complex with a Peptidoglycan Mimetic Peptide. *J. Mol. Biol.* **371**, 528–539
68. McDonough, M. A., Anderson, J. W., Silvaggi, N. R., Pratt, R. F., Knox, J. R., and Kelly, J. A. (2002) Structures of two kinetic intermediates reveal species specificity of penicillin-binding proteins. *J. Mol. Biol.* **322**, 111–122
69. Kühlbrandt, W. (2014) The resolution revolution. *Science (80-)*. **343**, 1443–1444
70. Caveney, N. A., Li, F. K., and Strynadka, N. C. (2018) Enzyme structures of the bacterial peptidoglycan and wall teichoic acid biogenesis pathways. *Curr. Opin. Struct. Biol.* **53**, 45–58
71. Qiao, Y., Lebar, M. D., Schirner, K., Schaefer, K., Tsukamoto, H., Kahne, D., and Walker, S. (2014) Detection of Lipid-Linked Peptidoglycan Precursors by Exploiting an Unexpected Transpeptidase Reaction. *J. Am. Chem. Soc.* **136**, 14678–81
72. Fishovitz, J., Hermoso, J. A., Chang, M., and Mobashery, S. (2014) Penicillin-binding protein 2a of methicillin-resistant *Staphylococcus aureus*. *IUBMB Life*. **66**, 572–577
73. Reed, P., Atilano, M. L., Alves, R., Hoiczky, E., Sher, X., Reichmann, N. T., Pereira, P. M., Roemer, T., Filipe, S. R., Pereira-Leal, J. B., Ligoxygakis, P., and Pinho, M. G. (2015) *Staphylococcus aureus* Survives with a Minimal Peptidoglycan Synthesis Machine but Sacrifices Virulence and Antibiotic Resistance. *PLoS Pathog.* **11**, e1004891
74. Pereira, S. F. F., Henriques, A. O., Pinho, M. G., De Lencastre, H., and Tomasz, A. (2007) Role of PBP1 in cell division of *Staphylococcus aureus*. *J. Bacteriol.* **189**, 3525–3531
75. Pereira, S. F. F., Henriques, A. O., Pinho, M. G., De Lencastre, H., and Tomasz, A. (2009) Evidence for a dual role of PBP1 in the cell division and cell separation of *Staphylococcus aureus*. *Mol. Microbiol.* **72**, 895–904
76. Łeski, T. A., and Tomasz, A. (2005) Role of penicillin-binding protein 2 (PBP2) in the antibiotic susceptibility and cell wall cross-linking of *Staphylococcus aureus*: Evidence

- for the cooperative functioning of PBP2, PBP4, and PBP2A. *J. Bacteriol.* **187**, 1815–1824
77. Wu, S., Piscitelli, C., de Lencastre, H., and Tomasz, A. (1996) Tracking the Evolutionary Origin of the Methicillin Resistance Gene: Cloning and Sequencing of a Homologue of *mecA* from a Methicillin Susceptible Strain of *Staphylococcus sciuri*. *Microb. Drug Resist.* **2**, 435–441
 78. Otero, L. H., Rojas-Altuve, A., Llarrull, L. I., Carrasco-Lopez, C., Kumarasiri, M., Lastochkin, E., Fishovitz, J., Dawley, M., Heseck, D., Lee, M., Johnson, J. W., Fisher, J. F., Chang, M., Mobashery, S., Hermoso, J. A., Carrasco-López, C., Kumarasiri, M., Lastochkin, E., Fishovitz, J., Dawley, M., Heseck, D., Lee, M., Johnson, J. W., Fisher, J. F., Chang, M., Mobashery, S., and Hermoso, J. A. (2013) How allosteric control of *Staphylococcus aureus* penicillin binding protein 2a enables methicillin resistance and physiological function. *Proc. Natl. Acad. Sci.* **110**, 16808–16813
 79. Laudano, J. B. (2011) Ceftaroline fosamil: A new broad-spectrum cephalosporin. *J. Antimicrob. Chemother.* **66**, iii11–iii18
 80. Fishovitz, J., Hermoso, J. A., Chang, M., and Mobashery, S. (2014) Penicillin-binding protein 2a of methicillin-resistant *Staphylococcus aureus*. *IUBMB Life.* **66**, 572–577
 81. Yoshida, H., Kawai, F., Obayashi, E., Akashi, S., Roper, D. I., Tame, J. R. H., and Park, S. Y. (2012) Crystal structures of penicillin-binding protein 3 (PBP3) from methicillin-resistant *Staphylococcus aureus* in the Apo and cefotaxime-bound forms. *J. Mol. Biol.* **423**, 351–364
 82. Pinho, M. G., De Lencastre, H., and Tomasz, A. (2000) Cloning, characterization, and inactivation of the gene *pbpC*, encoding penicillin-binding protein 3 of *Staphylococcus aureus*. *J. Bacteriol.* **182**, 1074–1079
 83. Memmi, G., Filipe, S. R., Pinho, M. G., Fu, Z., and Cheung, A. (2008) *Staphylococcus aureus* PBP4 is essential for β -lactam resistance in community-acquired methicillin-resistant strains. *Antimicrob. Agents Chemother.* **52**, 3955–3966
 84. Katayama, Y., Zhang, H.-Z., and Chambers, H. F. (2003) Effect of disruption of *Staphylococcus aureus* PBP4 gene on resistance to beta-lactam antibiotics. *Microb. drug Resist.* **9**, 329–336
 85. Hamilton, S. M., Alexander, J. A. N., Choo, E. J., Basuino, L., Da Costa, T. M., Severin, A., Chung, M., Aedo, S., Strynadka, N. C. J., Tomasz, A., Chatterjee, S. S., and Chambers, H. F. (2017) High-level resistance of *Staphylococcus aureus* to β -Lactam antibiotics mediated by penicillin-binding protein 4 (PBP4). *Antimicrob. Agents Chemother.* **61**, AAC.02727-16
 86. Loskill, P., Pereira, P. M., Jung, P., Bischoff, M., Herrmann, M., Pinho, M. G., and Jacobs, K. (2014) Reduction of the peptidoglycan crosslinking causes a decrease in stiffness of the *Staphylococcus aureus* cell envelope. *Biophys. J.* **107**, 1082–1089
 87. Pasquina-Lemonche, L., Burns, J., Turner, R. D., Kumar, S., Tank, R., Mullin, N., Wilson, J. S., Chakrabarti, B., Bullough, P. A., Foster, S. J., and Hobbs, J. K. (2020) The architecture of the Gram-positive bacterial cell wall. *Nature.* 10.1038/s41586-020-2236-6
 88. Fleming, A. (1929) On the antibacterial action of cultures of a penicillium, with special reference to their use in the isolation of B. influenzae. *Br. J. Exp. Pathol.* **10**, 226
 89. Osthoff, M., Siegemund, M., Balestra, G., Abdul-Aziz, M. H., and Roberts, J. A. (2016) Prolonged administration of β -lactam antibiotics - a comprehensive review and critical appraisal. *Swiss Med. Wkly.* **146**, w14368

90. Klein, E. Y., Van Boeckel, T. P., Martinez, E. M., Pant, S., Gandra, S., Levin, S. A., Goossens, H., and Laxminarayan, R. (2018) Global increase and geographic convergence in antibiotic consumption between 2000 and 2015. *Proc. Natl. Acad. Sci. U. S. A.* **115**, E3463–E3470
91. Tipper, D. J., and Strominger, J. L. (1965) Mechanism of action of penicillins: a proposal based on their structural similarity to acyl-D-alanyl-D-alanine. *Proc. Natl. Acad. Sci. U. S. A.* **54**, 1133–1141
92. King, A. M., King, D. T., French, S., Brouillette, E., Asli, A., Alexander, J. A. N., Vuckovic, M., Maiti, S. N., Parr, T. R., Brown, E. D., Malouin, F., Strynadka, N. C. J., and Wright, G. D. (2016) Structural and Kinetic Characterization of Diazabicyclooctanes as Dual Inhibitors of Both Serine- β -Lactamases and Penicillin-Binding Proteins. *ACS Chem. Biol.* **11**, 864–868
93. Tomasz, A., and Waks, S. (1975) Mechanism of action of penicillin: triggering of the pneumococcal autolytic enzyme by inhibitors of cell wall synthesis. *Proc. Natl. Acad. Sci. U. S. A.* **72**, 4162–4166
94. Tomasz, A., Albino, A., and Zanati, E. (1970) Multiple antibiotic resistance in a Bacterium with suppressed autolytic System. *Nature.* **227**, 138–140
95. Kohlrausch, U., and Holtje, J. V. (1991) Analysis of murein and murein precursors during antibiotic-induced lysis of *Escherichia coli*. *J. Bacteriol.* **173**, 3425–3431
96. Cho, H., Uehara, T., and Bernhardt, T. G. (2014) Beta-lactam antibiotics induce a lethal malfunctioning of the bacterial cell wall synthesis machinery. *Cell.* **159**, 1300–1311
97. Herzberg, O. (1991) Refined crystal structure of β -lactamase from *Staphylococcus aureus* PC1 at 2.0 Å resolution. *J. Mol. Biol.* **217**, 701–719
98. Nomura, R., Nakaminami, H., Takasao, K., Muramatsu, S., Kato, Y., Wajima, T., and Noguchi, N. (2020) A class A β -lactamase produced by borderline oxacillin-resistant *Staphylococcus aureus* hydrolyzes oxacillin. *J. Glob. Antimicrob. Resist.* 10.1016/j.jgar.2020.03.002
99. Stapleton, P. D., and Taylor, P. W. (2002) Methicillin resistance in *Staphylococcus aureus*: mechanisms and modulation. *Sci. Prog.* **85**, 57–72
100. Brown, D. F. J., and Reynolds, P. E. (1980) Intrinsic resistance to β -lactam antibiotics in *Staphylococcus aureus*. *FEBS Lett.* **122**, 275–278
101. Kerff, F., Charlier, P., Colombo, M.-L., Sauvage, E., Brans, A., Frère, J.-M., Joris, B., and Fonzé, E. (2003) Crystal structure of the sensor domain of the BlaR penicillin receptor from *Bacillus licheniformis*. *Biochemistry.* **42**, 12835–43
102. Mazuet, C., Yoon, E.-J., Boyer, S., Pignier, S., Blanc, T., Doehring, I., Meziane-Cherif, D., Dumant-Forest, C., Sautereau, J., Legeay, C., Bouvet, P., Bouchier, C., Quijano-Roy, S., Pestel-Caron, M., Courvalin, P., and Popoff, M. R. (2016) A penicillin- and metronidazole-resistant *Clostridium botulinum* strain responsible for an infant botulism case. *Clin. Microbiol. Infect.* **22**, 644.e7–644.e12
103. Hackbarth, C. J., and Chambers, H. F. (1993) blaI and blaR1 regulate beta-lactamase and PBP 2a production in methicillin-resistant *Staphylococcus aureus*. *Antimicrob. Agents Chemother.* **37**, 1144–9
104. Zhang, H. Z., Hackbarth, C. J., Chansky, K. M., and Chambers, H. F. (2001) A proteolytic transmembrane signaling pathway and resistance to beta-lactams in staphylococci. *Science.* **291**, 1962–5

105. Cha, J., Vakulenko, S. S. B., and Mobashery, S. (2007) Characterization of the β -lactam antibiotic sensor domain of the MecR1 signal sensor/transducer protein from methicillin-resistant *Staphylococcus aureus*. *Biochemistry*. **46**, 7822–7831
106. Safo, M. K., Zhao, Q., Ko, T., Musayev, F. N., Robinson, H., Scarsdale, N., Wang, A. H.-J., and Archer, G. L. (2005) Crystal Structures of the BlaI Repressor from *Staphylococcus aureus* and Its Complex with DNA : Insights into Transcriptional Regulation of the bla and mec Operons Crystal Structures of the BlaI Repressor from *Staphylococcus aureus* and Its Complex with DNA. *J. Bacteriol.* **187**, 1833–1844
107. Safo, M. K., Ko, T. P., Musayev, F. N., Zhao, Q., Wang, A. H. J., and Archer, G. L. (2006) Structure of the MecI repressor from *Staphylococcus aureus* in complex with the cognate DNA operator of mec. *Acta Crystallogr. Sect. F. Struct. Biol. Cryst. Commun.* **62**, 320–4
108. Llarrull, L. I., Prorok, M., and Mobashery, S. (2010) Binding of the gene repressor BlaI to the bla operon in methicillin-resistant *Staphylococcus aureus*. *Biochemistry*. **49**, 7975–7977
109. Tesch, W., Ryffel, C., Strasle, A., Kayser, F. H., and Berger-Bachi, B. (1990) Evidence of a novel staphylococcal mec-encoded element (mecR) controlling expression of penicillin-binding protein 2'. *Antimicrob. Agents Chemother.* **34**, 1703–1706
110. Kobayashi, T., Zhu, Y. F., Nicholls, N. J., and Lampen, J. O. (1987) A second regulatory gene, blaR1, encoding a potential penicillin-binding protein required for induction of β -lactamase in *Bacillus licheniformis*. *J. Bacteriol.* **169**, 3873–3878
111. Belluzo, B. S., Abriata, L. A., Giannini, E., Mihovilcevic, D., Dal Peraro, M., and Llarrull, L. I. (2019) An experiment-informed signal transduction model for the role of the *Staphylococcus aureus* MecR1 protein in β -lactam resistance. *Sci. Rep.* 10.1038/s41598-019-55923-z
112. Sobhanifar, S., Prehna, G., and Strynadka, N. (2012) BlaR1 and MecR1 gene products of *Staphylococcus aureus*. in *Handbook of Proteolytic Enzymes* (Barrett, A., Rawlings, J., and Woessner, J. eds), pp. 1237–1243, Academic Press
113. Hardt, K., Joris, B., Lepage, S., Brasseur, R., Lampen, J. O., Frère, J. M., Fink, A. L., and Ghuysen, J. M. (1997) The penicillin sensory transducer, BlaR, involved in the inducibility of β -lactamase synthesis in *Bacillus licheniformis* is embedded in the plasma membrane via a four- α -helix bundle. *Mol. Microbiol.* **23**, 935–944
114. Madeira, F., Park, Y. M., Lee, J., Buso, N., Gur, T., Madhusoodanan, N., Basutkar, P., Tivey, A. R. N., Potter, S. C., Finn, R. D., and Lopez, R. (2019) The EMBL-EBI search and sequence analysis tools APIs in 2019. *Nucleic Acids Res.* **47**, W636–W641
115. Sievers, F., Wilm, A., Dineen, D., Gibson, T. J., Karplus, K., Li, W., Lopez, R., McWilliam, H., Remmert, M., Söding, J., Thompson, J. D., and Higgins, D. G. (2011) Fast, scalable generation of high-quality protein multiple sequence alignments using Clustal Omega. *Mol. Syst. Biol.* **7**, 539
116. Robert, X., and Gouet, P. (2014) Deciphering key features in protein structures with the new ENDscript server. *Nucleic Acids Res.* **42**, W320–W324
117. Quigley, a., Dong, Y. Y., Pike, a. C. W., Dong, L., Shrestha, L., Berridge, G., Stansfeld, P. J., Sansom, M. S. P., Edwards, a. M., Bountra, C., von Delft, F., Bullock, a. N., Burgess-Brown, N. a., and Carpenter, E. P. (2013) The Structural Basis of ZMPSTE24-Dependent Laminopathies. *Science (80-.).* **339**, 1604–1607

118. Pryor, E. E., Horanyi, P. S., Clark, K. M., Fedoriw, N., Connelly, S. M., Koszelak-Rosenblum, M., Zhu, G., Malkowski, M. G., Wiener, M. C., and Dumont, M. E. (2013) Structure of the integral membrane protein CAAX protease Ste24p. *Science*. **339**, 1600–4
119. Wilke, M. S., Hills, T. L., Zhang, H.-Z., Chambers, H. F., and Strynadka, N. C. J. (2004) Crystal structures of the Apo and penicillin-acylated forms of the BlaR1 beta-lactam sensor of *Staphylococcus aureus*. *J. Biol. Chem.* **279**, 47278–87
120. Marrero, A., Mallorquí-Fernández, G., Guevara, T., García-Castellanos, R., and Gomis-Rüth, F. X. (2006) Unbound and acylated structures of the MecR1 extracellular antibiotic-sensor domain provide insights into the signal-transduction system that triggers methicillin resistance. *J. Mol. Biol.* **361**, 506–21
121. Thumanu, K., Cha, J., Fisher, J. F., Perrins, R., Mobashery, S., and Wharton, C. (2006) Discrete steps in sensing of beta-lactam antibiotics by the BlaR1 protein of the methicillin-resistant *Staphylococcus aureus* bacterium. *Proc. Natl. Acad. Sci. U. S. A.* **103**, 10630–5
122. Golemi-Kotra, D., Cha, J. Y., Meroueh, S. O., Vakulenko, S. B., and Mobashery, S. (2003) Resistance to beta-lactam antibiotics and its mediation by the sensor domain of the transmembrane BlaR signaling pathway in *Staphylococcus aureus*. *J. Biol. Chem.* **278**, 18419–25
123. Hanique, S., Colombo, M.-L. L., Goormaghtigh, E., Soumillon, P., Frère, J.-M. M., and Joris, B. (2004) Evidence of an Intramolecular Interaction between the Two Domains of the BlaR1 Penicillin Receptor during the Signal Transduction. *J. Biol. Chem.* **279**, 14264–14272
124. Frederick, T. E., Wilson, B. D., Cha, J., Mobashery, S., and Peng, J. W. (2014) Revealing cell-surface intramolecular interactions in the BlaR1 protein of methicillin-resistant *Staphylococcus aureus* by NMR spectroscopy. *Biochemistry*. **53**, 10–12
125. Staude, M. W., Frederick, T. E., Natarajan, S. V., Wilson, B. D., Tanner, C. E., Ruggiero, S. T., Mobashery, S., and Peng, J. W. (2015) Investigation of signal transduction routes within the sensor/transducer protein BlaR1 of *Staphylococcus aureus*. *Biochemistry*. **54**, 1600–10
126. Mescola, A., Dauvin, M., Amoroso, A., Duwez, A. S., and Joris, B. (2019) Single-molecule force spectroscopy to decipher the early signalling step in membrane-bound penicillin receptors embedded into a lipid bilayer. *Nanoscale*. **11**, 12275–12284
127. Boudreau, M. A., Fishovitz, J., Llarrull, L. I., Xiao, Q., and Mobashery, S. (2015) Phosphorylation of BlaR1 in Manifestation of Antibiotic Resistance in Methicillin-Resistant *Staphylococcus aureus* and Its Abrogation by Small Molecules. *ACS Infect. Dis.* **1**, 454–459
128. Hooper, N. M. (1994) Families of zinc metalloproteases. *FEBS Lett.* **354**, 1–6
129. Matthews, B. W. (1988) Structural Basis of the Action of Thermolysin and Related Zinc Peptidases. *Acc. Chem. Res.* **21**, 333–340
130. Berzigotti, S., Benlafya, K., Sépulchre, J., Amoroso, A., and Joris, B. (2012) *Bacillus licheniformis* BlaR1 L3 loop is a zinc metalloprotease activated by self-proteolysis. *PLoS One*. **7**, e36400
131. Arêde, P., Milheiriço, C., de Lencastre, H., and Oliveira, D. C. (2012) The anti-repressor MecR2 promotes the proteolysis of the mecA repressor and enables optimal expression of β -lactam resistance in MRSA. *PLoS Pathog.* **8**, e1002816

132. Amoroso, A., Boudet, J., Berzigotti, S., Duval, V., Teller, N., Mengin-Lecreulx, D., Luxen, A., Simorre, J.-P., and Joris, B. (2012) A peptidoglycan fragment triggers β -lactam resistance in *Bacillus licheniformis*. *PLoS Pathog.* **8**, e1002571
133. Llarrull, L. I., and Mobashery, S. (2012) Dissection of events in the resistance to β -lactam antibiotics mediated by the protein BlaR1 from *Staphylococcus aureus*. *Biochemistry.* **51**, 4642–9
134. Ye, J., Davé, U. P., Grishin, N. V., Goldstein, J. L., and Brown, M. S. (2000) Asparagine-proline sequence within membrane-spanning segment of SREBP triggers intramembrane cleavage by Site-2 protease. *Proc. Natl. Acad. Sci. U. S. A.* **97**, 5123–5128
135. Llarrull, L. I., Toth, M., Champion, M. M., and Mobashery, S. (2011) Activation of BlaR1 protein of methicillin-resistant *Staphylococcus aureus*, its proteolytic processing, and recovery from induction of resistance. *J. Biol. Chem.* **286**, 38148–58
136. Henze, U. U., and Berger-Bächi, B. (1995) *Staphylococcus aureus* penicillin-binding protein 4 and intrinsic beta-lactam resistance. *Antimicrob. Agents Chemother.* **39**, 2415–2422
137. Henze, U. U., and Berger-Bächi, B. (1996) Penicillin-binding protein 4 overproduction increases beta-lactam resistance in *Staphylococcus aureus*. *Antimicrob. Agents Chemother.* **40**, 2121–5
138. Banerjee, R., Gretes, M., Basuino, L., Strynadka, N., and Chambers, H. F. (2008) In vitro selection and characterization of ceftobiprole-resistant methicillin-resistant *Staphylococcus aureus*. *Antimicrob. Agents Chemother.* **52**, 2089–2096
139. Chan, L. C., Gilbert, A., Basuino, L., Da Costa, T. M., Hamilton, S. M., Dos Santos, K. R., Chambers, H. F., and Chatterjee, S. S. (2016) PBP 4 mediates high-level resistance to new-generation cephalosporins in *Staphylococcus aureus*. *Antimicrob. Agents Chemother.* **60**, 3934–3941
140. Lahiri, S. D., and Alm, R. A. (2016) Identification of non-PBP2a resistance mechanisms in *Staphylococcus aureus* after serial passage with ceftaroline: involvement of other PBPs. *J. Antimicrob. Chemother.* **71**, 3050–3057
141. Hebeisen, P., Heinze-Krauss, I., Angehrn, P., Hohl, P., Page, M. G., and Then, R. L. (2001) In vitro and in vivo properties of Ro 63-9141, a novel broad-spectrum cephalosporin with activity against methicillin-resistant staphylococci. *Antimicrob. Agents Chemother.* **45**, 825–36
142. Banerjee, R., Gretes, M., Harlem, C., Basuino, L., and Chambers, H. F. (2010) A mecA-negative strain of methicillin-resistant *Staphylococcus aureus* with high-level β -lactam resistance contains mutations in three genes. *Antimicrob. Agents Chemother.* **54**, 4900–4902
143. Basuino, L., Jouselin, A., Alexander, J. A. N., Strynadka, N. C. J., Pinho, M. G., Chambers, H. F., and Chatterjee, S. S. (2018) PBP4 activity and its overexpression are necessary for PBP4-mediated high-level β -lactam resistance. *J. Antimicrob. Chemother.* **73**, 1177–1180
144. Greninger, A. L., Chatterjee, S. S., Chan, L. C., Hamilton, S. M., Chambers, H. F., and Chiu, C. Y. (2016) Whole-Genome Sequencing of Methicillin-Resistant *Staphylococcus aureus* Resistant to Fifth-Generation Cephalosporins Reveals Potential Non-mecA Mechanisms of Resistance. *PLoS One.* **11**, e0149541
145. Angeles Argudín, M., Roisin, S., Nienhaus, L., Dodémont, M., De Mendonça, R.,

- Nonhoff, C., Deplano, A., and Denisa, O. (2018) Genetic diversity among staphylococcus aureus isolates showing oxacillin and/or ceftoxitin resistance not linked to the presence of mec genes. *Antimicrob. Agents Chemother.* **62**, AAC.00091-18
146. Argudín, M. A., Dodémont, M., Taguemount, M., Roisin, S., de Mendonça, R., Deplano, A., Nonhoff, C., and Denis, O. (2017) In vitro activity of ceftaroline against clinical *Staphylococcus aureus* isolates collected during a national survey conducted in Belgian hospitals. *J. Antimicrob. Chemother.* **72**, 56–59
147. Davies, T. A., Page, M. G. P., Shang, W., Andrew, T., Kania, M., and Bush, K. (2007) Binding of ceftobiprole and comparators to the penicillin-binding proteins of *Escherichia coli*, *Pseudomonas aeruginosa*, *Staphylococcus aureus*, and *Streptococcus pneumoniae*. *Antimicrob. Agents Chemother.* **51**, 2621–2624
148. Kosowska-Shick, K., McGhee, P. L., and Appelbaum, P. C. (2010) Affinity of ceftaroline and other β -lactams for penicillin-binding proteins from *Staphylococcus aureus* and *Streptococcus pneumoniae*. *Antimicrob. Agents Chemother.* **54**, 1670–1677
149. Chambers, H., and Sachdeva, M. (1990) Binding of β -Lactam Antibiotics to Penicillin-Binding Proteins in Methicillin-Resistant *Staphylococcus aureus*. *J. Infect. Dis.* **161**, 1170–1176
150. Ehmann, D. E., Jahić, H., Ross, P. L., Gu, R. F., Hu, J., Durand-Réville, T. F., Lahiri, S., Thresher, J., Livchak, S., Gao, N., Palmer, T., Walkup, G. K., and Fisher, S. L. (2013) Kinetics of avibactam inhibition against class A, C, and D β -lactamases. *J. Biol. Chem.* **288**, 27960–27971
151. Chambers, H. F. (1997) Methicillin Resistance in Staphylococci : Molecular and Biochemical Basis and Clinical Implications. *Clin. Microbiol. Rev.* **10**, 781–791
152. Chatterjee, S. S., Chen, L., Gilbert, A., da Costa, T. M., Nair, V., Datta, S. K., Kreiswirth, B. N., and Chambers, H. F. (2017) PBP4 mediates β -lactam resistance by altered function. *Antimicrob. Agents Chemother.* 10.1128/AAC.00932-17
153. Zapun, A., Macheboeuf, P., and Vernet, T. (2017) Penicillin-Binding Proteins and β -Lactam Resistance. in *Antimicrobial Drug Resistance*, pp. 177–211, Springer International Publishing, Cham, 10.1007/978-3-319-46718-4_13
154. Navratna, V., Nadig, S., Sood, V., Prasad, K., Arakere, G., and Gopal, B. (2010) Molecular basis for the role of *Staphylococcus aureus* penicillin binding protein 4 in antimicrobial resistance. *J. Bacteriol.* **192**, 134–44
155. Dyke, K. G. H., Jevons, M. P., and Parker, M. T. (1966) Penicillinase production and intrinsic resistance to penicillins in *Staphylococcus aureus*. *Lancet.* **287**, 835–838
156. Katayama, Y., Zhang, H. Z., Hong, D., and Chambers, H. F. (2003) Jumping the barrier to β -lactam resistance in *Staphylococcus aureus*. *J. Bacteriol.* **185**, 5465–5472
157. Griffiths, J. M., and O'Neill, A. J. (2012) Loss of function of the GdpP protein leads to joint β -lactam/ glycopeptide tolerance in *Staphylococcus aureus*. *Antimicrob. Agents Chemother.* **56**, 579–581
158. Page, M. G. (2004) Cephalosporins in clinical development. *Expert Opin. Investig. Drugs.* **13**, 973–985
159. Schweizer, M. L., Furuno, J. P., Harris, A. D., Johnson, J. K., Shardell, M. D., McGregor, J. C., Thom, K. A., Cosgrove, S. E., Sakoulas, G., and Perencevich, E. N. (2011) Comparative effectiveness of nafcillin or cefazolin versus vancomycin in methicillin-susceptible *Staphylococcus aureus* bacteremia. *BMC Infect. Dis.* **11**, 279

160. Winter, G., Lobley, C. M. C., and Prince, S. M. (2013) Decision making in xia2. *Acta Crystallogr. D. Biol. Crystallogr.* **69**, 1260–73
161. Kabsch, W. (2010) XDS. *Acta Crystallogr. Sect. D Biol. Crystallogr.* **66**, 125–132
162. Evans, P. R., and Murshudov, G. N. (2013) How good are my data and what is the resolution? *Acta Crystallogr. Sect. D Biol. Crystallogr.* **69**, 1204–1214
163. Winn, M. D., Ballard, C. C., Cowtan, K. D., Dodson, E. J., Emsley, P., Evans, P. R., Keegan, R. M., Krissinel, E. B., Leslie, A. G. W., McCoy, A., McNicholas, S. J., Murshudov, G. N., Pannu, N. S., Potterton, E. A., Powell, H. R., Read, R. J., Vagin, A., and Wilson, K. S. (2011) Overview of the CCP4 suite and current developments. *Acta Crystallogr. Sect. D Biol. Crystallogr.* **67**, 235–242
164. McCoy, A. J., Grosse-Kunstleve, R. W., Adams, P. D., Winn, M. D., Storoni, L. C., and Read, R. J. (2007) Phaser crystallographic software. *J. Appl. Crystallogr.* **40**, 658–674
165. Adams, P. D., Afonine, P. V., Bunkóczi, G., Chen, V. B., Davis, I. W., Echols, N., Headd, J. J., Hung, L. W., Kapral, G. J., Grosse-Kunstleve, R. W., McCoy, A. J., Moriarty, N. W., Oeffner, R., Read, R. J., Richardson, D. C., Richardson, J. S., Terwilliger, T. C., and Zwart, P. H. (2010) PHENIX: A comprehensive Python-based system for macromolecular structure solution. *Acta Crystallogr. Sect. D Biol. Crystallogr.* **66**, 213–221
166. Terwilliger, T. C., Grosse-Kunstleve, R. W., Afonine, P. V., Moriarty, N. W., Zwart, P. H., Hung, L. W., Read, R. J., and Adams, P. D. (2007) Iterative model building, structure refinement and density modification with the PHENIX AutoBuild wizard. in *Acta Crystallographica Section D: Biological Crystallography*, pp. 61–69, International Union of Crystallography, **64**, 61–69
167. Emsley, P., Lohkamp, B., Scott, W. G., and Cowtan, K. (2010) Features and development of Coot. *Acta Crystallogr. Sect. D Biol. Crystallogr.* **66**, 486–501
168. Afonine, P. V., Grosse-Kunstleve, R. W., Echols, N., Headd, J. J., Moriarty, N. W., Mustyakimov, M., Terwilliger, T. C., Urzhumtsev, A., Zwart, P. H., and Adams, P. D. (2012) Towards automated crystallographic structure refinement with phenix.refine. *Acta Crystallogr. Sect. D Biol. Crystallogr.* **68**, 352–367
169. Chen, V. B., Arendall, W. B., Headd, J. J., Keedy, D. A., Immormino, R. M., Kapral, G. J., Murray, L. W., Richardson, J. S., and Richardson, D. C. (2010) MolProbity: All-atom structure validation for macromolecular crystallography. *Acta Crystallogr. Sect. D Biol. Crystallogr.* **66**, 12–21
170. Joosten, R. P., Long, F., Murshudov, G. N., and Perrakis, A. (2014) The PDB_REDO server for macromolecular structure model optimization. *IUCrJ.* **1**, 213–220
171. Krissinel, E., and Henrick, K. (2007) Inference of Macromolecular Assemblies from Crystalline State. *J. Mol. Biol.* **372**, 774–797
172. Laskowski, R. A., and Swindells, M. B. (2011) LigPlot+: Multiple Ligand–Protein Interaction Diagrams for Drug Discovery. *J. Chem. Inf. Model.* **51**, 2778–2786
173. Gasteiger, E., Hoogland, C., Gattiker, A., Duvaud, S., Wilkins, M. R., Appel, R. D., and Bairoch, A. (2005) Protein Identification and Analysis Tools on the ExPASy Server. *Proteomics Protoc. Handb.* 10.1385/1-59259-890-0:571
174. Ourghanlian, C., Soroka, D., and Arthur, M. (2017) Inhibition by avibactam and clavulanate of the β -lactamases KPC-2 and CTX-M-15 harboring the substitution N132G in the conserved SDN motif. *Antimicrob. Agents Chemother.* **61**, e02510-16
175. Queenan, A. M., Shang, W., Kania, M., Page, M. G. P., and Bush, K. (2007) Interactions

- of ceftobiprole with β -lactamases from molecular classes A to D. *Antimicrob. Agents Chemother.* **51**, 3089–3095
176. Holm, L., and Laakso, L. M. (2016) Dali server update. *Nucleic Acids Res.* **44**, W351-5
 177. Morlot, C., Pernot, L., Le Gouellec, A., Di Guilmi, A. M., Vernet, T., Dideberg, O., and Dessen, A. (2005) Crystal structure of a peptidoglycan synthesis regulatory factor (PBP3) from *Streptococcus pneumoniae*. *J. Biol. Chem.* **280**, 15984–15991
 178. Nicola, G., Tomberg, J., Pratt, R. F., Nicholas, R. A., and Davies, C. (2010) Crystal structures of covalent complexes of β -Lactam antibiotics with *Escherichia coli* penicillin-binding protein 5: Toward an understanding of antibiotic specificity. *Biochemistry.* **49**, 8094–8104
 179. Chen, Y., Zhang, W., Shi, Q., Heseck, D., Lee, M., Mobashery, S., and Shoichet, B. K. (2009) Crystal Structures of Penicillin-Binding Protein 6 from *Escherichia coli*. *J. Am. Chem. Soc.* **131**, 14345–14354
 180. Nicholas, R. A., Krings, S., Tomberg, J., Nicola, G., and Davies, C. (2003) Crystal Structure of Wild-type Penicillin-binding Protein 5 from *Escherichia coli*. *J. Biol. Chem.* **278**, 52826–52833
 181. Chambers, H. F., Sachdeva, M. J., and Hackbarth, C. J. (1994) Kinetics of penicillin binding to penicillin-binding proteins of *Staphylococcus aureus*. *Biochem. J.* **301**, 139–144
 182. Hamilton, S. M., Alexander, J. A. N., Choo, E. J., Basuino, L., Da Costa, T. M., Severin, A., Chung, M., Aedo, S., Strynadka, N. C. J. J., Tomasz, A., Chatterjee, S. S., and Chambers, H. F. (2017) High-Level Resistance of *Staphylococcus aureus* to β -Lactam Antibiotics Mediated by Penicillin-Binding Protein 4 (PBP4). *Antimicrob. Agents Chemother.* **61**, AAC.02727-16
 183. Welsh, M. A., Taguchi, A., Schaefer, K., Van Tyne, D., Lebreton, F., Gilmore, M. S., Kahne, D., and Walker, S. (2017) Identification of a Functionally Unique Family of Penicillin-Binding Proteins. *J. Am. Chem. Soc.* **139**, 17727–17730
 184. Nicola, G., Fedarovich, A., Nicholas, R. A., and Davies, C. (2005) A large displacement of the SXN motif of Cys115-modified penicillin-binding protein 5 from *Escherichia coli*. *Biochem. J.* **392**, 55–63
 185. Tomberg, J., Temple, B., Fedarovich, A., Davies, C., and Nicholas, R. A. (2012) A highly conserved interaction involving the middle residue of the SXN active-site motif is crucial for function of class B penicillin-binding proteins: Mutational and computational analysis of PBP 2 from *N. gonorrhoeae*. *Biochemistry.* **51**, 2775–2784
 186. Dessen, A., Mouz, N., Gordon, E., Hopkins, J., and Dideberg, O. (2001) Crystal structure of PBP2x from a highly penicillin-resistant *Streptococcus pneumoniae* clinical isolate: A mosaic framework containing 83 mutations. *J. Biol. Chem.* **276**, 45106–45112
 187. Becker, K., Denis, O., Roisin, S., Mellmann, A., Idelevich, E. A., Knaack, D., Van Alen, S., Kriegeskorte, A., Köck, R., Schaumburg, F., Peters, G., and Ballhausen, B. (2016) Detection of mecA- and mecC-positive methicillin-resistant *Staphylococcus aureus* (MRSA) isolates by the new Xpert MRSA Gen 3 PCR assay. *J. Clin. Microbiol.* **54**, 180–184
 188. Lee, A. S., de Lencastre, H., Garau, J., Kluytmans, J., Malhotra-Kumar, S., Peschel, A., and Harbarth, S. (2018) Methicillin-resistant *Staphylococcus aureus*. *Nat. Rev. Dis. Prim.* **4**, 18033

189. Wertheim, H. F., Melles, D. C., Vos, M. C., Van Leeuwen, W., Van Belkum, A., Verbrugh, H. A., and Nouwen, J. L. (2005) The role of nasal carriage in *Staphylococcus aureus* infections. *Lancet Infect. Dis.* **5**, 751–762
190. Bush, K., and Bradford, P. A. (2016) β -lactams and β -lactamase inhibitors: An overview. *Cold Spring Harb. Perspect. Med.* **6**, a025247
191. García-Castellanos, R., Mallorquí-Fernández, G., Marrero, A., Potempa, J., Coll, M., and Gomis-Rüth, F. X. (2004) On the transcriptional regulation of methicillin resistance: MecI repressor in complex with its operator. *J. Biol. Chem.* **279**, 17888–96
192. Poirel, L., Naas, T., and Nordmann, P. (2010) Diversity, epidemiology, and genetics of class D β -lactamases. *Antimicrob. Agents Chemother.* **54**, 24–38
193. Golemi, D., Maveyraud, L., Vakulenko, S., Samama, J. P., and Mobashery, S. (2001) Critical involvement of a carbamylated lysine in catalytic function of class D β -lactamases. *Proc. Natl. Acad. Sci. U. S. A.* **98**, 14280–14285
194. Borbulevych, O., Kumarasiri, M., Wilson, B., Llarrull, L. I., Lee, M., Heseck, D., Shi, Q., Peng, J., Baker, B. M., and Mobashery, S. (2011) Lysine N ζ -decarboxylation switch and activation of the β -lactam sensor domain of BlaR1 protein of methicillin-resistant *Staphylococcus aureus*. *J. Biol. Chem.* **286**, 31466–31472
195. Kumarasiri, M., Llarrull, L. I., Borbulevych, O., Fishovitz, J., Lastochkin, E., Baker, B. M., and Mobashery, S. (2012) An amino acid position at crossroads of evolution of protein function: Antibiotic sensor domain of BlaR1 protein from *Staphylococcus aureus* versus class D β -lactamases. *J. Biol. Chem.* **287**, 8232–8241
196. Docquier, J. D., and Mangani, S. (2018) An update on β -lactamase inhibitor discovery and development. *Drug Resist. Updat.* **36**, 13–29
197. Stachyra, T., Péchereau, M. C., Bruneau, J. M., Claudon, M., Frère, J. M., Miossec, C., Coleman, K., and Black, M. T. (2010) Mechanistic studies of the inactivation of TEM-1 and P99 by NXL104, a novel non- β -lactam β -lactamase inhibitor. *Antimicrob. Agents Chemother.* **54**, 5132–5138
198. Ehmann, D. E., Jahić, H., Ross, P. L., Gu, R.-F. R.-F., Hu, J., Kern, G., Walkup, G. K., Fisher, S. L., Jahic, H., Ross, P. L., Gu, R.-F. R.-F., Hu, J., Kern, G., Walkup, G. K., and Fisher, S. L. (2012) Avibactam is a covalent, reversible, non- β -lactam β -lactamase inhibitor. *Proc. Natl. Acad. Sci. U. S. A.* **109**, 11663–11668
199. Avycaz (Ceftazidime-Avibactam) [package insert] [online] <https://www.allergan.com> (Accessed April 28, 2019)
200. Sader, H. S., Flamm, R. K., and Jones, R. N. (2013) Antimicrobial Activity of Ceftaroline-Avibactam Tested against Clinical Isolates Collected from U.S. Medical Centers in 2010-2011. *Antimicrob. Agents Chemother.* **57**, 1982–1988
201. Karlowsky, J. A., Adam, H. J., Baxter, M. R., Lagacé-Wiens, P. R. S., Walkty, A. J., Hoban, D. J., and Zhanel, G. G. (2013) In Vitro Activity of Ceftaroline-Avibactam against Gram-Negative and Gram-Positive Pathogens Isolated from Patients in Canadian Hospitals from 2010 to 2012: Results from the CANWARD Surveillance Study. *Antimicrob. Agents Chemother.* **57**, 5600–5611
202. Castanheira, M., Sader, H. S., Farrell, D. J., Mendes, R. E., and Jones, R. N. (2012) Activity of Ceftaroline-Avibactam Tested against Gram-Negative Organism Populations, including Strains Expressing One or More β -Lactamases and Methicillin-Resistant *Staphylococcus aureus* Carrying Various Staphylococcal Cassette Chromosome mec

- Types. *Antimicrob. Agents Chemother.* **56**, 4779–4785
203. Miossec, C., Cclaudon, M., Levasseur, P., Black, M. T., Claudon, M., Levasseur, P., and Black, M. T. (2013) The β -lactamase inhibitor avibactam (NXL104) does not induce ampC β -lactamase in *Enterobacter cloacae*. *Infect. Drug Resist.* **6**, 235–240
 204. Livermore, D. M., Jamrozy, D., Mushtaq, S., Nichols, W. W., Young, K., and Woodford, N. (2017) AmpC β -lactamase induction by avibactam and relebactam. *J. Antimicrob. Chemother.* **72**, 3342–3348
 205. Thurlow, L. R., Joshi, G. S., and Richardson, A. R. (2012) Virulence strategies of the dominant USA300 lineage of community-associated methicillin-resistant *Staphylococcus aureus* (CA-MRSA). *FEMS Immunol. Med. Microbiol.* **65**, 5–22
 206. Challagundla, L., Luo, X., Tickler, I. A., Didelot, X., Coleman, D. C., Shore, A. C., Coombs, G. W., Sordelli, D. O., Brown, E. L., Skov, R., Larsen, A. R., Reyes, J., Robledo, I. E., Vazquez, G. J., Rivera, R., Fey, P. D., Stevenson, K., Wang, S. H., Kreiswirth, B. N., Mediavilla, J. R., Arias, C. A., Planet, P. J., Nolan, R. L., Tenover, F. C., Goering, R. V., and Robinson, D. A. (2018) Range expansion and the origin of USA300 north american epidemic methicillin-resistant *Staphylococcus aureus*. *MBio*. 10.1128/mBio.02016-17
 207. Painter, J., and Merritt, E. A. (2006) TLSMD web server for the generation of multi-group TLS models. *J. Appl. Crystallogr.* **39**, 109–111
 208. Painter, J., and Merritt, E. A. (2006) Optimal description of a protein structure in terms of multiple groups undergoing TLS motion. *Acta Crystallogr. Sect. D Biol. Crystallogr.* **62**, 439–450
 209. Dolinsky, T. J., Nielsen, J. E., McCammon, J. A., and Baker, N. A. (2004) PDB2PQR: An automated pipeline for the setup of Poisson-Boltzmann electrostatics calculations. *Nucleic Acids Res.* 10.1093/nar/gkh381
 210. Jurrus, E., Engel, D., Star, K., Monson, K., Brandi, J., Felberg, L. E., Brookes, D. H., Wilson, L., Chen, J., Liles, K., Chun, M., Li, P., Gohara, D. W., Dolinsky, T., Konecny, R., Koes, D. R., Nielsen, J. E., Head-Gordon, T., Geng, W., Krasny, R., Wei, G. W., Holst, M. J., McCammon, J. A., and Baker, N. A. (2018) Improvements to the APBS biomolecular solvation software suite. *Protein Sci.* **27**, 112–128
 211. Goto, J., Kataoka, R., Muta, H., and Hirayama, N. (2008) ASEDock-docking based on alpha spheres and excluded volumes. *J. Chem. Inf. Model.* **48**, 583–590
 212. Schrödinger Release 2019-1: Desmond Molecular Dynamics System DESR, New York, NY, 2019. Maestro-Desmond Interoperability Tools, Schrödinger, New York, NY, 2019
 213. Birck, C., Cha, J. Y., Cross, J., Schulze-Briese, C., Meroueh, S. O., Schlegel, H. B., Mobashery, S., and Samama, J.-P. (2004) X-ray crystal structure of the acylated beta-lactam sensor domain of BlaR1 from *Staphylococcus aureus* and the mechanism of receptor activation for signal transduction. *J. Am. Chem. Soc.* **126**, 13945–7
 214. González-Bello, C., Rodríguez, D., Pernas, M., Rodríguez, Á., and Colchón, E. (2019) β -Lactamase Inhibitors to Restore the Efficacy of Antibiotics against Superbugs. *J. Med. Chem.* 10.1021/acs.jmedchem.9b01279
 215. A Study to Investigate the Intrapulmonary Lung Penetration of Nacubactam in Healthy Participants - Full Text View - ClinicalTrials.gov [online]
<https://clinicaltrials.gov/ct2/show/NCT03182504?term=nacubactam&draw=2&rank=1>
 (Accessed February 8, 2020)

216. Efficacy and Safety of Imipenem+Cilastatin/Relebactam (MK-7655A) in Japanese Participants With Complicated Intra-abdominal Infection or Complicated Urinary Tract Infection (MK-7655A-017) - Full Text View - ClinicalTrials.gov [online] <https://clinicaltrials.gov/ct2/show/NCT03293485?term=relebactam&draw=2&rank=2> (Accessed February 8, 2020)
217. Mallalieu, N. L., Winter, E., Fettner, S., Patel, K., Zwanziger, E., Attley, G., Rodriguez, I., Kano, A., Salama, S. M., Bentley, D., and Geretti, A. M. (2020) Safety and Pharmacokinetic Characterization of Nacubactam, a Novel β -Lactamase Inhibitor, Alone and in Combination with Meropenem, in Healthy Volunteers. *Antimicrob. Agents Chemother.* 10.1128/AAC.02229-19
218. Antunes, N. T., Lamoureaux, T. L., Toth, M., Stewart, N. K., Frase, H., and Vakulenko, S. B. (2014) Class D β -lactamases: are they all carbapenemases? *Antimicrob. Agents Chemother.* **58**, 2119–25
219. Evans, B. A., and Amyes, S. G. B. (2014) OXA β -lactamases. *Clin. Microbiol. Rev.* **27**, 241–63
220. King, D. T., King, A. M., Lal, S. M., Wright, G. D., and Strynadka, N. C. J. (2015) Molecular Mechanism of Avibactam-Mediated β -Lactamase Inhibition. *ACS Infect. Dis.* **1**, 175–184
221. Schroder, E. C., Klamer, Z. L., Saral, A., Sugg, K. A., June, C. M., Wymore, T., Szarecka, A., and Leonard, D. A. (2016) Clinical variants of the native class D β -lactamase of *Acinetobacter baumannii* pose an emerging threat through increased hydrolytic activity against carbapenems. *Antimicrob. Agents Chemother.* **60**, 6155–6164
222. Szarecka, A., Lesnock, K. R., Ramirez-Mondragon, C. A., Nicholas, H. B., and Wymore, T. (2011) The Class D β -lactamase family: Residues governing the maintenance and diversity of function. *Protein Eng. Des. Sel.* **24**, 801–809
223. June, C. M., Muckenthaler, T. J., Schroder, E. C., Klamer, Z. L., Wawrzak, Z., Powers, R. A., Szarecka, A., and Leonard, D. A. (2016) The structure of a doripenem-bound OXA-51 class D β -lactamase variant with enhanced carbapenemase activity. *Protein Sci.* **25**, 2152–2163
224. Santillana, E., Beceiro, A., Bou, G., and Romero, A. (2007) Crystal structure of the carbapenemase OXA-24 reveals insights into the mechanism of carbapenem hydrolysis. *Proc. Natl. Acad. Sci. U. S. A.* **104**, 5354–5359

Appendices

Appendix A – Research publications

First author publications arising from PhD work

- 2020 **Alexander, J.A.N.**, Radaeva, M., King, D.T., Chambers, H.F., Cherkasov, A., Chatterjee, S.S., & Strynadka, N.C.J. Structural analysis of avibactam mediated activation of the bla and mec divergons in methicillin-resistant *Staphylococcus aureus*. *J. Biol. Chem.* In press.
- 2018 **Alexander, J.A.N.**, Chatterjee, S.S., Hamilton, S.M., Eltis, L.D., Chambers, H.F., and Strynadka, N.C.J. Structural and kinetic analysis of penicillin-binding protein 4 (PBP4)-mediated antibiotic resistance in *Staphylococcus aureus*. *J. Biol. Chem.* **293**, 19854–19865

Additional publications arising from graduate work

- 2020 Zeytuni, N., Dickey, S.W., Hu, J., Chou, H.T., Worrall, L.J., **Alexander, J.A.N.**, Carlson, M.L., Nosella, M., Duong, F., Yu, Z., Otto, M., Strynadka, N.C.J. Structural insight into the *Staphylococcus aureus* ATP-driven exporter of virulent peptide toxins. *Science Advances*. In press.
- 2019 Maya-Martinez, R., **Alexander, J.A.N.**, Otten, C.F., Ayala, I., Vollmer, D., Gray, J., Bougault, C.M., Burt, A., Laguri, C., Fonvielle, M., Arthur, M., Strynadka, N.C.J., Vollmer, W., and Simorre, J.-P. Recognition of peptidoglycan fragments by the transpeptidase PBP4 from *Staphylococcus aureus*. *Front. Microbiol.* **9**, 3223
- 2018 Basuino, L., Jouselin, A., **Alexander, J.A.N.**, Strynadka, N.C.J., Pinho, M.G., Chambers, H.F., and Chatterjee, S.S. PBP4 activity and its overexpression are necessary for PBP4-mediated high-level β -lactam resistance. *J. Antimicrob. Chemother.* **73**, 1177–1180
- 2017 Hamilton, S.M., **Alexander, J.A.N.**, Choo, E.J., Basuino, L., Da Costa, T.M., Severin, A., Chung, M., Aedo, S., Strynadka, N.C.J., Tomasz, A., Chatterjee, S.S., and Chambers, H.F. High-level resistance of *Staphylococcus aureus* to β -Lactam antibiotics mediated by penicillin-binding protein 4 (PBP4). *Antimicrob. Agents Chemother.* **61**, AAC.02727-16
- 2016 King, A.M., King, D.T., French, S., Brouillette, E., Asli, A., **Alexander, J.A.N.**, Vuckovic, M., Maiti, S.N., Parr, T.R., Brown, E.D., Malouin, F., Strynadka, N.C.J., and Wright, G.D. Structural and Kinetic Characterization of Diazabicyclooctanes as Dual Inhibitors of Both Serine- β -Lactamases and Penicillin-Binding Proteins. *ACS Chem. Biol.* **11**, 864–868

Publications arising from research conducted during my BSc.

- 2018 MacLeod, M.J., Vo, N.T.K., Mikhaeil, M.S., Monaghan, S.R., **Alexander, J.A.N.**, Saran, M.K., and Lee, L.E.J. Development of a continuous cell line from larval Atlantic cod (*Gadus morhua*) and its use in the study of the microsporidian, *Loma morhua*. *J. Fish Dis.* **41**, 1359–1372

- 2014 Gignac, S.J., Vo, N.T.K., Mikhaeil, M.S., **Alexander, J.A.N.**, MacLatchy, D.L., Schulte, P.M., and Lee, L.E.J. Derivation of a continuous myogenic cell culture from an embryo of common killifish, *Fundulus heteroclitus*. *Comp. Biochem. Physiol. Part A Mol. Integr. Physiol.* **175**, 15–27

Appendix B – Chapter 2 supplementary information

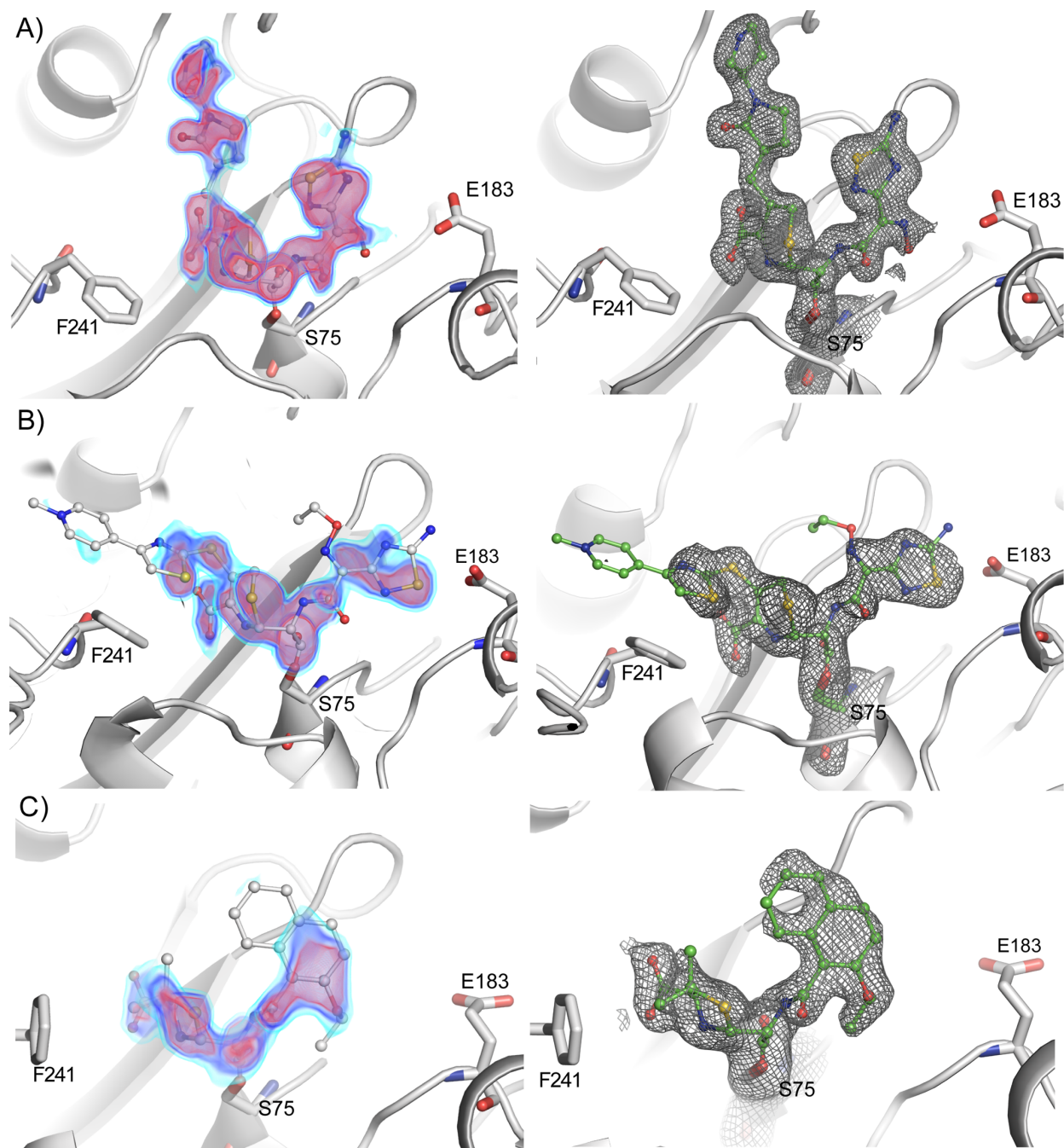


Figure B1: The active site of PBP4 in grey cartoon representation with the catalytic serine (S75) and residues mutated in PBP4^{CRB} shown in stick form. A volume mF_o-DF_c omit map shown in cyan, dark blue, and red, contoured at 3.0, 4.0, 5.0 σ , respectively, is shown in the column on the left while the column on the right shows a $2mF_o-DF_c$ electron density map contoured at 1.0 σ is shown in grey mesh. PBP4 is shown in complex with A) ceftobiprole, B) ceftaroline, and C) nafcillin with the ligands represented by thin sticks and balls. Atoms are coloured by type with C in green or white, N in blue, S in yellow and O in red.

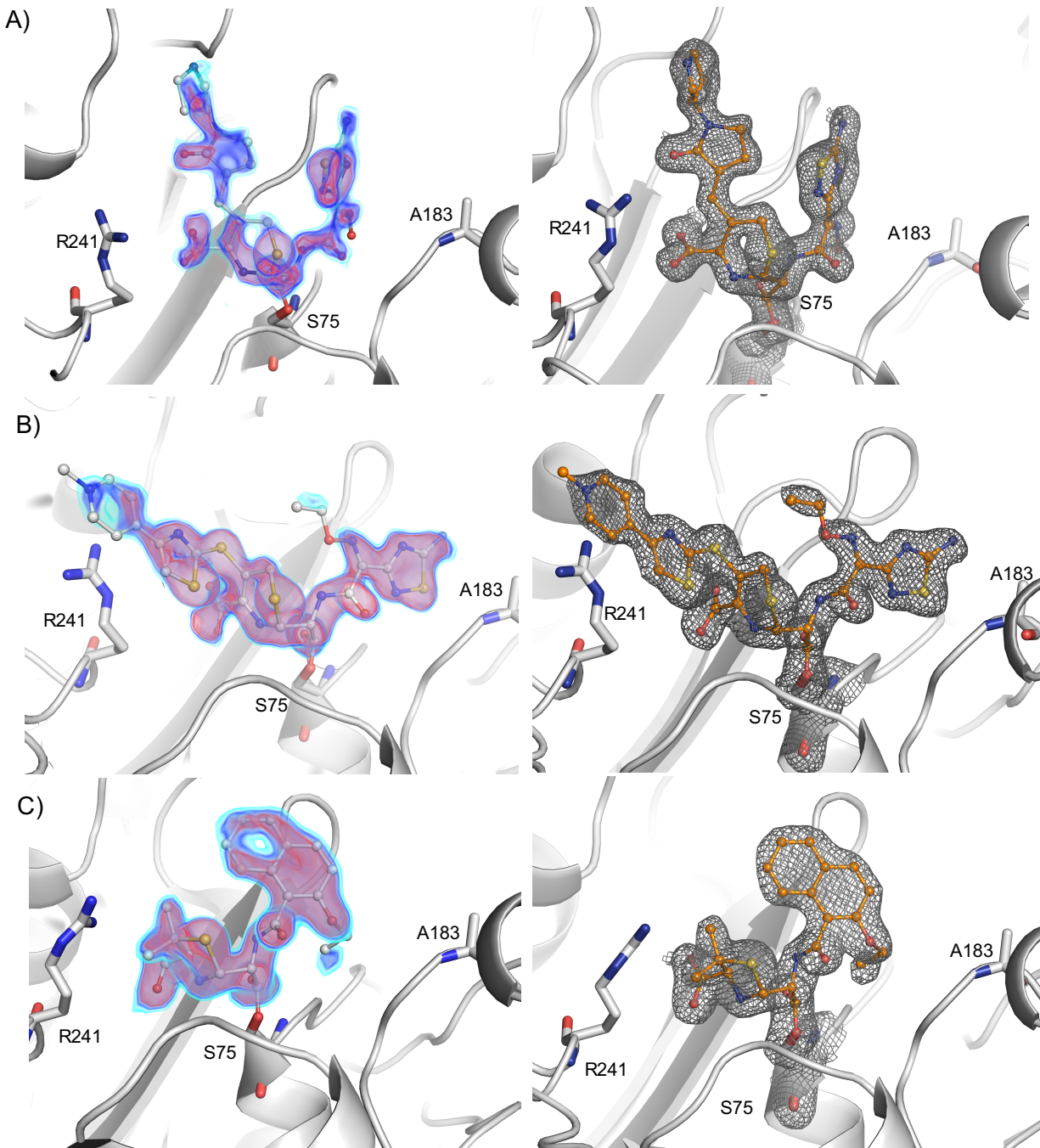


Figure B2: The active site of PBP4^{CRB} in grey cartoon representation with the catalytic serine (S75) and residues mutated in PBP4^{CRB} shown in stick form. A volume $mF_o - DF_c$ omit map shown in cyan, dark blue, and red, contoured at 3.0, 4.0, 5.0 σ , respectively, is shown in the column on the left while the column on the right shows a $2mF_o - DF_c$ electron density map contoured at 1.0 σ is shown in grey mesh. PBP4^{CRB} is shown in complex with A) ceftobiprole, B) ceftaroline, and C) nafcillin with the ligands represented by thin sticks. Atoms are coloured by type with C in orange or white, N in blue, S in yellow and O in red.

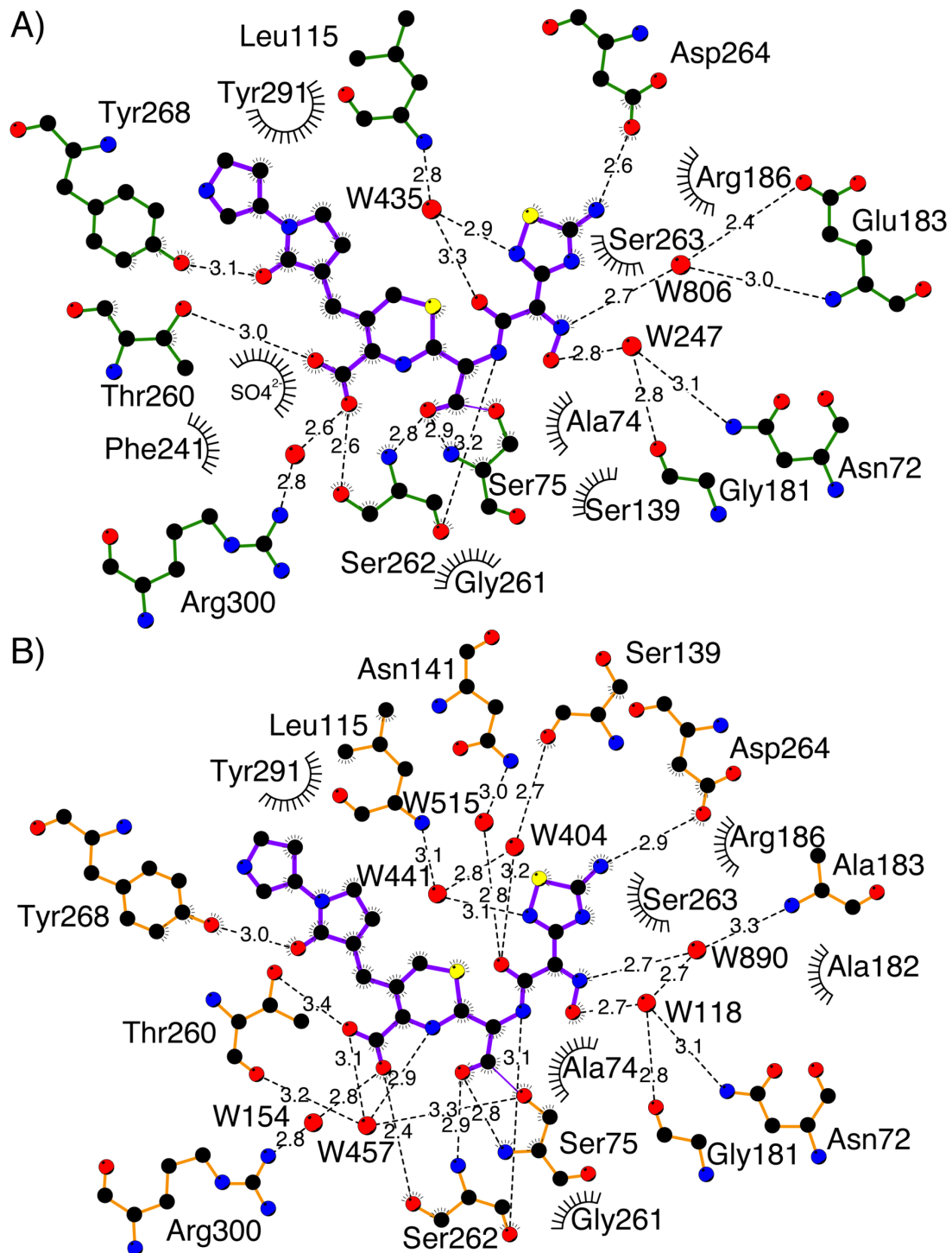


Figure B3: A) PBP4 and B) PBP4^{CRB} interactions with ceftobiprole are shown using LigPlot+. Atoms are coloured by type and ceftobiprole is shown with purple bond while PBP4 and PBP4^{CRB} bonds are shown in green and orange respectively. Water molecules hydrogen bonding distance from protein and ligand are represented with red spheres. Hydrogen bonds are depicted as black dashes with distances shown in angstroms while hydrophobic contacts are represented by black combs.

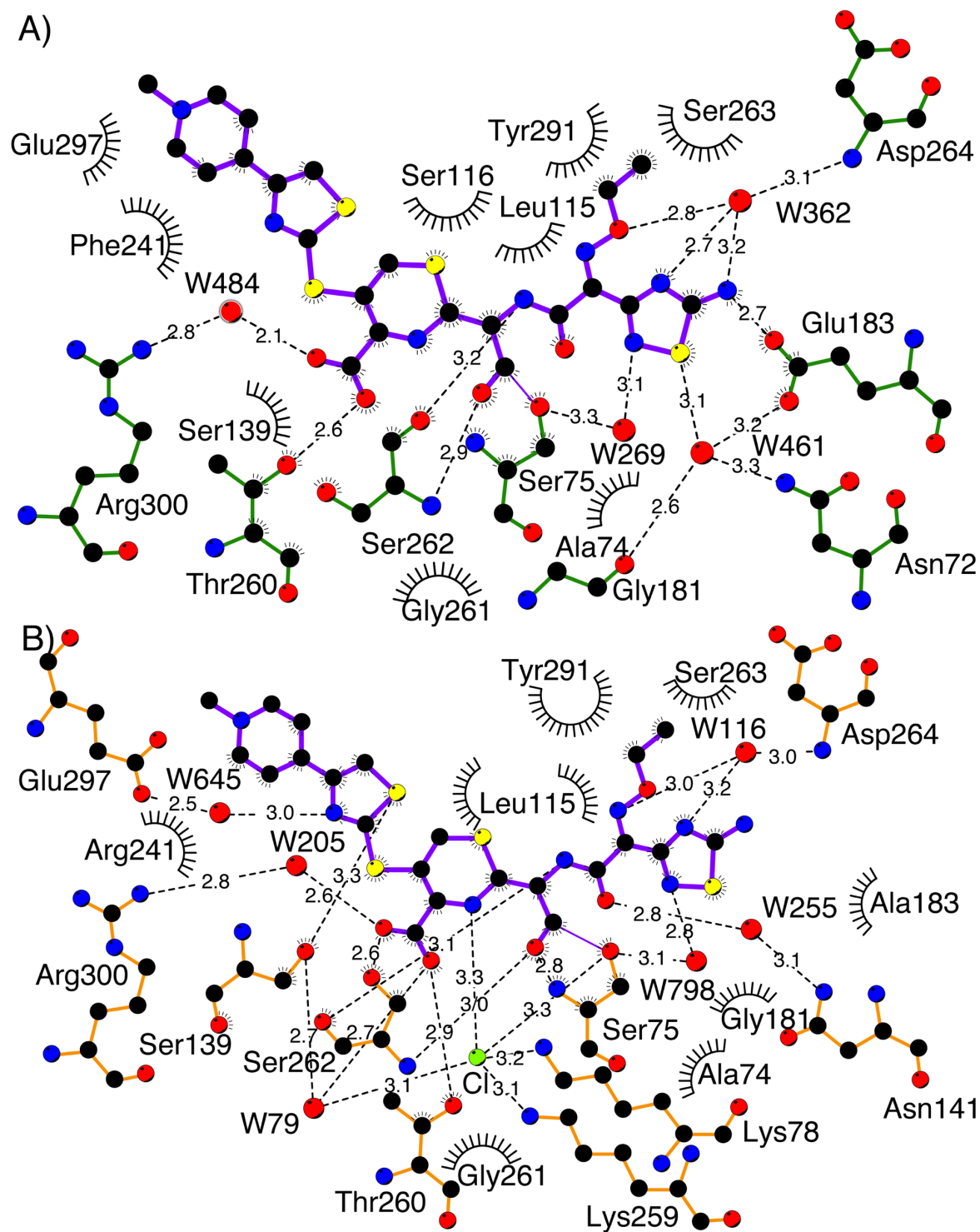


Figure B4: A) PBP4 and B) PBP4^{CRB} interactions with ceftaroline are shown using LigPlot+. Atoms are coloured by type and ceftaroline is shown with purple bond while PBP4 and PBP4^{CRB} bonds are shown in green and orange respectively. Water molecules hydrogen bonding distance from protein and ligand are represented with red spheres. Hydrogen bonds are depicted as black dashes with distances shown in angstroms while hydrophobic contacts are represented by black combs.

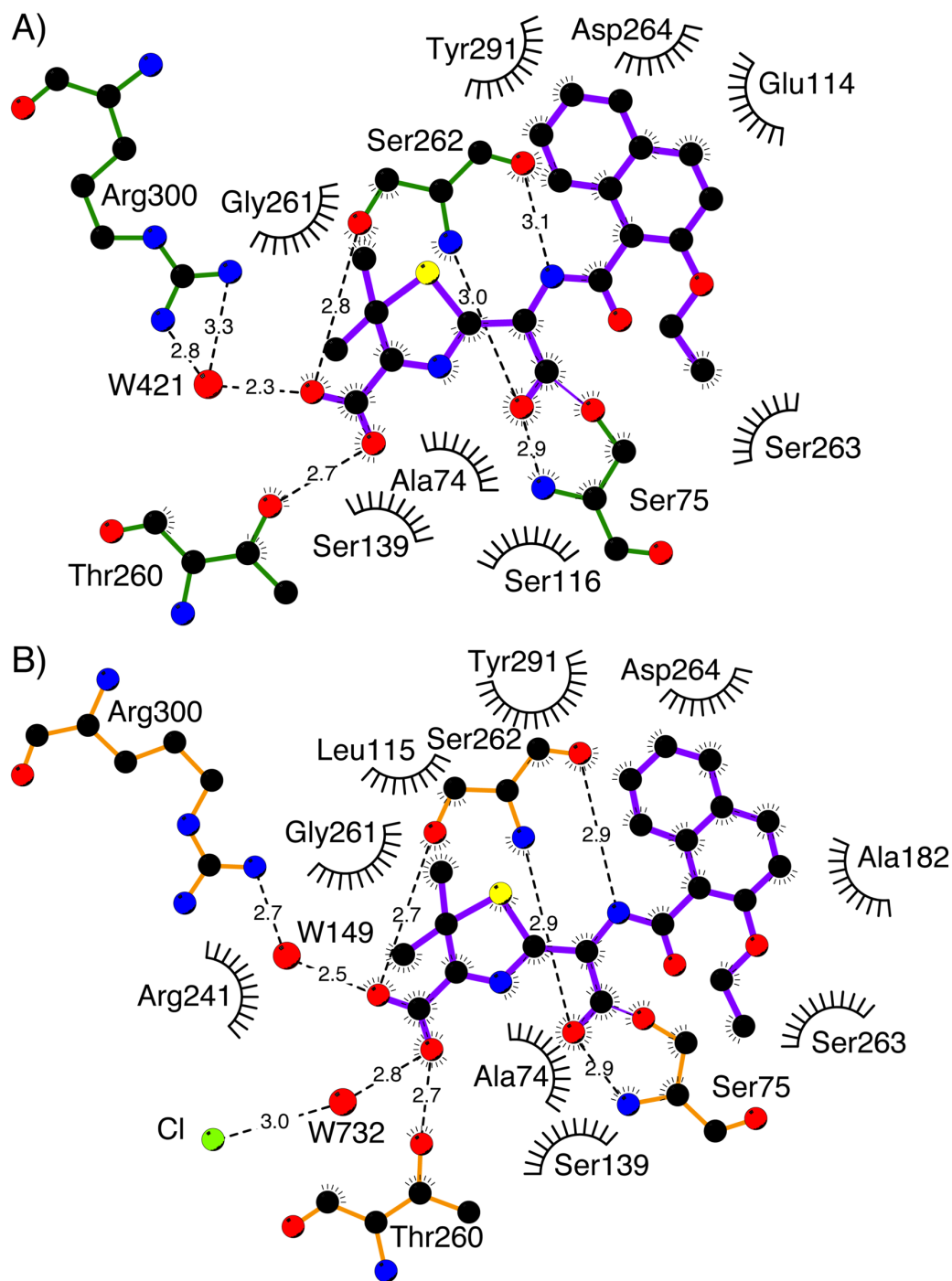


Figure B5: A) PBP4 and B) PBP4^{CRB} interactions with nafcillin are shown using LigPlot+. Atoms are coloured by type and nafcillin is shown with purple bond while PBP4 and PBP4^{CRB} bonds are shown in green and orange respectively. Water molecules hydrogen bonding distance from protein and ligand are represented with red spheres. Hydrogen bonds are depicted as black dashes with distances shown in angstroms while hydrophobic contacts are represented by black combs.

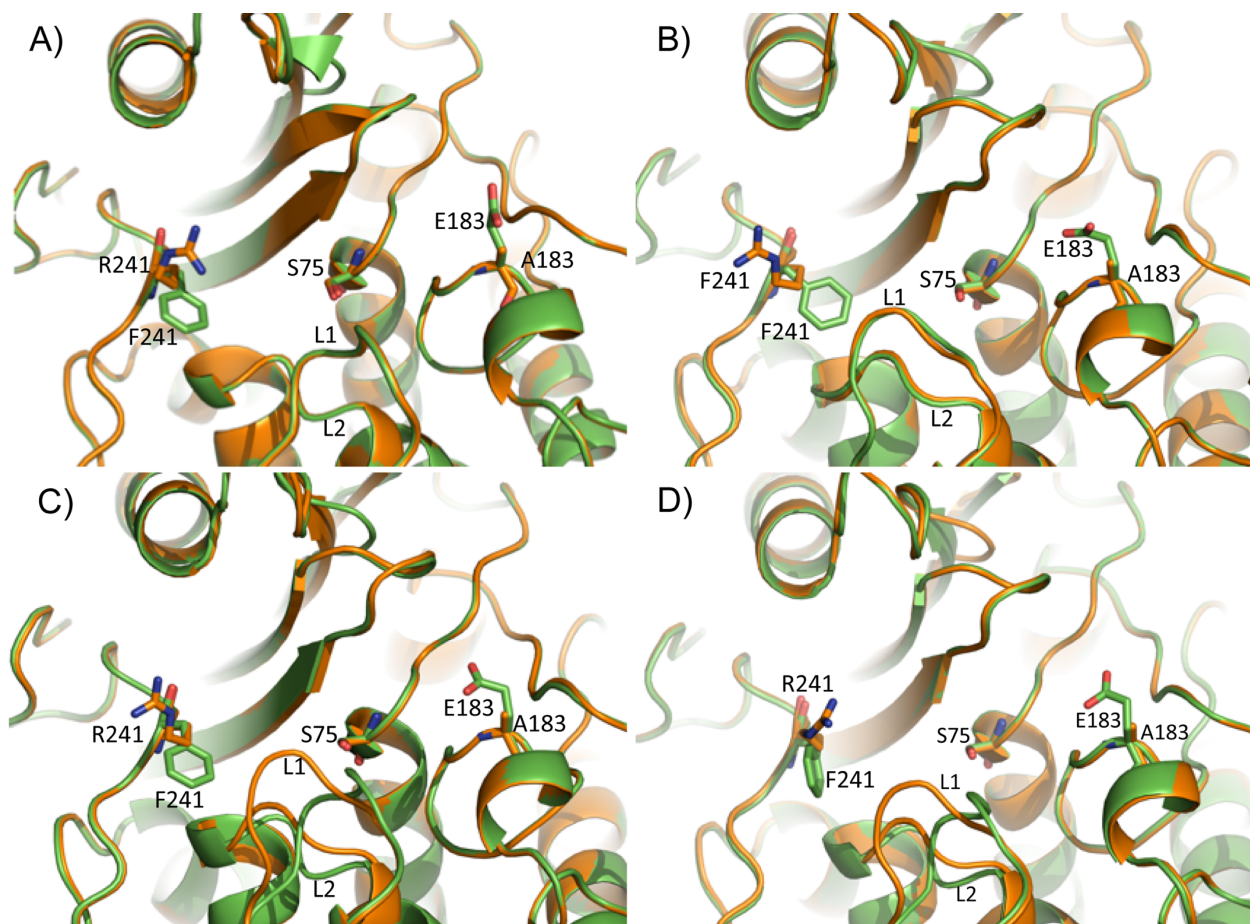


Figure B6: Cartoon representation of the aligned active site clefts of PBP4 (shown in green) and PBP4^{CRB} (shown in orange) in A) the ligand-free form and in complex with B) ceftobiprole, C) ceftaroline, and D) nafcillin (ligands not shown for clarity). The ligand-free PBP4 and PBP4^{CRB} structures as well as those in complex with ceftobiprole, ceftaroline, and nafcillin were aligned with an all matched atom C α RMSD of 0.13Å, 0.14Å, 0.57Å, and 0.54Å, respectively. The loops (L1 and L2) with significant variation are labelled. L1 includes residues 112-122 for the ligand-free, ceftaroline and ceftobiprole structures and residues 112-118 for the nafcillin bound structures. L2 includes residues 138 to 140.

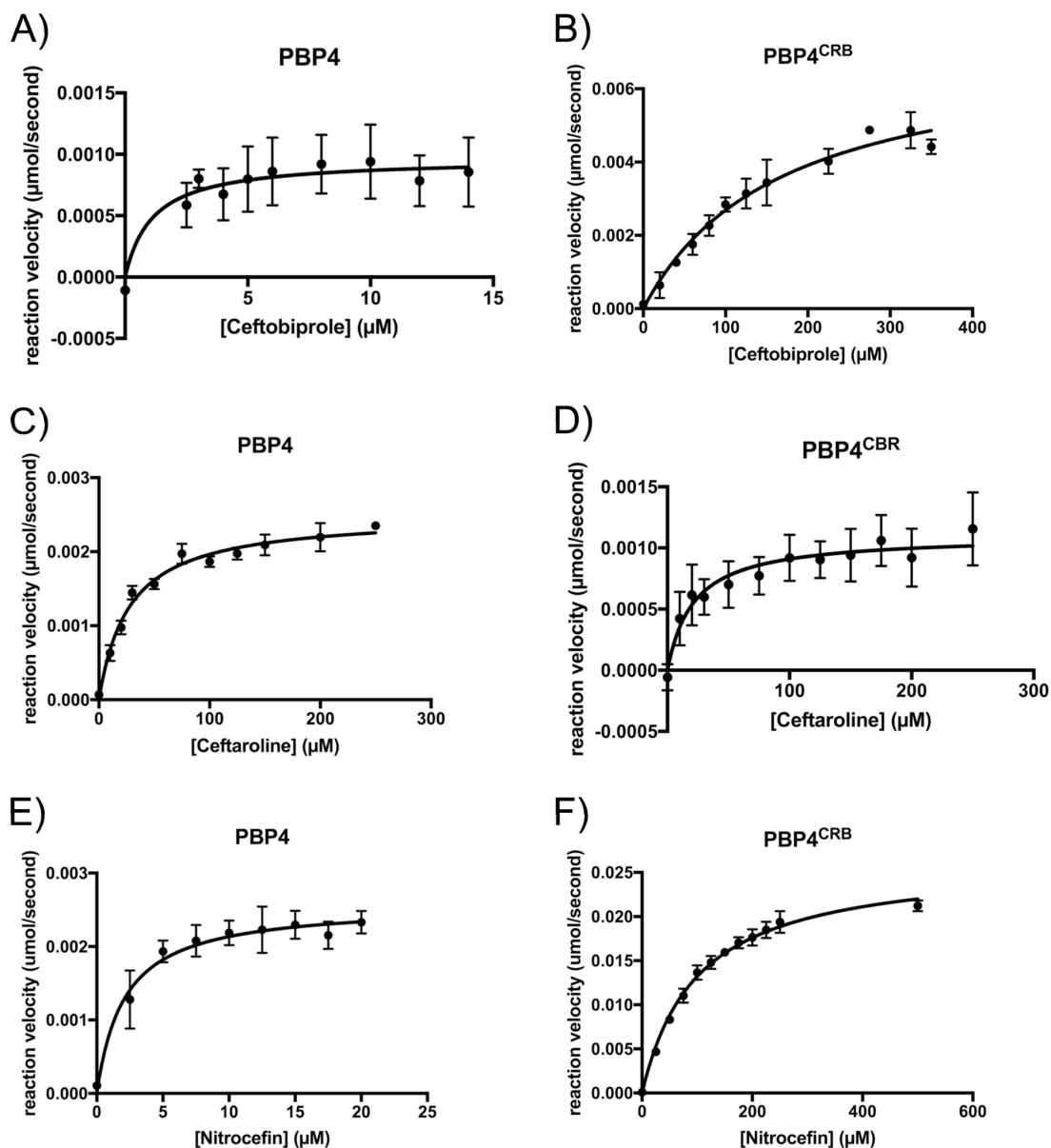


Figure B7: Plots of initial reaction velocity versus substrate concentration for PBP4 and PBP4^{CRB}. Panels A, C and E show PBP4 with ceftaroline, ceftobiprole, and nitrocefin as substrates. Panels B, D, and F show PBP4^{CRB} with ceftaroline, ceftobiprole, and nitrocefin as substrates. Steady-state kinetic parameters were calculated using data from two different protein purifications. The error bars show standard deviations.

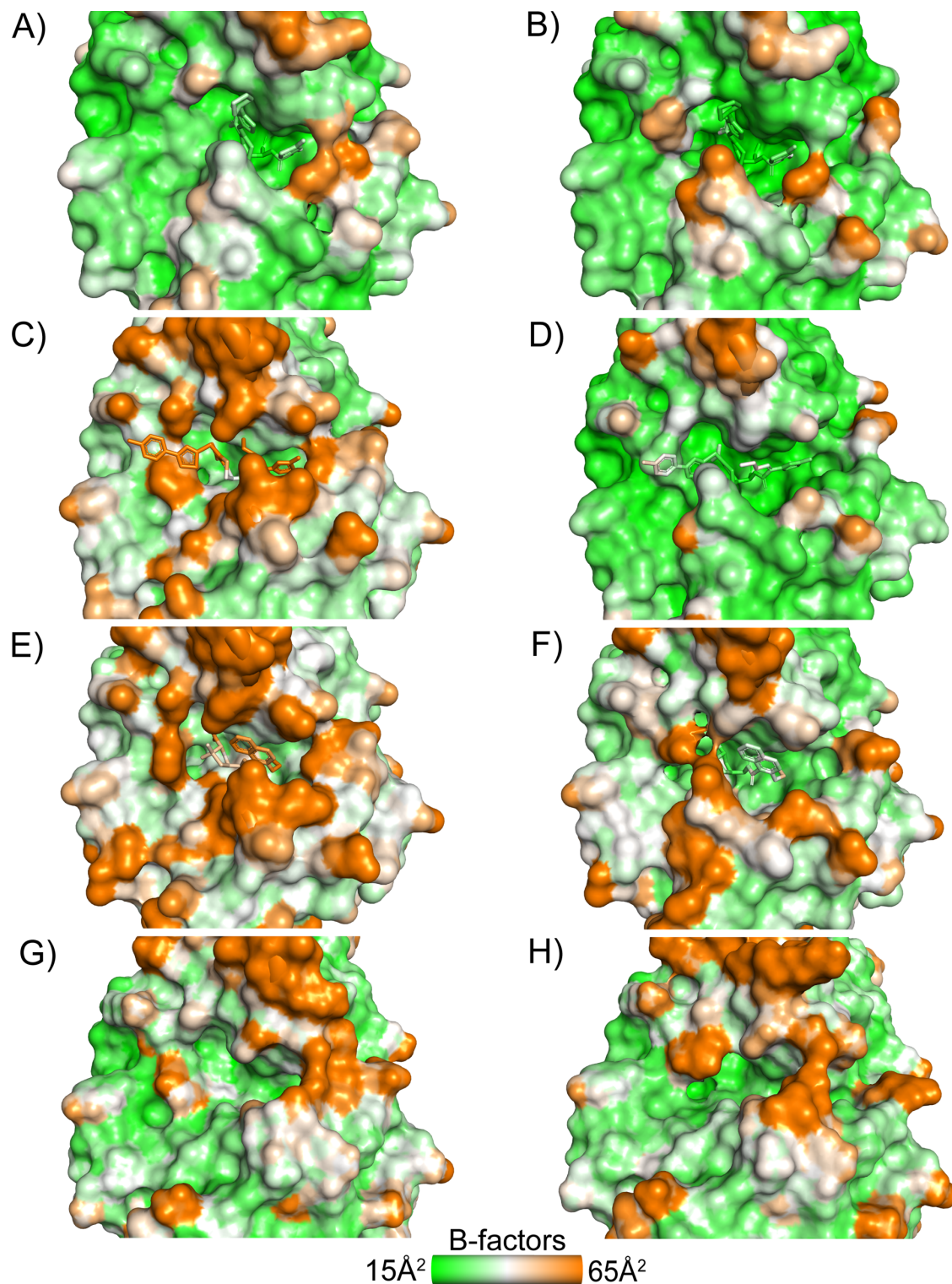


Figure B8: PBP4 and PBP4^{CRB} active site clefts coloured according to B-factor value and depicted as surfaces with ligands shown as sticks. PBP4 structures are shown on the left with A) ceftobiprole, C) ceftaroline E) nafcillin, and G) no ligand while PBP4^{CRB} structures are shown on the right with B) ceftobiprole, D) ceftaroline, F) nafcillin, and H) no ligand.

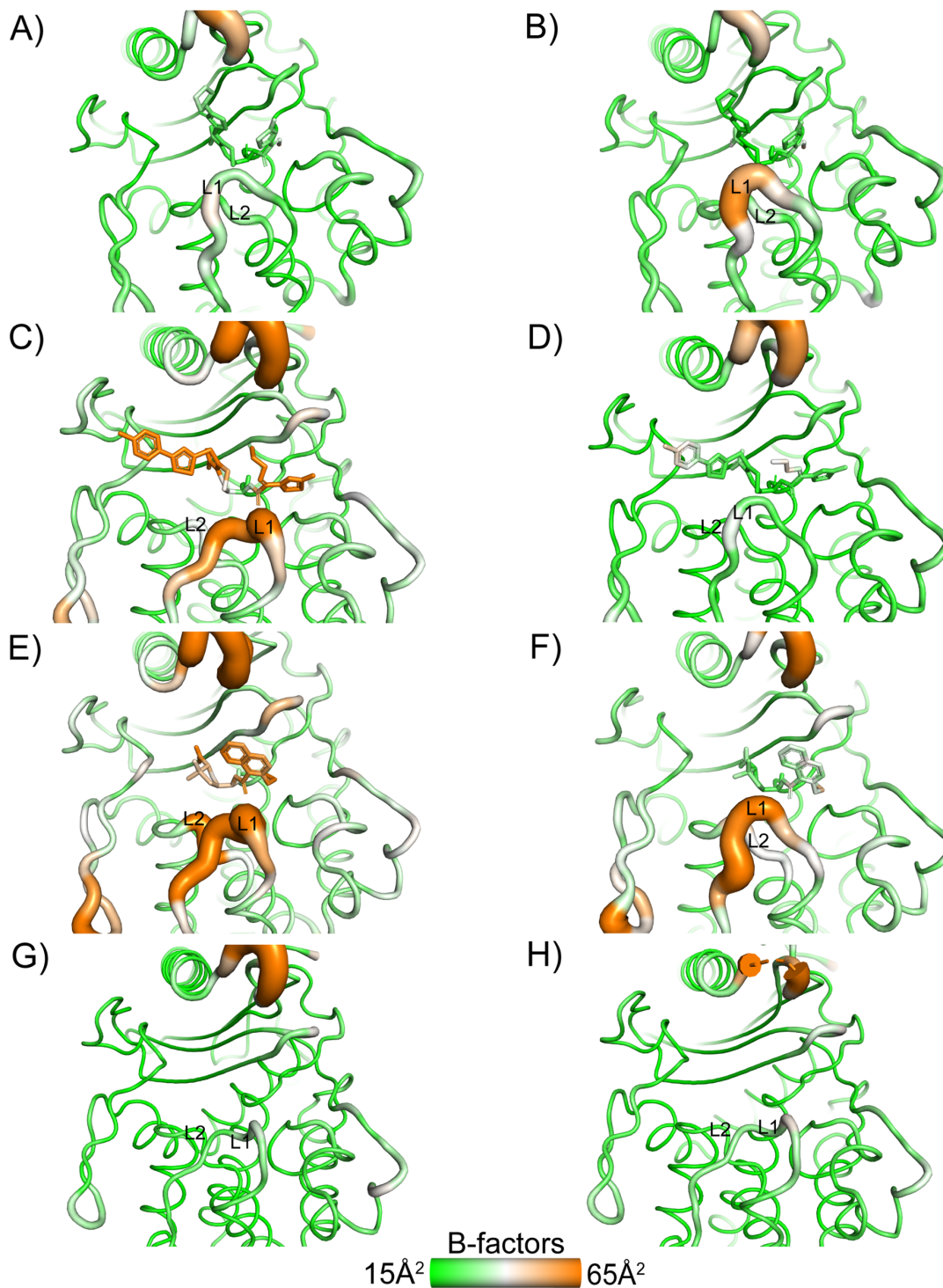


Figure B9: PBP4 and PBP4^{CRB} active site clefts coloured according to B-factor value and depicted as putty cartoons with ligands shown as sticks. PBP4 structures are shown on the left with A) ceftobiprole, C) ceftaroline E) nafcillin, and G) no ligand while PBP4^{CRB} structures are shown on the right with B) ceftobiprole, D) ceftaroline, F) nafcillin, and H) no ligand. The loops (L1 and L2) with significant variation in several of the structures are labelled.

Appendix C – Chapter 3 supplementary information

Table C1: Primers used for qRT-PCR

Primer	Sequence
<i>gyrB</i> -for	ATTGCTCTAGTAAAAGTCCTGAAGAATG
<i>gyrB</i> -rev	TAATCGTGCTTTTTCAACATTTAATATC
<i>pbp2a</i> -for	ACTTAAAACAAGCAATAGAATCATCAG
<i>pbp2a</i> -rev	AATTTGAGCATTATAAAAATGGATAATCAC
<i>blaZ</i> -for	TGCTTTAAATACTAAAAGTGGTAAGG
<i>blaZ</i> -rev	AGCAACTATATCATCTTTGTTAATATG

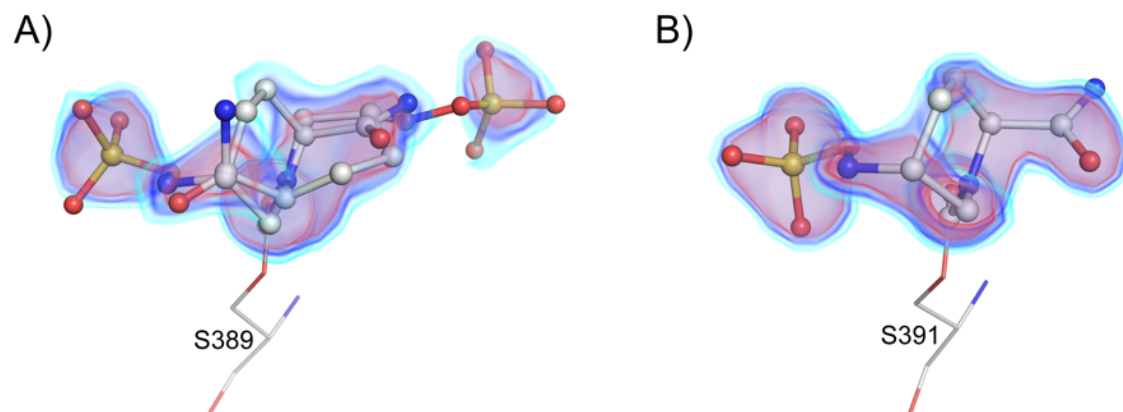


Figure C1: Volume mF_o-DF_c omit maps around avibactam modelled into the active sites of A) BlaR1^{SD} and B) MecR1^{SD}. The omit map is shown in cyan, dark blue, and red, contoured at 3.0, 4.0, 5.0 σ , respectively. Avibactam is represented by thin sticks and balls. Atoms are coloured by type with C in green or white, N in blue, S in yellow and O in red.

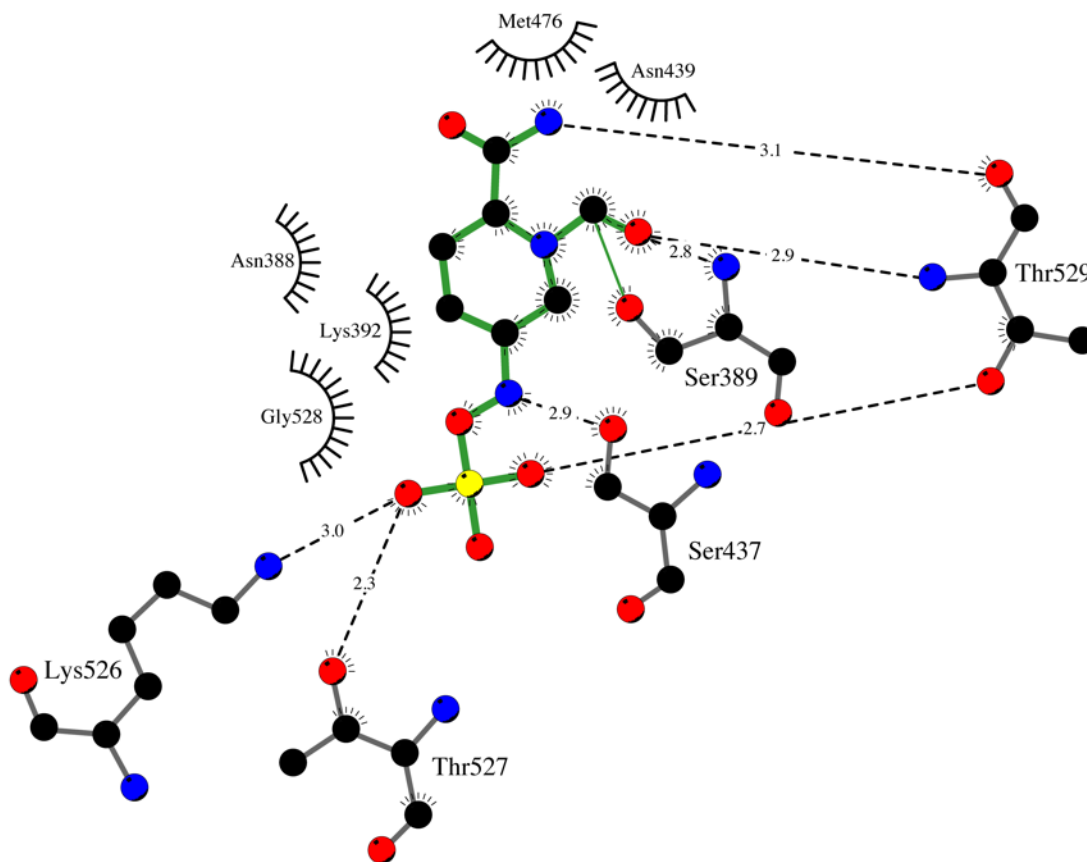


Figure C2: BlaR1^{SD} interactions with avibactam in conformation A are shown using LigPlot+. Atoms are coloured by type and avibactam is shown with green bonds while BlaR1^{SD} bonds are shown in dark-grey. Hydrogen bonds are depicted as black dashes with distances shown in angstroms while hydrophobic contacts are represented by black combs.

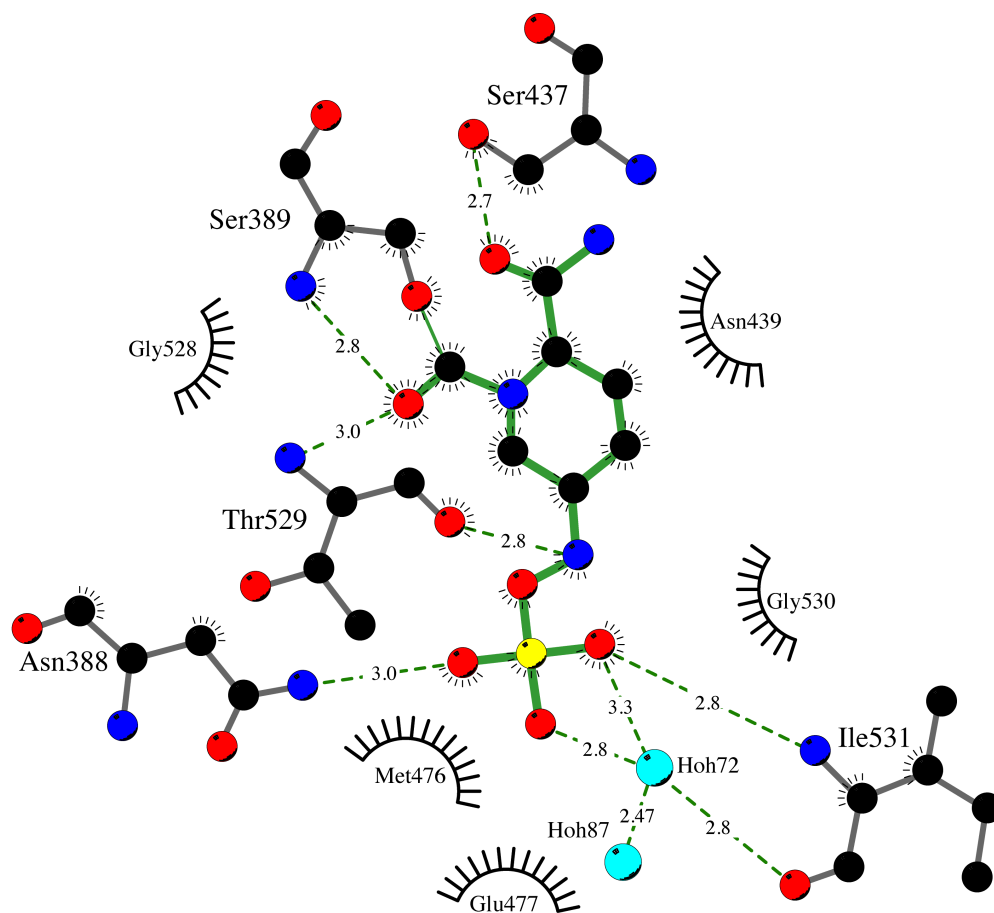


Figure C3: BlaR1^{SD} interactions with avibactam in conformation B are shown using LigPlot+. Water molecules hydrogen bonding distance from protein and ligand are represented with cyan spheres. Other atoms are coloured by type and avibactam is shown with green bonds while BlaR1^{SD} bonds are shown in dark-grey. Hydrogen bonds are depicted as black dashes with distances shown in angstroms while hydrophobic contacts are represented by black combs.

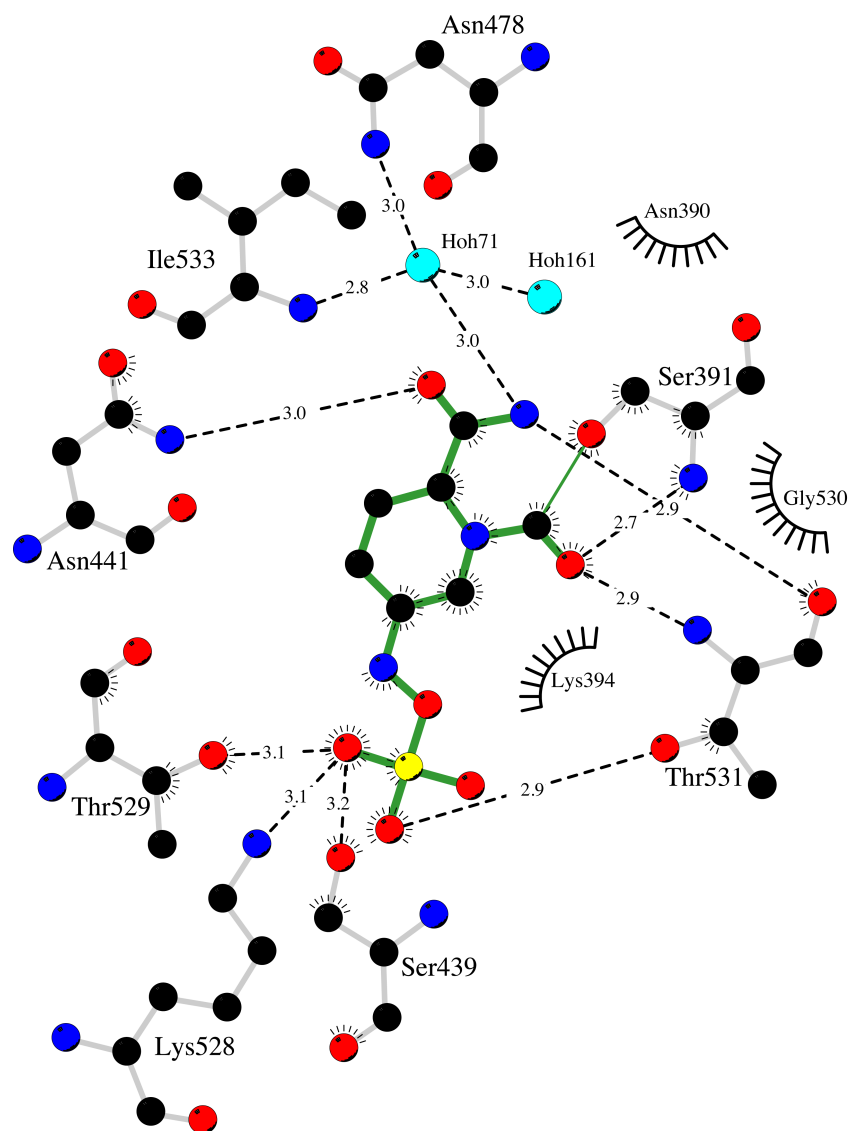


Figure C4: MecR1^{SD} interactions with avibactam are depicted using LigPlot+. Water molecules hydrogen bonding distance from protein and ligand are represented with cyan spheres. Other atoms are coloured by type and avibactam is shown with green bonds while MecR1^{SD} bonds are shown in light grey. Hydrogen bonds are depicted as black dashes with distances shown in angstroms while hydrophobic contacts are represented by black combs.

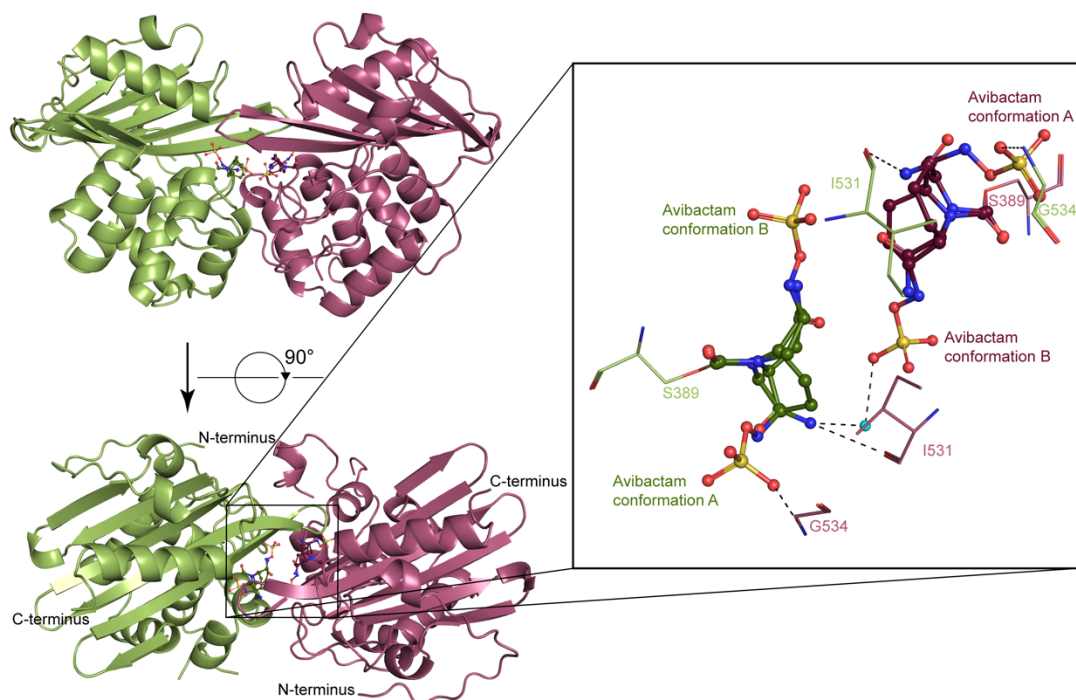


Figure C5: The BlaR1^{SD} chains A and B are shown in green and purple cartoons, respectively. Avibactam is shown as stick and balls with carbon atoms coloured by the chain they belong to while the rest of the atoms are coloured by type. The inset shows the relative positions of avibactam within the asymmetric unit with residues that coordinate avibactam in the opposite chain shown as lines. Hydrogen bonds between avibactam and the opposite chain are depicted as black dashed lines.

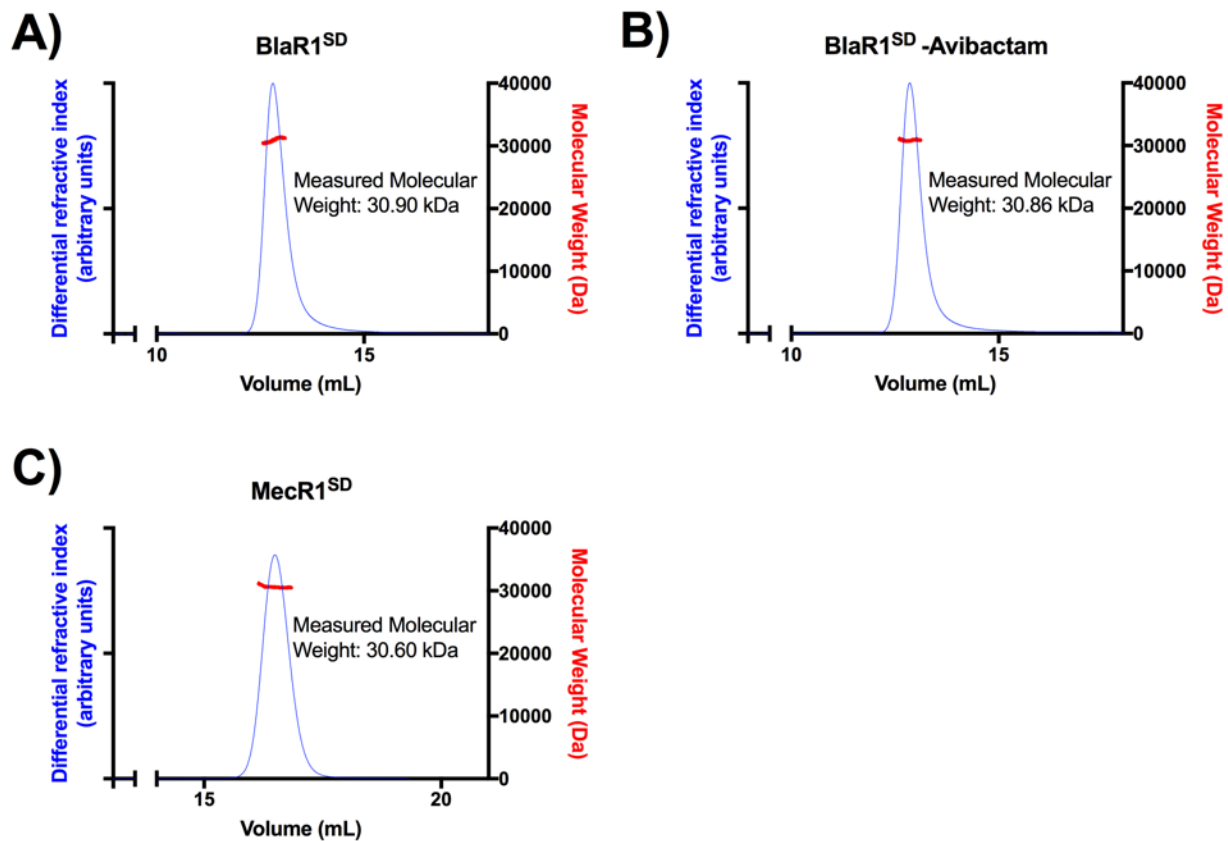


Figure C6: SEC-MALS of A) BlaR1^{SD}, B) BlaR1^{SD} with 5 mM avibactam, and C) MecR1^{SD}. In solution, BlaR1^{SD}, BlaR1^{SD}-Avibactam, and MecR1^{SD} both give a single monomeric peak. The molecular weights for both proteins closely align to the theoretical values of 30.4 and 30.2 kDa for BlaR1^{SD} and MecR1^{SD} respectively.

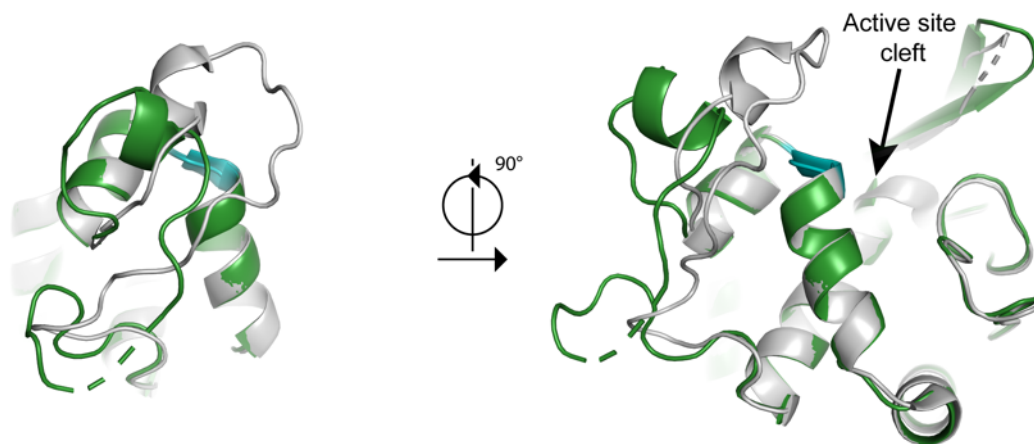


Figure C7: Structural alignment of BlaR1^{SD} in complex with avibactam and a previously solved representative BlaR1^{SD} structure. BlaR1^{SD} is shown as a green cartoon while the BlaR1^{SD} structure in complex with Benzylpenicillin (PDB ID: 1xa7) is depicted in grey. The Sx(N/T) motif is shown in cyan and any ligands are not shown for greater clarity.

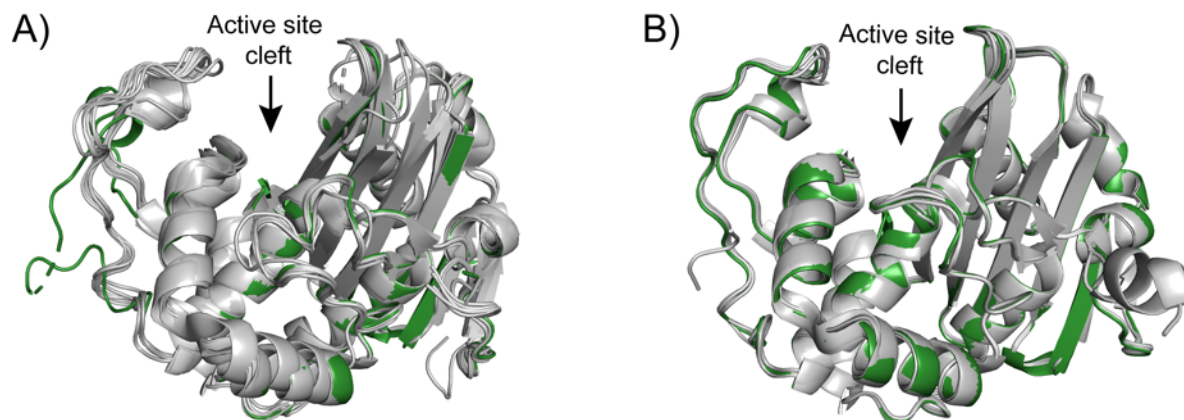


Figure C8: Structural alignments of A) the BlaR1^{SD} avibactam structures and existing BlaR1^{SD} structures in the PDB (PDB IDs: 1nrf, 1xkz, 1xa1, 1xa7, 3uy6, 3q7v, 3q7z, 3q81, 3q82) and B) MecR1^{SD} avibactam existing MecR1^{SD} structures in the PDB (PDB IDs: 2iwb, 2iwc, 2iwd). BlaR1^{SD} and MecR1^{SD} avibactam structures are shown as a green cartoon while other BlaR1^{SD} / MecR1^{SD} structures are shown in grey. Ligands are not shown for greater clarity.

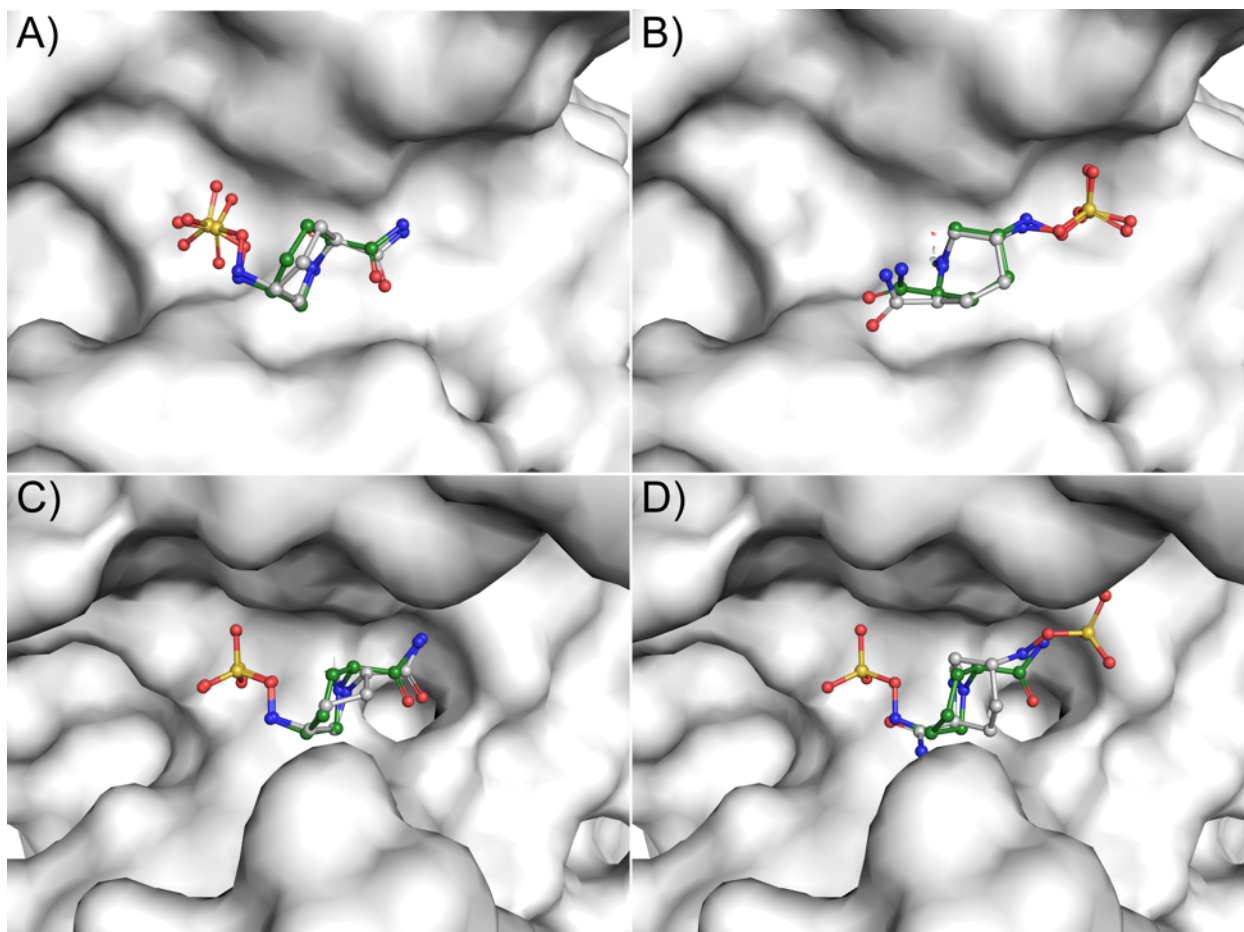


Figure C9: Docking poses calculated for avibactam and BlaR1^{SD} and MecR1^{SD}. Panels A and B show avibactam in conformation A and B respectively in the BlaR1^{SD} structure while panels C and D show avibactam in conformation A and B respectively in the MecR1^{SD} structure. The solvent-accessible surface area of each protein active site cleft is shown in white while avibactam modelled from X-ray density is shown in forest. The docked avibactam is shown in grey. Atoms other than carbon are coloured by type.

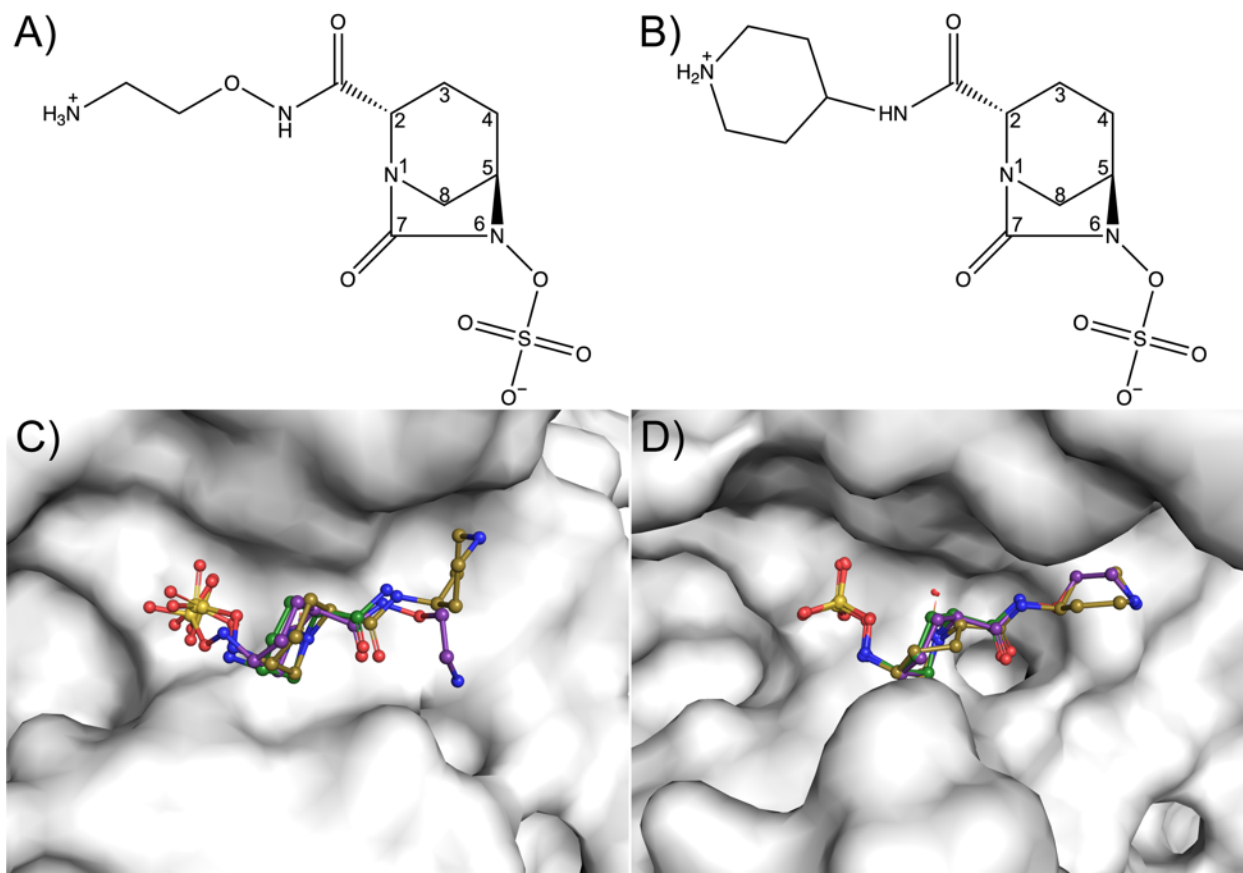
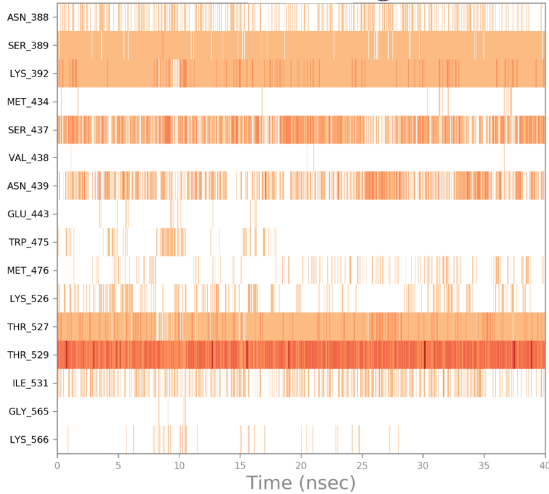
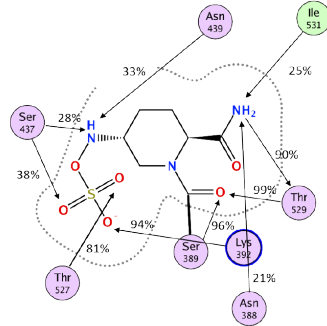


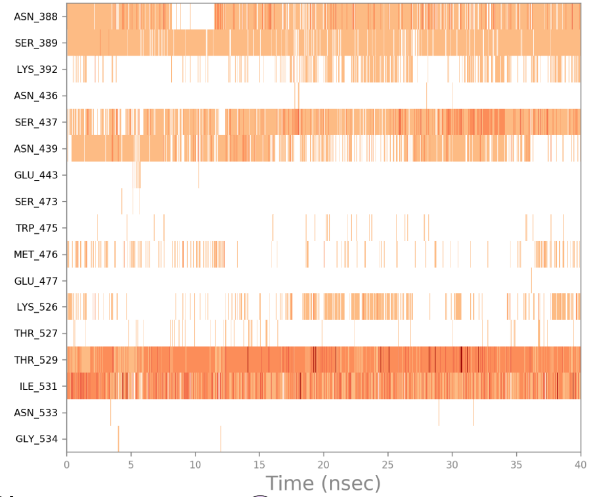
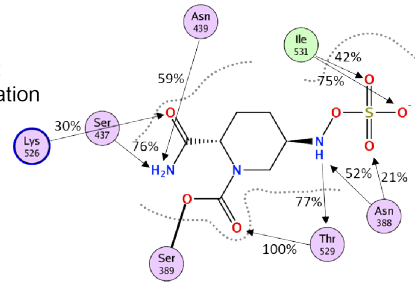
Figure C10: Structures of A) nacubactam, B) relebactam and their docking poses calculated for C) BlaR1^{SD} and D) MecR1^{SD}. The solvent-accessible surface area of each protein active site cleft is shown in white, while avibactam modelled from X-ray density is shown in forest. The docked nacubactam and relebactam ligands are shown in purple and olive respectively. Atoms other than carbon are coloured by type.

A)

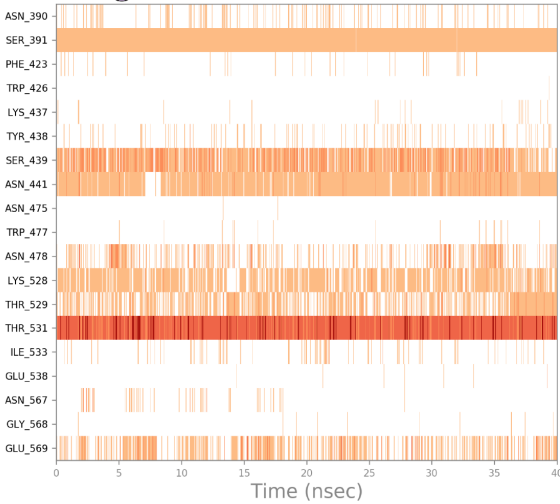
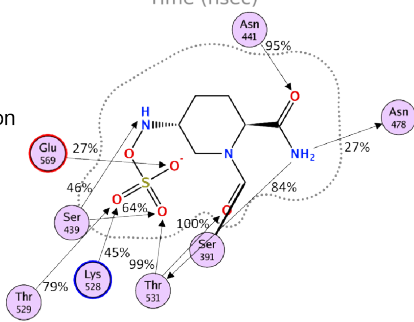
BlaR1^{SD}
 Avibactam:
 A conformation

**B)**

BlaR1^{SD}
 Avibactam:
 B conformation

**C)**

MecR1^{SD}
 Avibactam:
 A conformation

**D)**

MecR1^{SD}
 Avibactam:
 B conformation

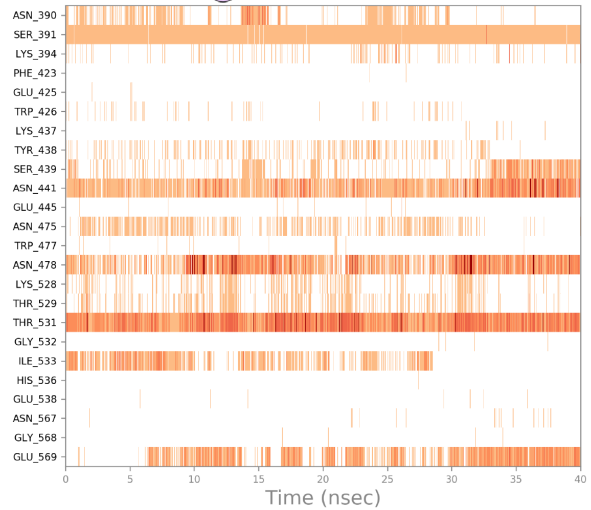
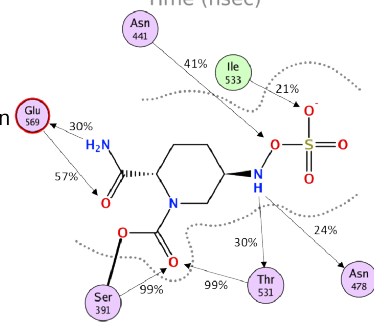


Figure C11: Molecular dynamics simulations of avibactam bound to BlaR1^{SD} and MecR1^{SD} in poses A and B in panels A-C as labelled. The top of each panel shows a 2D representation of active site residues that interact with avibactam for at least 20% of the duration of the simulation. In the bottom of each panel, interactions between avibactam and BlaR1^{SD}/MecR1^{SD} active site residues for each trajectory frame of the simulation are depicted in the interaction plots with either a light orange line (single interaction) or dark orange line (multiple interactions).

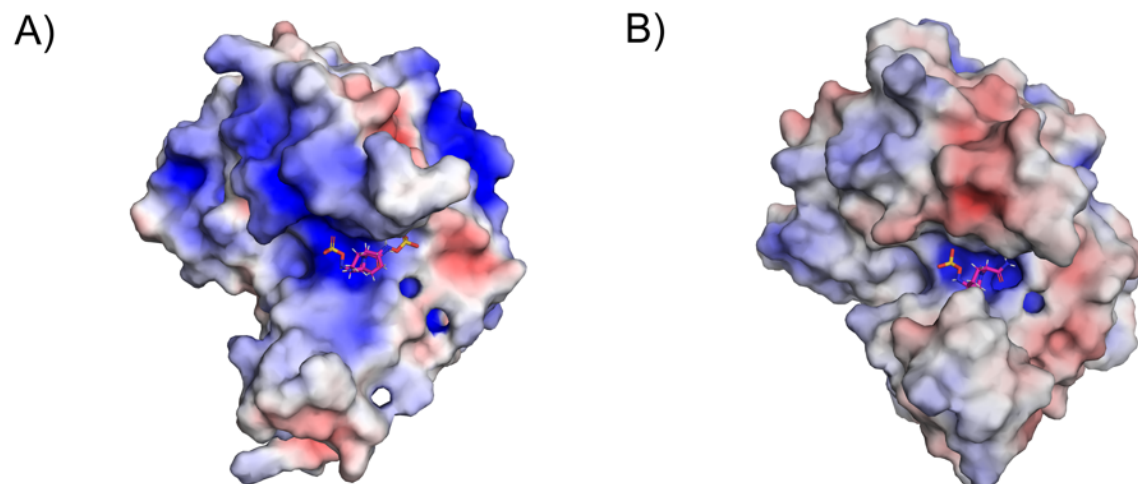


Figure C12: Electrostatic surface of the catalytic binding cleft of A) BlaR1^{SD} and B) MecR1^{SD} in complex with avibactam. The surface is coloured red for negative charges (-5 kTe^{-1}), white for uncharged, and blue for positive charges (5 kTe^{-1}). Avibactam is shown in sticks with carbon atoms coloured pink and other atoms coloured by type.

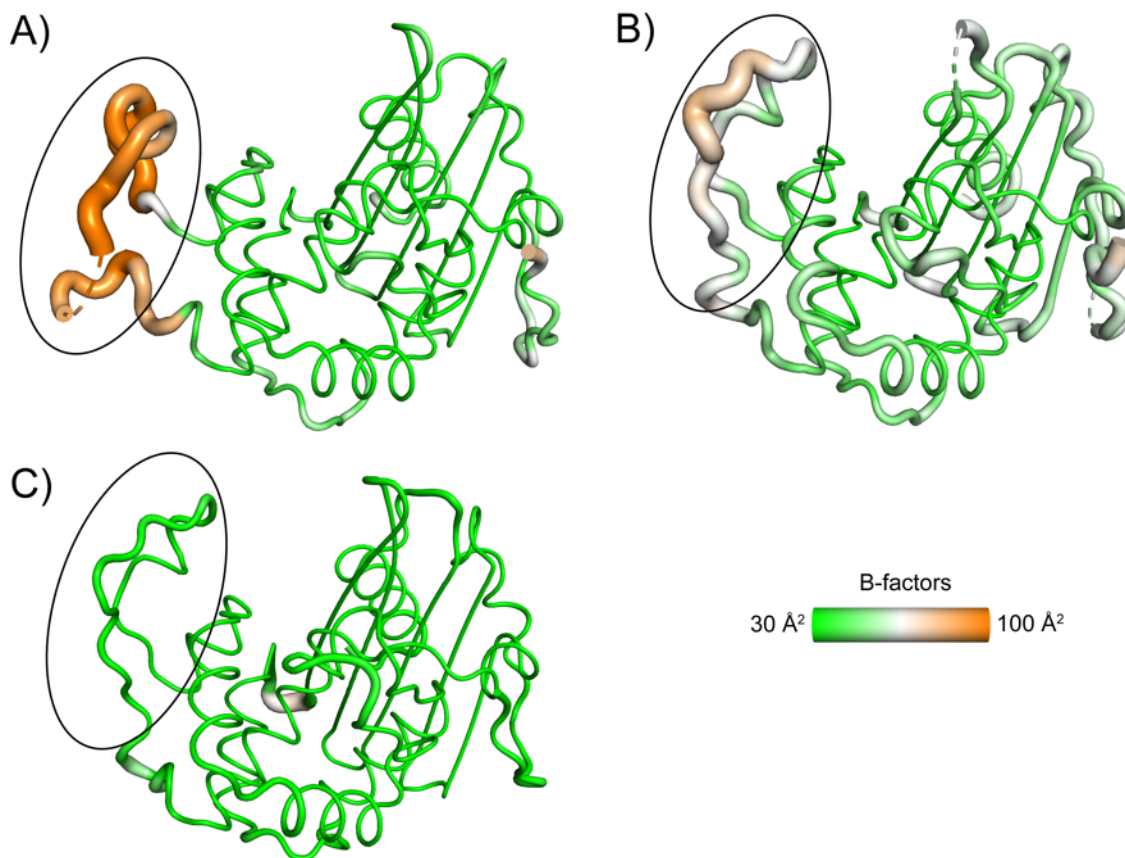


Figure C13: BlaR1 and MecR1 structures coloured according to B-factor value and depicted as putty cartoons. A) BlaR1SD avibactam, B) BlaR1SD with benzylpenicillin (PDB ID: 1xa7), and C) MecR1SD with avibactam. The loop with significant variation in several of the structures is indicated with a black oval.